The Pennsylvania State University

The Graduate School

LOW TEMPERATURE POST-PROCESSING OF ADDITIVELY MANUFACTURED 316 STAINLESS STEEL

A Thesis in

Mechanical Engineering

by

James Kidd

Submitted in Partial Fulfillment
of the Requirements
for the Degree of

Master of Science

May 2020

The thesis of James Kidd was reviewed and approved by the following:

Aman Haque
Professor of Mechanical Engineering
Thesis Advisor

Guha Manogharan
Associate Professor of Mechanical Engineering

Karen Thole
Professor of Mechanical Engineering
Head of the Department of Mechanical Engineering

ABSTRACT

Post processing has been dominated for the last few centuries by heat treatments with relatively little advancements in technology. These processes require extreme temperatures for extended periods of time. The need for high temperatures to promote mobility in materials has become a fundamental part of altering microstructures in materials. This thesis aims to challenge this idea. Post processes utilizing electricity have recently become an interest of material researchers due to observations of energy and time savings. Even though the use of electricity to affect microstructures was first realized in the 1960's, studies have only just come out detailing how to control microstructures with a constant electrical current. Some research has hinted that this electrical annealing process does not require heat in order to achieve microstructural changes. This thesis details a unique electrical processing technique that can be done at room temperature. With a focus on austenitic stainless steel, special material properties, such as low stacking fault energy, allows for a unique microstructural characteristic such as a large number of annealing twins. Analysis is performed using electron backscattered diffraction, grain boundary misorientation plots, grain size analysis, and x-ray diffraction. This novel annealing and grain refinement process resulted in the grain size increasing by up to 74 percent for the grain growth experiments and the grain size decreasing by up to 74 percent for the refinement experiments. The results also showed significant changes in misorientation angle distributions for both grain growth and grain refinement with the average misorientation angle increasing up to 500 percent.

TABLE OF CONTENTS

LIST OF FIGURES

LIST OF TABLES

Acknowledgments

This thesis would not be possible without the support of my thesis advisor Dr. Haque. I would like to thank him for his continued support during the past three years and will always remember that, with the appropriate amount of work, any problem can be solved. I would also like to thank my family for motivating and inspiring me to pursue higher levels of education.

This work was supported by the Division of Civil, Mechanical, & Manufacturing Innovation (Nanomanufacturing program) of the National Science Foundation through award #1760931. The findings and conclusions of this work do not necessarily reflect the view of the National Science Foundation.

Chapter 1

Introduction

The Microstructure of a metal is crucial in determining the properties of the material. Often the properties of the material are undesirable and need to be altered by changing the material's microstructure. Unfortunately, methods of altering microstructure is limited with most methods having an approach of starting the microstructure over from scratch and controlling the process until the desirable grain size and shape is achieved. These methods are called heat treatments and have been around since the bronze age. New methods of altering microstructure, such as strain induced grain boundary migration, have been discovered within the last century that utilize unique mechanisms that completely skip the starting over step. Even more recently, a new form of strain induced grain boundary migration has been discovered that has exciting efficiencies and unique results. This method utilizes electrical current to drive microstructures to achieve states of superior mechanical properties. This process completely eliminates the archaic need for high temperature and can be completed in a fraction of the time required for traditional heat treatments. By first reviewing the necessary background information, then performing practical experiments, and finally discussing the experimental results, this thesis will demonstrate how electrical annealing can drastically change a microstructure as seen in Figure 1-1. This thesis will also demonstrate how this type of post processing differentiates itself from other post processes.

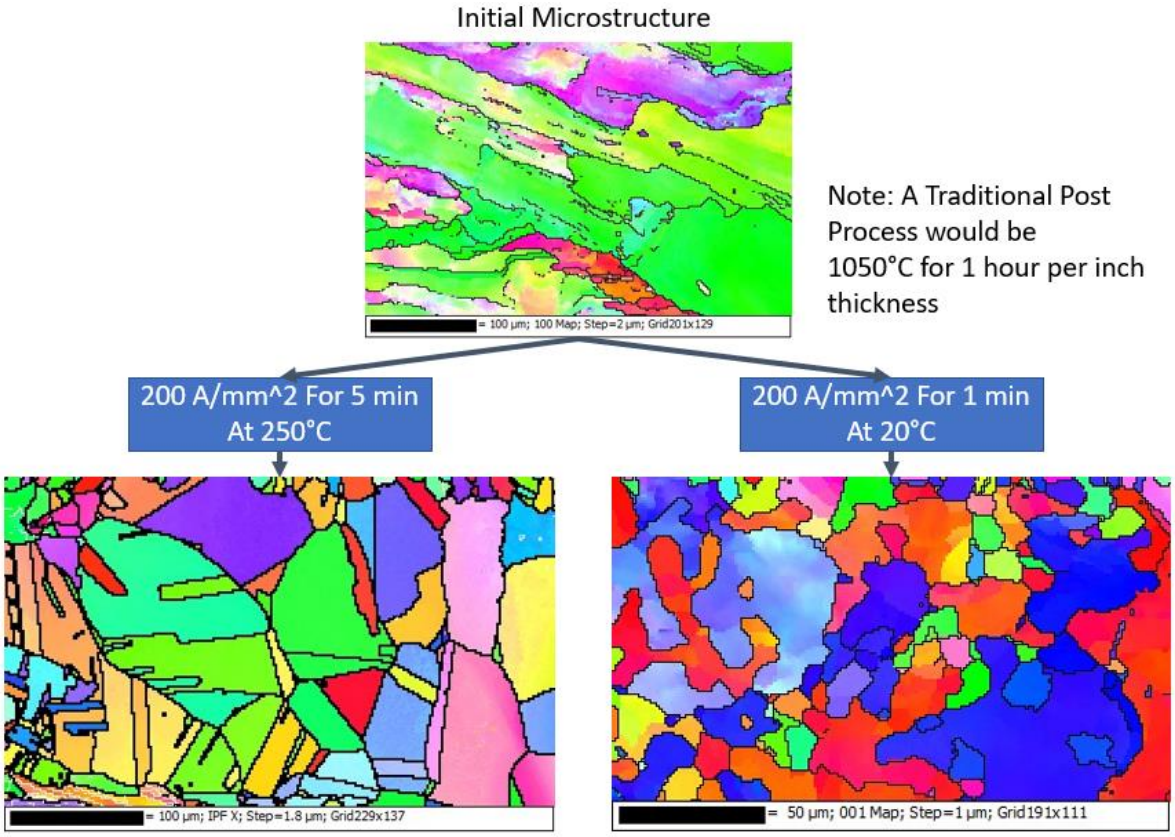

Figure 1-1: A Graphical abstract of the electrical annealing process.

Traditional Post Processing

Traditional post processing steps that would compete with the electrical annealing process would include heat treatments since the goal of these processes are to normalize and control the microstructure. It is worthy to mention the process of hot isostatic pressing since it would be commonly used for materials that are additively manufactured, like the material that is the focus of this study. Hot isostatic pressing has a primary goal of eliminating porosity defects which differs from electrical annealing. Hot isostatic pressing can often be combined with heat treatment by performing a HIP step and then controlling the cooling rate to perform the desired heat treatment. The HIP process consists of three major parameters: temperature, pressure, and holding time. These parameters allow for large variations in recipes. The thermal annealing process can be broken down into three stages: recovery, recrystallization,

and grain growth. These three stages only depend on temperature and time and allow for simple parameters-grain size relationships. Both the HIP process and the heat-treating processes require large temperatures and large amounts of time to promote diffusion in the material. HIP will also use longer periods of time to apply creep effects. The end goal of these processes is to improve or alter the mechanical properties of the material. HIP mainly focuses on improving the material's fatigue life, while heat treatments focus on altering the materials strength and ductility.

Hot iso-static pressing closes porosity defects to improve density. A schematic of the components of a hot isostatic pressing machine can be seen Figure 1-2. Hot isostatic pressing is done by plastically deforming a weakened material due to creep effects and allowing the newly created surface to surface interfaces to diffuse together. The elevated temperatures for long periods of time allow for creep effects in a material. These creep effects allow for plastic deformation even though the stress in the material is below the material's yield limit. The mechanical stress in the material stems from the high-pressure environment. This environment needs to be made of an inert gas in order to prevent contamination of the material. The iso-static pressure environment applies a force on all sides of the material putting the material in a compression state. The goal of this loading scenario is to compress any porosity defects to a point where the cavity buckles and new surface-surface interfaces are created. Once these interfaces are created, the enhanced diffusion will work to permanently fuse the interface into a continuous piece of material. Once the defect is permanently closed, there will be less voids and therefore a higher density. The process will also result in the part shrinking equally in all dimensions.

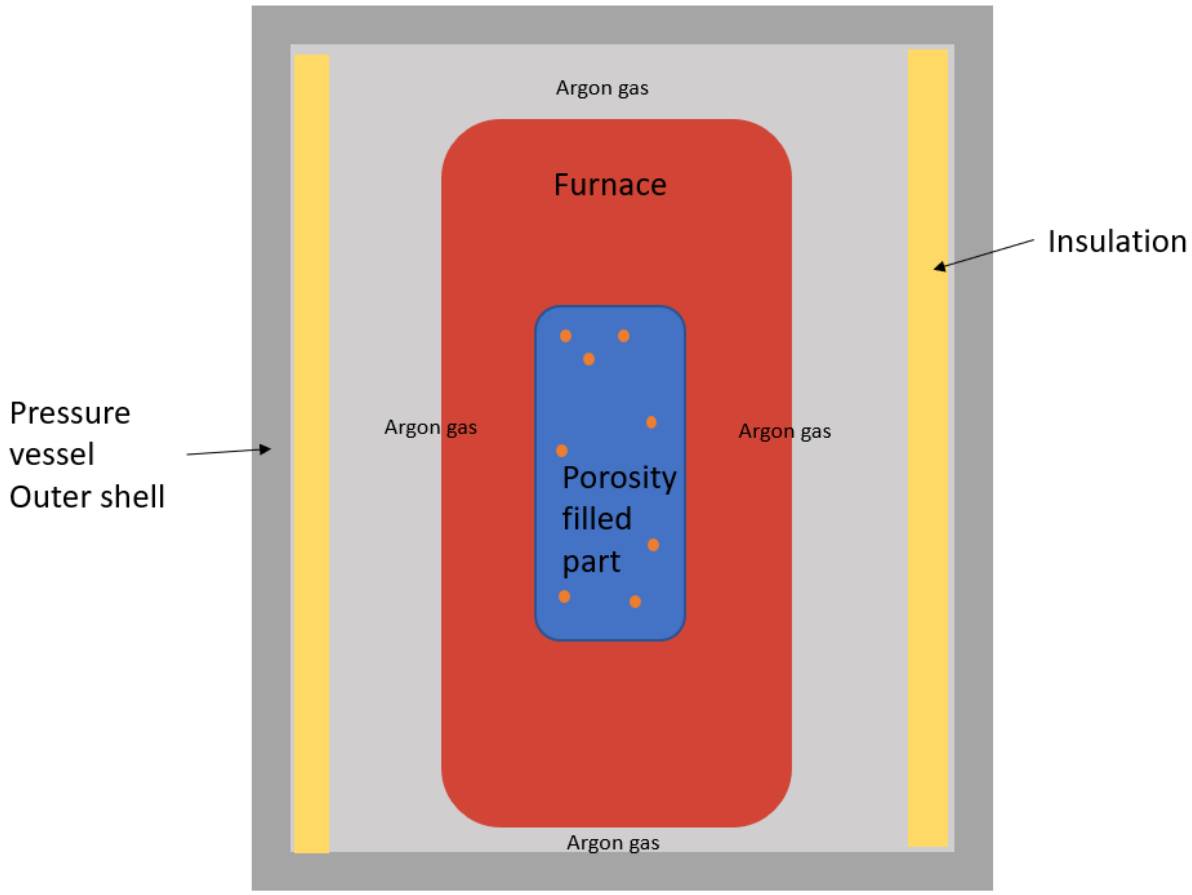

Figure 1-2: A schematic of how most HIP machines are setup.

Hot iso-static pressing is not a perfect process and will not remove all porosity in the material. A common issue found in additive materials that have undergone a HIP process is that porosity will increase during heat treatments after hot iso-static pressing. This problem has been demonstrated in the additive field [1]. This problem occurs because diffusion cannot take place across the interface boundary of a collapsed void if the void contains a significant amount of elements like argon. These elements line the interface and prevent the base material from contacting itself. The lining acts as a large barrier to diffusion. Once the part is undergoing the heat treatment process, these collapsed voids eventually expand due to the interface surfaces breaking from being poorly fused. Figure 1-3 details how material density changes after HIP and then how the density changes after thermal annealing. Elements like argon can commonly be found inside the voids of additive materials due to the inert gas becoming entrapped in the

material during solidification. This gas entrapment can occur during processing or can come from entrapped gas inside of the powder feedstock. Another common problem with hot iso-static pressing is that it cannot close any surface connected porosity. This is because the gas from the environment fills the surface connected porosity and will prevent the void from closing when the pressure is raised.

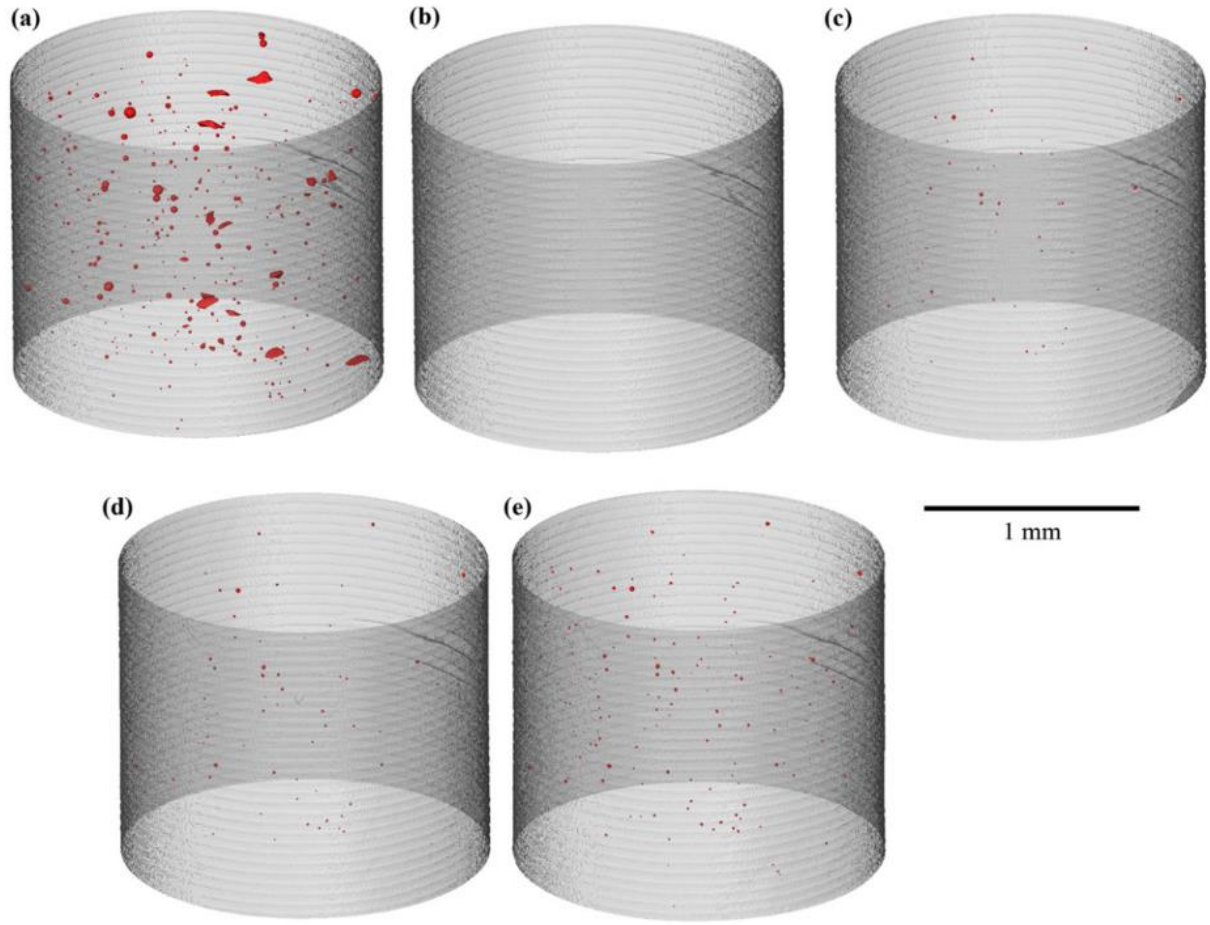

Figure 1-3: 3D visualization of material density as porosity (red volumes) in a sample (a) as received, (b) Post HIP, (c) 10 min at 1035 C, (d) 10 hrs at 1035 C, and (e) 10 min at 1200 C [1].

Thermal treatments to control microstructure and material properties were developed well before hot isostatic pressing. The processes of these treatments have been explored and are well understood. The first step in the process is recovery. In recovery, the internal strain energy of the microstructure is reduced due to dislocation motions in the crystal. Next is recrystallization, where the microstructure changes drastically. The elevated energy state of the grains allows for new grains to nucleate along the grain

boundaries. These new grains are strain free, equiaxed in shape, and will have lower dislocation densities. The recrystallization stage is complete when the previous grains are overtaken by newly nucleated grains. Finally, the grain growth step starts when the newly nucleated grains grow and compete with each other. The grains will continue to grow as the material is left in the high temperatures that facilitate atomic diffusion. The grain boundaries will move in the direction of each grain boundary's center of curvature due to an excess of strain energy driving the movement. The grains will eventually reach a state close to equilibrium. At this point the diffusion slows to a point where the grains will take a long time to grow [2]. Overall, the thermal annealing process requires a lot of energy to achieve the elevated temperatures for long periods of time (hours to days).

Thermal annealing occurs due to a static recrystallization process. In the case of thermal annealing, stored strain energy and high dislocation densities act as a driving force that produces new dislocation free grains. There is also another way to recrystallize materials which is referred to as dynamic recrystallization. Dynamic recrystallization happens when a material is being strained and the stored energy is large enough to create grain growth. This growth takes the form of bulges in the grain boundaries. This unique grain growth process is called strain induced grain growth [3].

Strain induced grain growth is a result of a grain boundary movement called strain induced grain boundary migration (also known as grain bulging). In strain induced grain boundary migration, the grain boundaries move in the direction that is opposite of the boundary's center of curvature. A key difference is that in strain induced grain growth, the grains that grew will retain the same crystal orientation as the original microstructure. This is different from the traditional grain growth process where the grains that grew will have the crystal orientation as that of the nucleated grains. While both processes will result in annealed microstructures with low strain energy and dislocation densities, the strain induced grain growth does not require the formation of nucleated grains [4].

Review of Additive Manufacturing

While the focus of this thesis is the process of altering microstructure by using electricity and not the process of additive manufacturing, information related to additive manufacturing will help better understand the as received material that will be used in this study. Additive manufacturing of metals can be done in several ways but primarily consists of building parts layer by layer using feedstock in the form of metal wires, strips, or powder. The processes can utilize various forms of energy inputs to fuse the layers together. Heat inputs from lasers and electron beams are the most common way to fuse layers together. Some less common ways would be to binder/sinter or to friction weld layers together. The additive field is currently dominated by powder-bed fusion and directed energy deposition processes with binder-jetting processes becoming more popular. Powder bed fusion can be seen in Figure 1-4 and consists of metal powder being spread and fused together into a new layer over the previously fused layer. Powder bed fusion can use lasers or electron beams to input the energy to fuse the powder layers. Directed energy deposition can be seen in Figure 1-4 as well. Directed energy deposition uses lasers, electron beams, or arc welders to fuse together a flowing feedstock into a weld track on top of the previous layer. Binder jetting can be seen in Figure 1-5 and is like powder bed fusion in that the powder feedstock is spread across the previous layers. It differs from powder bed fusion in that instead of fusing the feedstock it deposits a binder from a print head to lightly bind the layers together into a green part. This green part is then put into a traditional sintering furnace to fuse the particles into a solid part. Binder jetting is unique in the fact that it produces very low-density parts and requires certain post processing steps to have reliable part strength.

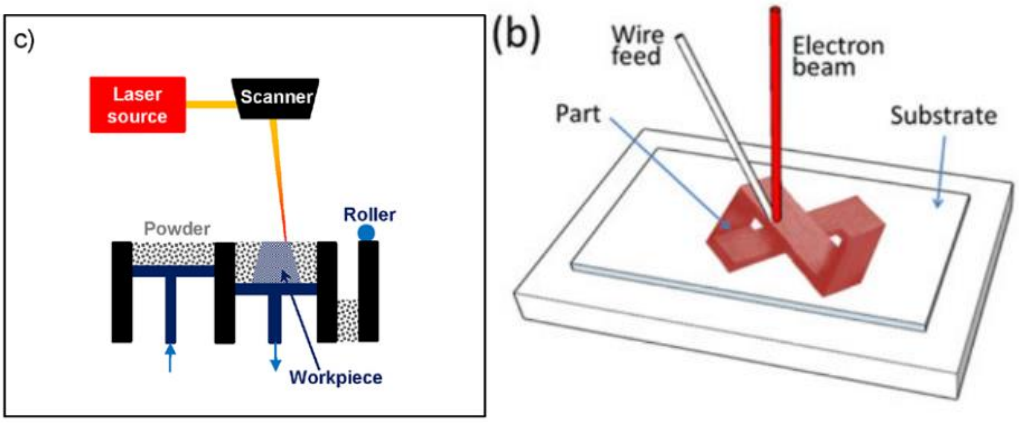

Figure 1-4: Diagrams of powder bed fusion (left) and directed energy deposition (right) processes [5][6].

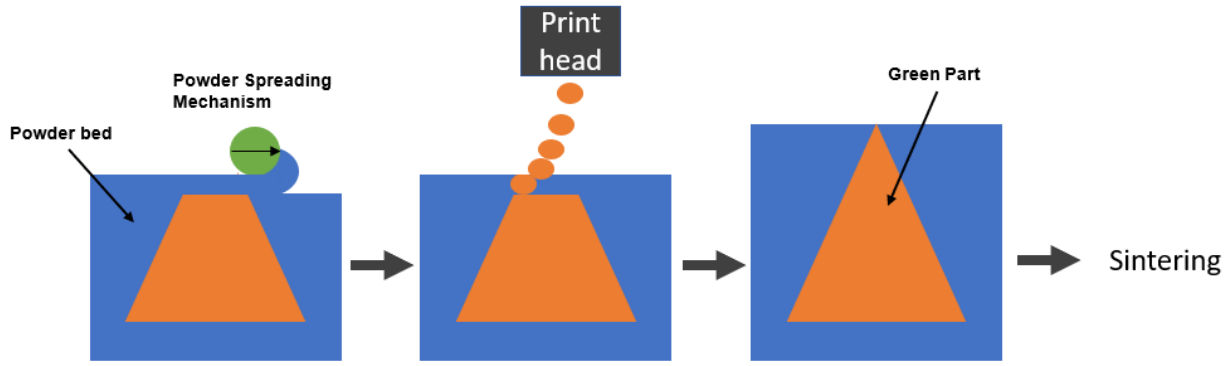

Figure 1-5: Illustration of how binder jetting processes work.

There are several problems that have become prevalent across all forms of additive manufacturing and are not subjected to one area. For instance, proper characterization of the process is needed for better understanding and control of the process. This characterization requires expert analysis and research in heat transfer, fluid flow, material science, solid mechanics, etc. Figure 1-6 demonstrates how complex a directed energy deposition process can be to control. Problems in this flow chart start at the feedstock level. More complexities are identified during the processing with a focus on melt pool characterization. Finally, once the part is finished building, complex relationships between what happened during processing and the microstructure or the distortion in the part become apparent.

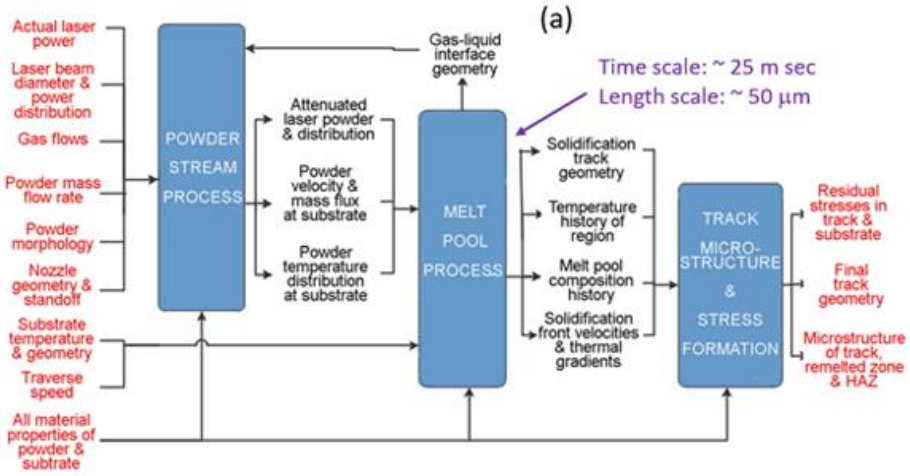

Figure 1-6: The parameters that go into controlling a directed energy deposition process. [7]

Research has shown how important the feedstock is to the final properties of parts made in additive manufacturing. These feedstock-property relationships apply to all forms of additive manufacturing. The most basic relationship is the feedstock chemistry effect on the final part properties. Some feedstock forms allow for easier control of the chemistry such as metal wires or sheets. The chemistry of these feedstock can be controlled with management of the melt chemistry that was used to create them. Control of the chemistry of metal powder is not as simple since along with melt chemistry, things such as the particle atomization environment and powder oxidation can affect the as-built part [8][9]. Other parameters that have potential to affect additive material properties are powder morphology, powder size distribution, and powder flowability. These powder characteristics have been shown to influence packing density which may result in lower final part densities [10][11].

Melt pool characterization is critical in understanding the relationship between processing and final part properties. It also plays a vital role in controlling additive manufacturing processes. Melt pools in metal additive manufacturing are complex, as seen in Figure 1-7, with influences coming from the powder bed, the flow in the melt pool, heat transfer mechanisms, the heat source, and evaporation. These dynamic molten pools affect both powder bed fusion and directed energy deposition processes. The Melt pools are the foundation for additive manufacturing and are what allow for the unique benefits of design freedoms and reduced wastes in additive manufacturing. Unfortunately, the instability of the melt pools is

also what form the defects in additive manufacturing. Understanding how these pools work and how to control them will allow for enhancing the aspects that benefit additive manufacturing while reducing the defects that are formed.

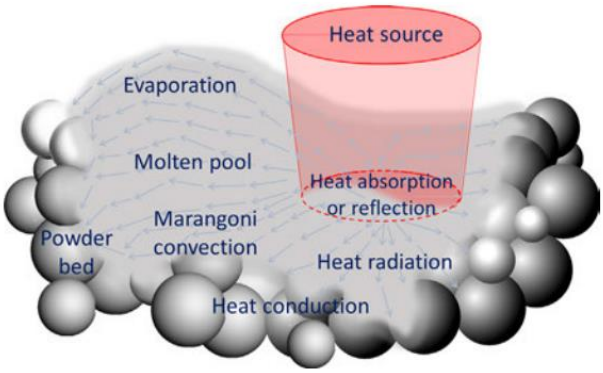

Figure 1-7: Factors that influence the molten pool in a powder bed fusion process [6].

In most additive processes, heat is put into the material through a laser or electron beam source. Some of this heat will be absorbed by the material which will lead to melting but some of the heat will be reflected. The absorptivity and reflectivity of the energy will constantly change and will lead to some of the dynamics of the melt pool. With the amount of absorbed heat constantly changing, imperfect packing densities, or imperfect powder flow rates, the shape of the melt pool will constantly change as seen in Figure 1-8 [12]. Another aspect of this dynamic melt pool is the mode of heat transfer. Lower levels of energy input will tend to lead to conduction mode welding while higher levels will lead to keyhole mode welding. Keyhole mode welding is where convection heat transfer takes over as the dominate mode of heat transfer. The convection results in more complex flows in the melt pool compared to conduction mode welding. Keyhole mode welding will have a larger pool depth to width ratio due to a vapor cavity caused from large amounts of evaporation. Evaporation of the melt pool is undesirable due to the complications that recoil pressure on the melt pool, spatter, and plumes have on the additive process. The vapor cavity caused by the evaporation will tend to collapse from instability and will result in keyhole porosity [6].

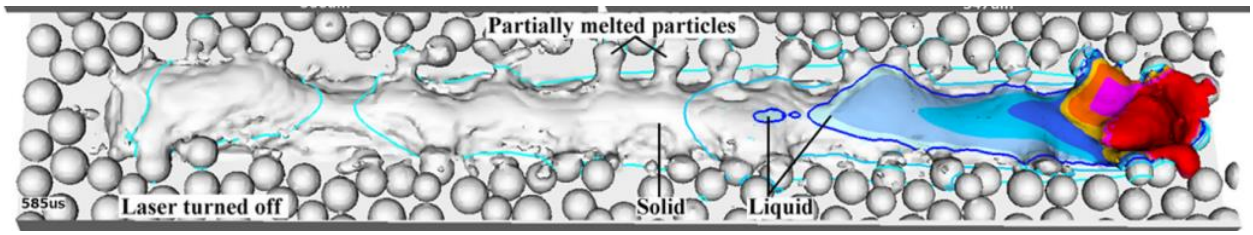

Figure 1-8: Dynamic melt pool shape in a powder bed fusion process [12].

The undesirable aspects of dynamic melt pools, such as keyhole collapse, spatter, and recoil pressure, will lead to porosity in the as-built part. The porosity in additive manufacturing is one of the biggest barriers preventing parts from being used in industry. Keyhole instability, that was previously discussed, leads to one form of porosity in additive manufacturing and can be seen in Figure 1-9 [6]. Porosity in additive manufacturing can also stem from a lack of full melting during processing. With the melt pool not properly melting all the material in its path, porosity can form in the track due to particle porosity or voids formed due to spatter [13][14]. The evaporation that can occur in a melt pool will also lead to porosity issues due to the denudation zone that forms along the side of melt tracks as seen in Figure 1-10 [15]. Solutions to these complex porosity issues need to be developed and implemented in order to properly control the additive manufacturing processes.

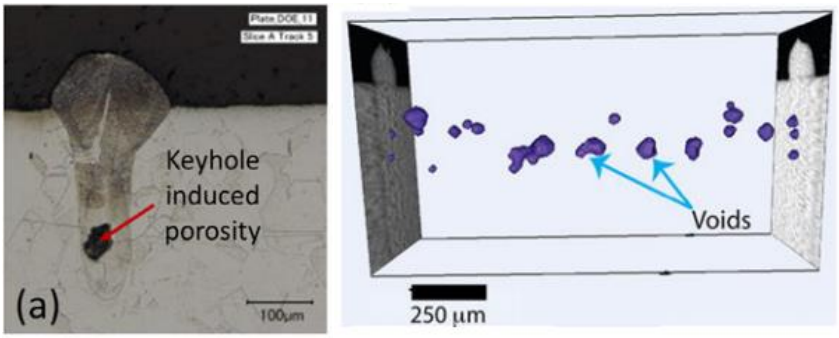

Figure 1-9: Keyhole porosity (left) and how unstable keyholes lead to porosity throughout a solidified melt track (right) [6].

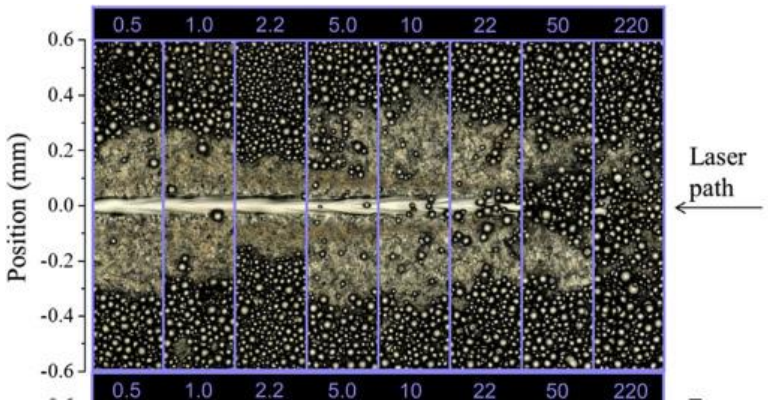

Figure 1-10: Denudation zone formed in a powder bed fusion process [15**]**.

After processing, more complexities occur when trying to relate resulting microstructure and part distortion to processing conditions. Additive manufacturing produces unique metallic microstructure due to the processing conditions. The process tends to have very high cooling rates due to having high energy dense heat sources which create large thermal gradients. The high cooling rates also develops from the small volumes of liquid metal that solidify quickly. The cooling rates seen in additive manufacturing often reach 10^3 to 10^6 K/s depending on the process [6]. These large cooling rates lead to non-equilibrium microstructures with large amounts of defects. The high cooling rates also lead to large contractions in the melt pool during solidification which leads to large residual stress and distortion in the part.

Distortions and residual stress are very hard to eliminate in processes such as powder bed fusion and directed energy deposition. During solidification of a melt pool, an initial large amount of residual stress will be formed due to differences in contraction. Additional buildup of residual stress will occur due to repeated changes from expansion and contraction from heating and cooling [6]. If the part is not properly anchored, the stress will turn into distortions in the part geometry. If the part is properly anchored, the stress has the potential to form cracks inside of the part.

The nonequilibrium conditions in additive manufactured metals will form long columnar grains across multiple layers in the build direction. An example of columnar grains can be seen in Figure 1-11. This epitaxial growth is formed due to a reduced amount of energy to form the solidifying crystal along the same orientation as the crystals from the previously deposited layer. It is worth mentioning that the

columnar grains can also be curved or slanted due to competitive growth. This competitive growth occurs because of the grains wanting to grow perpendicular to the solid-liquid interface of the melt pool [6]. This is the direction of maximum heat extraction also known as the largest thermal gradient. Figure 1-12 shows how the amount of curve in the columnar grains depends on the scanning speed of the process. If the scanning speed was slow, the grains will appear more curved, if it was fast, the grains will form straighter columnar shapes.

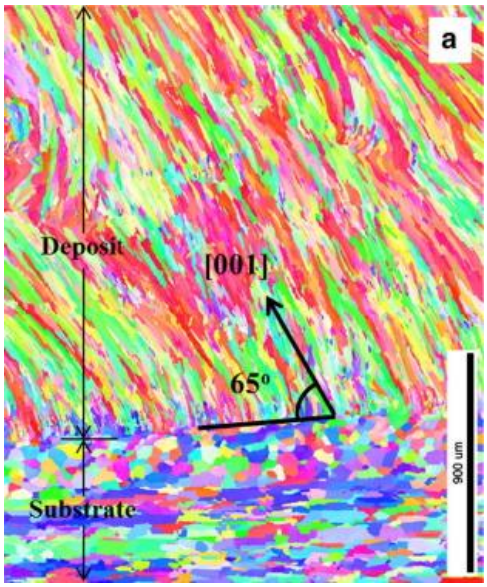

Figure 1-11: Columnar grains formed in additive materials across multiple build layers [6].

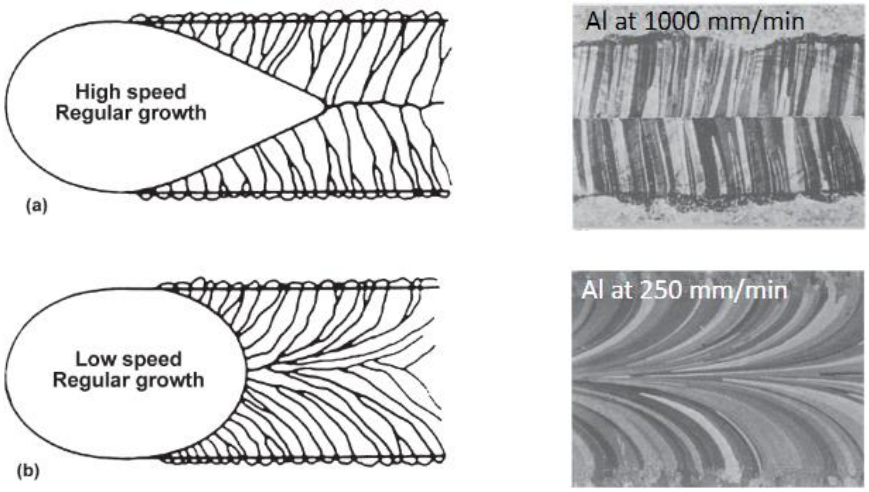

Figure 1-12: Relationship between scan speed and competitive growth [16].

In terms of the mechanical properties of these metals, the smaller microstructures tend to produce stronger parts which is predicted by the Hall-Petch equation. The Hall-Petch equation shows that smaller

microstructures will lead to a stronger material. This strength increase comes at the cost of a reduction in ductility of the material. Also, relatively large amounts of defects in the material due to non-optimal processing conditions lead to reduced mechanical properties. Figure 1-13 shows typical tensile test results from additively manufactured metals. The as-build conditions in additive materials typical contain very high strength levels due to refined microstructure but contain low ductility [17]. The ductility is partially low because of the small grain size but also because of the large number of defects in the material.

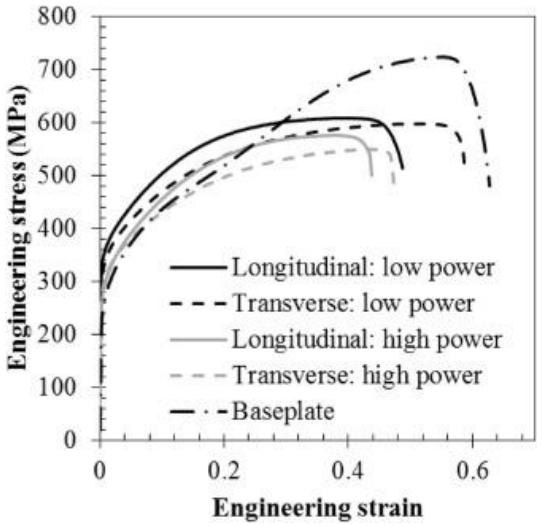

Figure 1-13: Tensile test results for additively manufactured 304L stainless steel [17].

The complex microstructure of additive metals complicates the analysis of mechanical properties since the direction at which a test sample is cut will greatly impact the measured mechanical properties [18]. If a sample of an additively manufactured part is cut perpendicular to the scanning direction, the grains will appear equiaxed if scanned at low speeds. When the sample is cut parallel to the scanning direction, as in Figure 1-14, the grains will appear columnar. This anisotropic microstructure directly results in the anisotropic mechanical properties due to the Hall-Petch relationship.

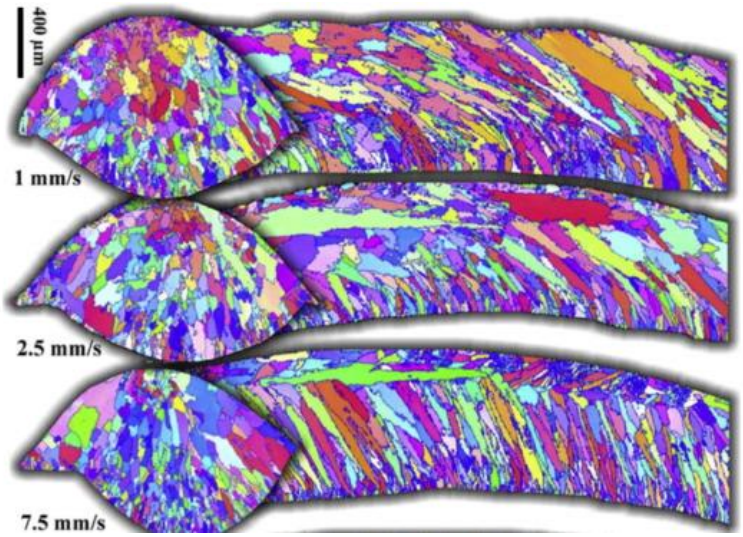

Figure 1-14: EBSD of multiple weld tracks with varying speed showing the differences in grain size and shape in different cross-sections [6].

Processing defects in additive manufacturing leads to a lower fracture toughness. Lower fracture toughness can disqualify AM parts for use in cyclic loading scenarios where the part will fail due to fatigue. Figure 1-15 shows how an additively manufactured material's fatigue life compares to the wrought alloy's fatigue life. In each of the loading scenarios, the additive material had lower cycles to failure [6]. The anisotropic strength in additively manufactured parts can also make the part not suitable. To overcome these problems, the parts require post processing. One of the most important post processing steps is the annealing that is done to eliminate the anisotropies and improving some of the mechanical properties.

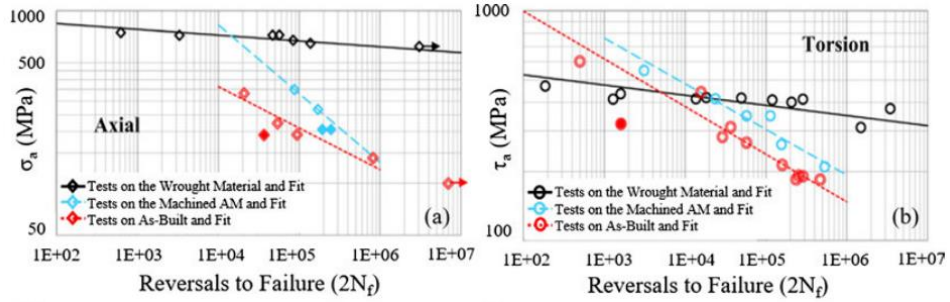

Figure 1-15: Fatigue life of an additively manufactured material compared to the life of the wrought alloy [6].

A specific research direction in the literature is aimed at the elimination of the post processing steps by optimizing the additive manufacturing processes [19][20]. So far nothing in the literature has been able to produce control of the process to the point that would eliminate post processing. The current lack of control and understanding is due to the complex relationships and problems that were previously discussed. Optimizing the processing parameters in additive process is difficult since the relationships between the feedstock, melt pools, and microstructure are intertwined. This difficulty is then compounded by the problems encountered such as porosity.

Twinning

Unique boundaries can form inside grains during the annealing process of materials. Twin boundaries are an example of this where the crystal inside of a grain gets split into two domains where the crystal orientation differs. This difference in crystal orientation can be described as a reflection where the two domains share some of the same lattice points in a symmetrical manner. A visualization of twins can be seen in Figure 1-16. This phenomenon will form in a material when the shear stress in a direction reaches a critical value. The formation of these twin boundaries allows for a reduction in interfacial energy in the material. Similar to grain boundaries, twin boundaries mark a change in crystal orientation that enables properties that suppress dislocation motion. Suppression of dislocation motion allows for increased strength of the material which has created interest from researchers to better understand twinning and what promotes twinning across multiple size scales [21] [22] [23].

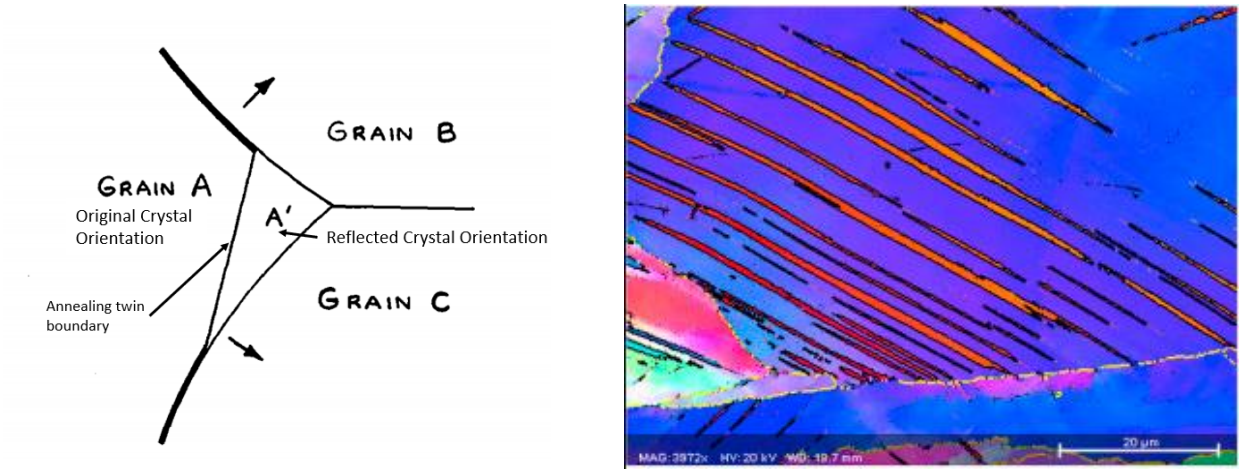

Figure 1-16: Visualization of annealing twins (left) and deformation twins (right) [24][25].

Twinning can be in the form of deformation twins or annealing twins with the cause of each being from plastic deformation and heat treatments respectively. The formation of both deformation twins and annealing twins are influenced by similar properties. The most influential property related to the formation of twins is the stacking fault energy. Materials like austenitic stainless steels have low stacking fault energies that result in large amounts of twins formed during heat treatments and deformation. The stacking fault energy of materials is sensitive to the chemistry of the alloy system. Larger amounts of elements like carbon and boron increases the stacking fault energy which would retard twin formation. Larger amounts of elements like nitrogen reduces the stacking fault energy and promotes twin formation [25]. Various other properties such as low temperatures during deformation, high temperatures during annealing, large strain rates (or growth rates), and large grain size promote the formation of twins [26][27].

The austenitic stainless steel used in this study is known for having a low stacking fault energy and tends to form twins. Since the material used is also additively manufactured, it is also worthy to mention that twinning in the additive literature is mostly associated with deformation twinning since the complex non-equilibrium microstructure tends to not form annealing twins. Some studies have shown superior mechanical properties from additively manufactured 316 stainless steel in the as built condition compared to mechanical properties of 316 stainless steel manufactured by traditional manufacturing

methods [25][28]. This can be seen in Figure 1-17. These results were surprising since additive materials tend to include significantly more porosity defects compared to traditional manufacturing. The porosity defects should result in weaker properties for the additive material. The explanation of these results lies within the fact that the additive material was more prone to deformation twinning. The twinning allowed for improved strength and greatly improved ductility. One reason the additive material was more prone to twinning could have been due to the larger variations in chemical compositions in additive material. In the case of Pham et al., the additive process was done inside of an inert nitrogen gas environment which increased the nitrogen content in material. The increased nitrogen content created a lower stacking fault energy in the material and helped to promote larger amounts of mechanical twinning [25].

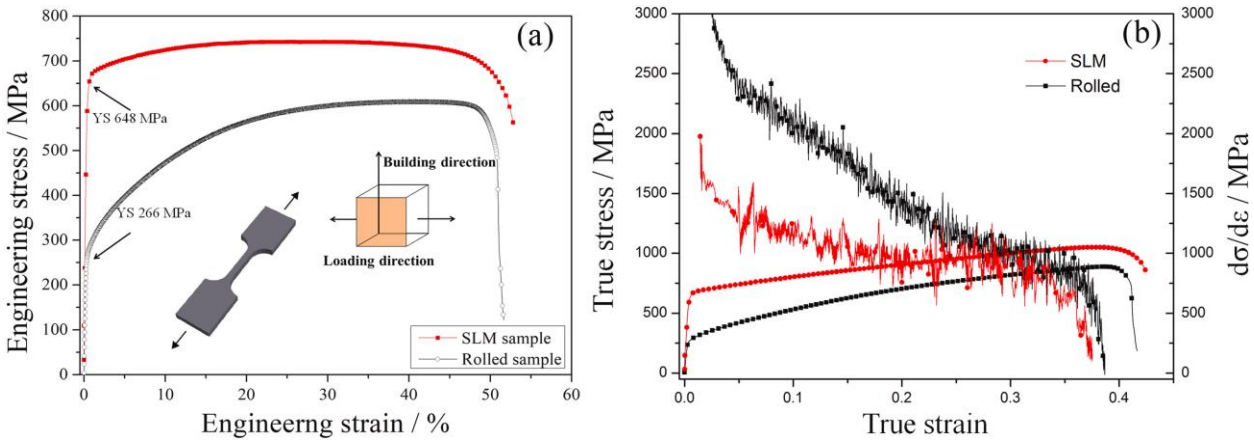

Figure 1-17: Twin tensile test results with an additively manufacturing sample performing better than a rolled sample [28].

The twinning phenomenon is important because it provides advantages when trying to improve material strength compared to other methods like reducing grain size. The most interesting aspect of twinning is that it allows for an increase in yield and ultimate tensile strength while also increasing the elongation before fracture. This contradicts other methods of strengthening materials where there is a tradeoff of improving the strength of the material at the cost of reducing the ductility. This unique aspect adds to the appeal of the twin phenomenon along with the benefits of thermal stability and high electrical conductivity [22] [23].

Twin boundaries have been shown to restrict dislocation motion and proliferation even though they are considered low angle boundaries in the crystal. This means that the addition of twins in the material will effectively reduce the average grain size seen in the material. The addition of twins inside of a grain effectively adds more restrictions on movement of dislocations and therefore can be equated to a microstructure of smaller grain size with no twins. Modified Hall-Petch equations have been made for both deformation twins and annealing twins. These equations follow the same relationship between size and strength but utilize the idea of effective grain size by implementing the variable of twinning density. Pande et al. created a modified Hall-Petch equation for annealing twins. This modified equation uses the twin spacing parameter to include the effects of twinning into the Hall-Petch equation [29]. Their modified equation was able to align well with data after implementing a correction factor that accounted for the fact that twin boundaries are not as effective as grain boundaries at inhibiting dislocation motion.

The increase in ductility of materials with twins is not as easily understood compared to the strengthening caused by twins, although, the increase in ductility is just as prevalent in the literature. Steinmetz et al. modeled twinning induced plasticity and described the increase in ductility as being from the dynamic increase of the twin-related interface density and its interaction with dislocations [30]. Their findings can be summarized as the changing rate of twin formation and growth during deformation is what allows for the large formability in the material.

The thermal stability of annealing twins was demonstrated by Chuang et al. where they showed how a microstructure with annealing twins was able to resist grain growth during an aging process [22]. Their experiments showed that twin boundaries had a “braking” effect on grain boundary migration that typically happens when a material is left at elevated temperatures for extended periods of time. This is another result of how a twin boundary reduces atomic mobility and diffusion within the crystal. They additionally demonstrated the improvements in mechanical properties that annealing twins had on the material. They concluded that the strengthening effect was related to the twins blocking dislocation motion.

The high conductivity of materials with twins comes from the fact that twin boundaries are low angle boundaries. These boundaries create less electron scatter compared to high angle grain boundaries. Less scatter leads to larger conductivity in the material. This property is important since applications that require good conductivity often need high strengths in the material. Lu et al. performed an experiment on a copper thin film that showed how promoting twin density is beneficial to retaining conductivity while improving strength and ductility in a pure copper sample [23]. Most methods of strengthening materials will result in a significant loss in conductivity since these methods ultimately increase the number of grain boundaries. Lu's work is more proof of the advantages of twinning over other microstructural methods used to improve properties of materials.

Using Electrical Current to Enhance Atomic Mobility

In order to anneal a material, there needs to be some driving force that allows for mobility in the material that changes the microstructure from a high energy state to a lower equilibrium state. Traditional heat treatments raise the temperature in the material to a point that allows for atomic bonds to break and therefore accelerate the diffusion process. A more advanced way to achieve the motion would be to add another driving force that would accelerate the process of achieving equilibrium. This addition of another driving force would fall under the strain induced grain growth and could be achieved by applying an electrical current to the material.

Applying an electrical current to a metal enhances diffusion inside the material by having the momentum of moving electrons transferred to the defects during collisions. The momentum transfer to metal ions increases the atomic mobility in the alloy. This momentum transfer will also increase defect mobility. This type of driving force has been given the name of electron wind force. The electron wind force has a critical point where there is enough current density to induce large grain growths and large amounts of defect annihilation in a short period of time. An example of the benefits that electricity can

provide is found in a study by Conrad et al. on the superplasticity of an aluminum alloy [31]. In this study, the electrical current was found to assist in the superplastic deformation due to its ability to enhance atomic mobility that affect the three main mechanisms involved during superplastic deformation.

The electron wind force is an efficient process to affect a materials microstructure since it can directly affect the grain boundaries of a material enhancing grain boundary migration. The focus on grain boundaries stems from the electrons deflecting to a greater degree when flowing from one grain to another due to the differences in crystal orientation. This larger deflection translates to larger momentum transfers. Comparatively, a Joule heating process will heat the entire crystal lattice which will require more energy and possibly more time in order to achieve the same amount of grain boundary migration [32]. The Figure 1-18 demonstrates how much energy is wasted by a Joule heating process by applying energy to irrelevant areas.

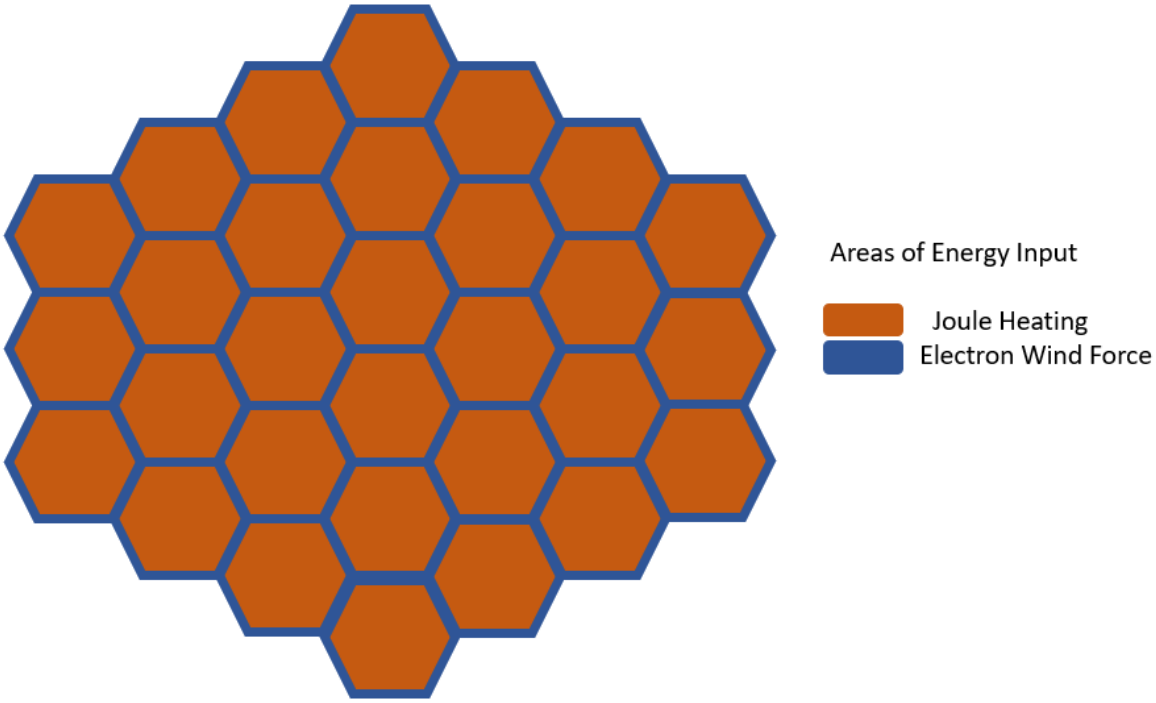

Figure 1-18: A comparison of the areas covered by Joule heating and electron wind force.

Applying an electrical current to a metal can also result in electromigration. Electromigration has mechanics similar to the electron wind force but happens at an order of magnitude higher current density. At lower current densities, the momentum transfer of electrons will promote diffusion, grain boundary migrations, and other microstructural changes. At higher current densities, the momentum transfer will result in mass transport in the material that leads to material damage or failure. The damage caused by electromigration has been extensively researched in electronics and material science [33][34][35][36].

Electrical Annealing

The use of electricity to induce changes in microstructures in metallic alloys has been observed in a few different fields of research. There is little or no research utilizing this method of microstructural change in the additive manufacturing field. This is surprising since this method of affecting microstructures has the advantage of being time and energy efficient compared to traditional thermal treatments [32][37]. For example, a traditional thermal annealing process will require a temperature that is around half of the material's melting temperature for a period of multiple hours. Comparatively, electrical annealing has been done at temperatures well below half the melting temperature for a period of minutes. The combination of additive manufacturing and this new method of microstructural control could cause waves of changes in the manufacturing industry and illustrates why the choice of using an additively manufactured material was made.

Microstructural changes caused by an electrical current have been achieved on smaller scales such as in thin films to enhance the creation of new phases and grow grain sizes [38][39]. Microstructural changes caused by an electrical current have also been achieved on a larger scale using constant and pulsed currents. Constant current has been shown to cause microstructural changes in materials from a couple of recent studies [32][40]. Pulsed current has been much more extensively researched under the term electropulsing [41][42][43][44]. The field of powder metallurgy has also explored the use of

electrical current to enhance sintering processes under the term spark plasma sintering [45][46][47]. In these spark plasma sintering studies, electrical current improved diffusion rates and lowered sintering times significantly. The electron wind force has been found to be one of the primary mechanisms in spark plasma sintering but is coupled with many other mechanisms due to the complex relationship between pressure, temperature, time, and current. Spark plasma sintering differs slightly from electrical annealing since spark plasma sintering has a goal of electromigration which would be detrimental in an electrical annealing process. These various fields of Study have all revealed high density electric current's ability to improve material properties in ways such as altering grain size, promotion of twin growth, promoting certain phases, or enhancing mobility.

The cause of these microstructure changes has been debated to be the result of the electron wind force, Joule heating, or the combination of the two effects. Joule heating or resistive heating is a natural effect of allowing current to pass through a material. Several papers have suggested that Joule heating plays a role in the dislocation motion and microstructural changes [48][49][50]. The degree of which Joule heating effects the microstructural changes has been debated primarily since the effects from Joule heating and the effects of the electron wind force are hard to decouple from each other. The Joule heating explanation for microstructural changes stems from the fact that the heat that is generated could act as a traditional thermal process. Arguments have also been made that the heat focuses at the grain boundaries which causes the changes in microstructure [48]. This explanation loses credibility when the microstructural changes occur in samples that were processed at temperatures far below the annealing temperature for a substantially shorter time than what would be used in a thermal annealing process. Meanwhile, the electron wind force has been suggested to be a definite cause in the microstructural changes by several studies [32][43][51][52].

Material Characterization

After any process that has claimed to alter a material's microstructure and therefore the material's mechanical properties, determination of the effectiveness of the annealing processes needs to be established. The best way to do this would be to prove that the properties of the material have changed. There are several ways to demonstrate changes of material properties such as surface observations and characterization through microscopy (optical, scanning electron, transmission electron), mechanical testing, or analysis such as x-ray diffraction.

X-ray diffraction gathers information on the material's crystal structure along with other information such as the chemistry and phases of the material. Using a Williamson-Hall analysis on an x-ray diffraction scan will allow for estimations of average crystallite size and average strain the crystal lattice. The Williamson-Hall analysis method differs from other methods by including the ability to estimate the size and strain in the crystals at the same time. A properly annealed metal would show an increase in size and a decrease in strain from the analysis [28]. Visual inspections of the 2-theta plots can also be informative since a properly annealed metal would show peak sharpening from the increased crystallite size [53]. For XRD analysis of Additive Manufactured parts, there could also be a noticeable change in peak locations due to changes of residual stress in the material after being annealed. The changes in peak location in additive metals could also be from the annealing processes changing the columnar texture of the as built part to a normalized equiaxed structure.

Electron backscattered diffraction is a very important tool that can verify annealing treatments done on a material. EBSD is done inside of a scanning electron microscope system and gathers data about grain orientation. Other data such as phase composition throughout a scanned area can also be obtained. Since grain boundaries mark a change of orientation inside of a polycrystalline material, the crystal orientation data that is gathered outlines the grain boundaries in the material. With this information grains can be identified, and the microstructure can be characterized. This analysis method is vital in confirming microstructural differences after a heat treatment. Even if partial changes take place, such as the recovery

stage in a thermal treatment, EBSD can identify the differences in the microstructure. The EBSD data can also be manipulated to extract more information from it, such as misorientation angle distributions. Materials created from additive manufacturing have nonequilibrium microstructures. These structures have large fractions of low angle grain boundaries that is evidence that the material has high levels of stored strain energy [54]. Once annealed, the stored strain energy is released, and the material will recrystallize into a more equilibrium condition with a large fraction of high angle grain boundaries [32]. With the data obtained from an EBSD scan of a material, plots can be made showing the percent fraction of grain boundaries at each of the angles seen in the material. Information from this plot can be used to access the degree of which the annealing process was effective. If the material went from a large fraction of low angles to a large fraction of high angles, it can be inferred that the material has undergone a successful annealing process.

Mechanical testing is crucial in confirming that the annealing process was successful. This testing is important since it can confirm that the properties of the material have changed throughout the material and not just in localized areas. The methods already discussed will only detect changes that are close to the surface of the material. The methods discussed above can give a better picture of what is going on, but without methods of mechanical testing, there is no practical way to ensure that the changes observed are consistent throughout the entire material. One of the most common forms of mechanical testing is the tensile test. This test can establish property relationships such as strength and ductility throughout the entire testing area. A successful annealing treatment would consist of a decrease in the yield strength and, more importantly, an increase in ductility shown as the increase in elongation at fracture [18]. Tensile tests of additive materials are dominated by large scale samples in the shape of dog bones. A lot of the literature related to the tensile testing in additive manufacturing provides the dog bone samples printed separately from a part and do not cut a dog bone from a larger part. It is possible to perform micro-tensile, and nano-tensile tests but these methods drastically increase the cost, time, and difficulty to perform the analysis.

Another method of mechanical testing is an indentation test [55]. An indentation on an annealed metal would show a softer hardness value. The lower hardness is evidence of an increase in ductility. This method benefits from being a nondestructive evaluation method for measuring mechanical properties of the metal. Thus, allowing for the same sample to be tested before annealing and after annealing. It also allows for the sample to be analyzed using methods such as electron backscatter diffraction. The indentation results are highly dependent on the tip geometry that is indenting on the sample. The geometry of the tip will determine which type of indentation test is being performed and will have its own standard hardness scale. Hardness values on these scales are not easily converted into one of the different scales. Typical tests will result in either a Rockwell hardness value or a Brinell hardness value. Indentation can also be scaled down to microscopic and nanoscopic levels with low amounts of sample preparation and cost. Nano-Indentation machines are more advanced and will typically allow for position data to be tracked which will allow for the creation of force-displacement graphs. These graphs will allow for visual confirmation of the accuracy and precision of the tests.

Chapter 2

Experimental Approach

Sample and Stage Preparation

An additively manufactured 316 stainless steel cube was cut into slices of approximately 1mm thick. These slices were cut parallel to the build direction to reveal the columnar shaped grains. The cube was manufactured using a powder bed fusion process. The powder feedstock used to create the cube was made from a nitrogen gas atomization process. Each slice was grinded down to 150 µm using grit paper. Then the strips were cut into long rectangular shapes of approximately 10 mm long, 0.5 mm wide and 150 µm thick using a dicer machine. From here each strip was individually polished down to approximately 40 or 50 µm using various grit paper with the final stage being a grit paper of 1200. The samples were then polished using microfiber pads and diamond, colloidal alumina, and colloidal silica suspensions with particle sizes ranging from 3 µm down to 0.02 µm.

The sample was mounted to an alumina nitride slab that acts as a heat sink. Copper tape was attached to the alumina nitride slab to act as electrical contacts on both sides of the sample. The sample was mounted on top of the electrical contacts to make it a free-standing object. Wires were also attached to the copper tape and Solder was used on top of the contact pads to enhance the electrical connections. This stage setup can be seen in Figure 2-1 and Figure 2-2.

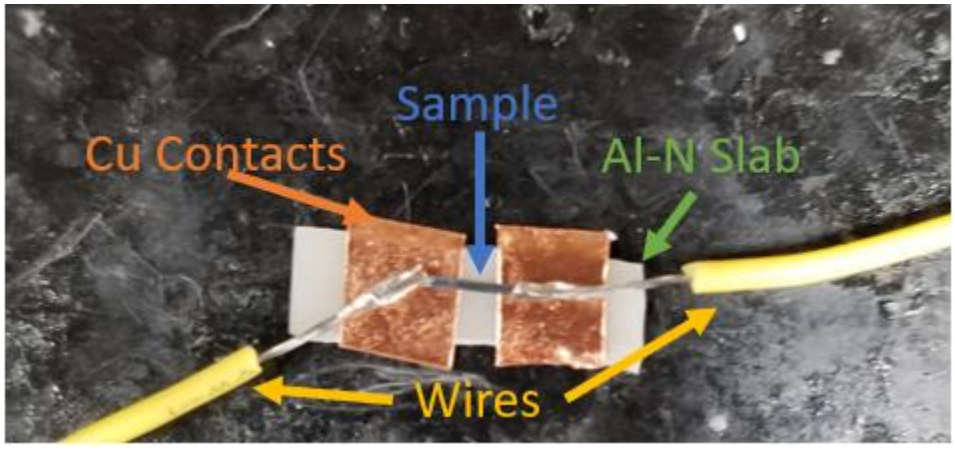

Figure 2-1: Sample and stage setup picture.

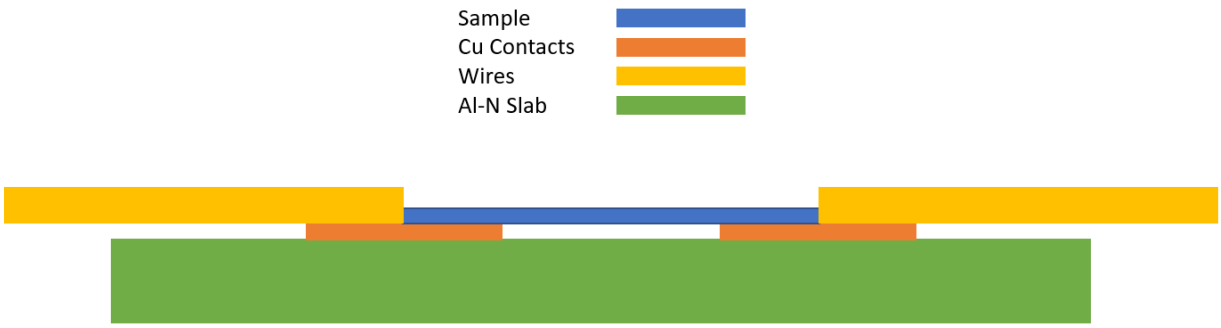

Figure 2-2: Sample and stage diagram

Experimental Setup

The sample and stage were mounted on a liquid nitrogen temperature-controlled stage inside of a SEM. The Liquid nitrogen cooled stage allowed for the extraction of heat from the stage to avoid the effects of Joule heating and possible surface contamination in the form of oxidation. Any oxidation of the surface would make it hard to see when the grain growth effects are taking place. The high vacuum conditions inside the SEM greatly increased the chances of achieving grain growth without failure from electromigration. The wires were connected through a pass through in the chamber and connected to a power supply capable of up to 3 Amps of biasing. The 3 A limitation dictated the sample dimensions in order to anneal the samples. This 3 A limit also prevented the electrical wires from failing and losing

connection. The high-resolution camera inside the SEM also allowed for the in-situ monitoring of the sample surface during the experiment. Images of the surface were obtained before, during, and after each experiment. During the experiment, the current was increased in small increments and held at each current level for a period ranging from about 30 seconds to a few minutes. The current level was increased faster when at the lower current densities that were found to be well below the activation densities. Once the current was providing densities that were close to what was expected to activate grain growth, the current levels were held for longer amounts of time as seen Figure 2-3. This longer time allowed for a more thorough surface observation and allowed for any surface changes to develop. Once the surface changes were observed, the current level was reduced slightly to avoid any failures in the sample. The slightly lowered current also allowed for the surface changes to continue to take place but at a much slower rate that can be more easily observed. If any sign of electromigration was taking place the current level was reduced more drastically to try to avoid sample failure.

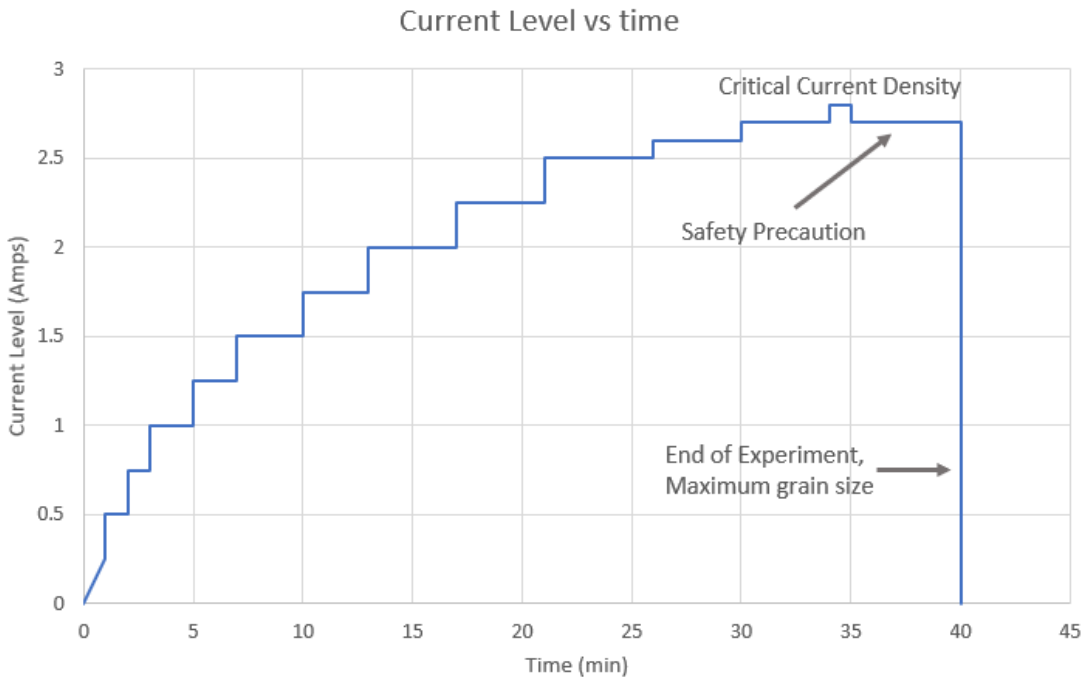

Figure 2-3: Current vs time during a typical annealing experiment.

Electromigration is the primary failure method that can occur when trying to induce microstructural changes using electrical current. While there is a difference in the current densities between the electron wind force and electromigration for a specific material, failure in these experiments can still occur due to pushing the current density limits to induce larger microstructural changes. Problems such as surface oxidation, effectively blinding the user from the surface changes that are taking place, can also lead to electromigration failure. Electromigration failure can also take place if the samples have variation in cross-sectional area that would lead to electromigration in the smallest section of the samples and grain growth in the larger sections of the sample.

Analysis

After the processing of a sample was complete, the sample was removed from the stage and prepared for X-ray diffraction analysis. Any residual solder was removed from the sample. The samples were placed in a PANalytical X'pert Pro MPD machine and scanned from a two-theta angle of approximately 40° to 100°. With the Intensity vs two-theta plots obtained from x-ray diffraction, Williamson-Hall analysis was performed to obtain size and strain estimations for the crystal. The annealed samples were then ion milled and placed in an EBSD capable SEM. Grain size analysis was performed on the as received and annealed materials. Grain boundary orientation analysis was performed as well in order to get an idea of the residual stresses in the material. After the microstructure was analyzed the samples were placed in a nano-indenter to measure the hardness and reduced elastic modulus of the samples.

For accurate micro-hardness measurements, the sample needs to be thick enough for the hardness value not to be influenced by the substrate on which the sample is mounted. The micro-hardness machines available at Penn State require a minimum thickness of approximately 60 μm. The minimum

thickness stems from the minimum indentation depth required to create an indent of a diameter that is large enough for the machine to identify the edge of the indent. A rough approximation of the minimum depth is found by multiplying the minimum diameter of the indent by a factor of one and a half, which is determined by the geometry of the indentation tip.

This 60 μm thickness requirement conflicts with the sample thicknesses created in this experiment. Enlarging the sample dimensions cannot be considered in this experiment due to the need of larger current densities to obtain the grain growth in the sample. The current density required to grow the grains in a 60 μm thick sample would cause failure in the electrical connections on the sample stage and in the electrical wires inside the SEM used to connect the stage to the power supply.

The only option for hardness measurements for these samples is using a nano-indentation machine. Nano-indentation requires more rigorous sample preparation to ensure accurate results. Nano-indentation requires a strict tolerance on the roughness of the surface of the sample. This tolerance is based off the relationship between the size of the peaks and valleys of the roughness and the depth of the indentation test. Since the indentation depths are nanoscale, the surface roughness will also need to be nano scale. This was obtained by the polishing and sample preparation explained above. Another requirement for accurate nano-indentation results is the tolerance of parallelism of the sample surface to the substrate. To ensure there is an acceptable amount of drift in the sample tip, which would affect the hardness and reduced elastic modulus measured, the sample surface needs to be as parallel to the substrate as possible. If the sample is not parallel, the indenter tip will drift along the surface of the sample and affect the results. Profilometry scans of a sample created using the above sample preparation showed that the sample had acceptable surface roughness and parallelism.

Chapter 3

Results

The following chapter will review the results from the experiments that were performed. First information will be given on the temperatures that can be seen in this type of electrical annealing process. Next, information will be given on experiments that were performed without any cooling and were confirmed to have microstructural changes. Finally, information on the microstructural changes of the cooled experiments will be given. A list of samples can be seen in Table 3-1. Various processing parameters were used in the different experiments that resulted in a variety of microstructures.

Table 3-1: Design of Experiments.

Specimen	Cooling	Current Density (A/mm^2)	Total Processing Time (min)	Resulting microstructure	Average Grain Size (µm)	Percent Change in size	Average Misorientation Angle	Percent Change in Average Misorientation angle
As-Received Material	-	-	-	Columnar Grains	43 (wide)	-	10°	-
1. Intermediate Sample	No	100	12	Columnar grains, Dislocation tangles	33 (wide)	-23%	5°	-50%
2. Annealed Sample with No Cooling	No	200	40	Large equiaxed grains, Twins, Electromigration damage	75	+74%	60°	500%
3. Sample with Localized Grain Growth	Yes	200	35	Large equiaxed grains, Small equiaxed grains, Twins, Columnar grains	11	-74%	55°	450%
4. Fully Annealed Sample	Yes	200	40	Large equiaxed grains, Twins	45	+5%	60°	500%
5. Sample Annealed under a Short Period of Time	Yes	200	30	Small equiaxed grains, Columnar grains	15	-65%	Mixture of 5° and 50°	400%

Temperature Measurements

The first experiment was performed with no cooling stage under a microscope with infrared temperature reading capabilities in order to better understand the temperatures that the sample can see

during an experiment. This sample was not cooled and represents the worst-case scenario. From Figure 3-1, the average temperature that the sample will see when processing at a high current density is in the range of 200°C. This is interesting since this temperature is well below the temperature required for thermal annealing. This supports the evidence in literature that Joule heating plays less of a role in this type of annealing.

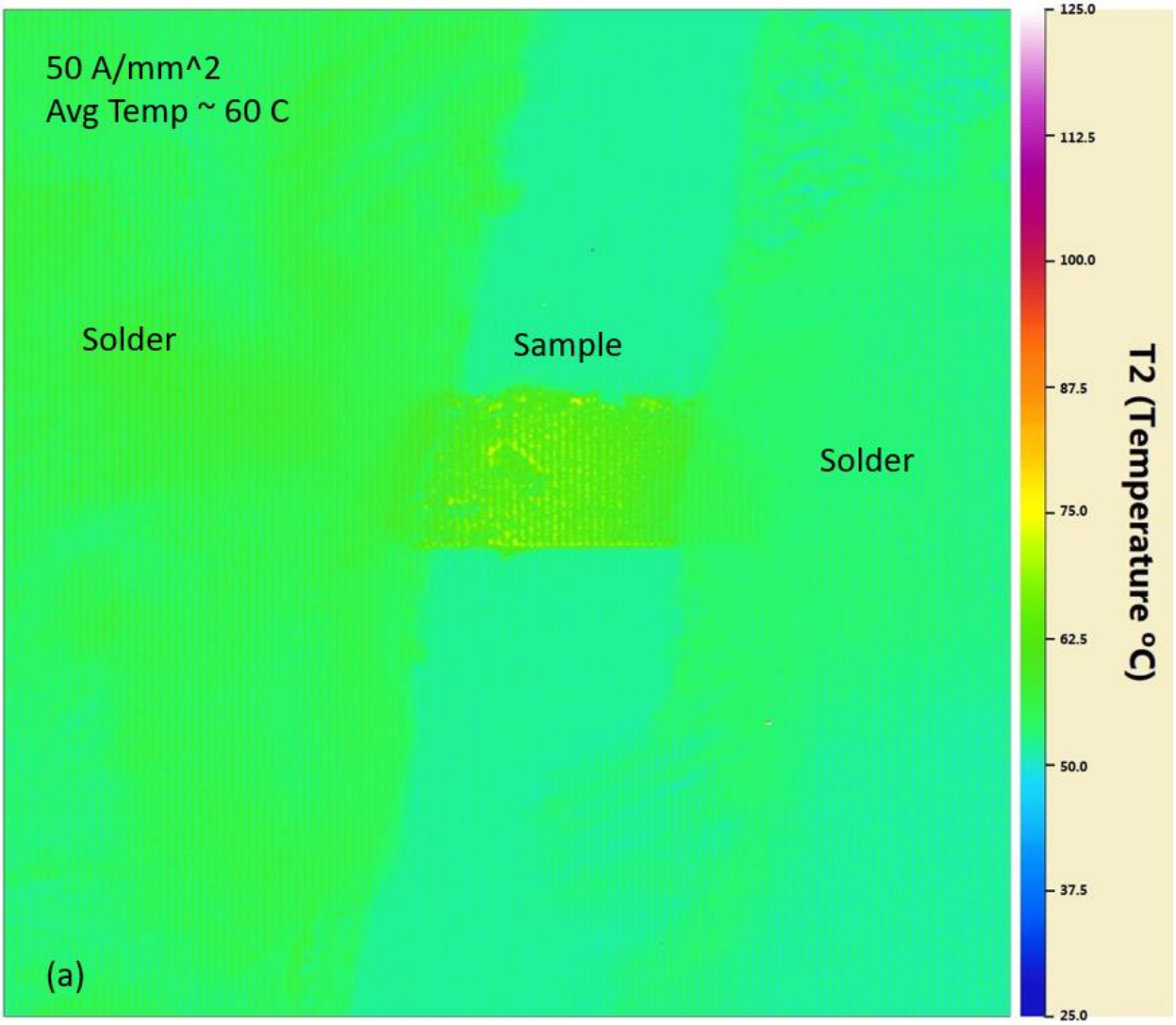
50 A/mm^2
Avg Temp ~ 60 C
Solder
Sample
Solder
(a)
125.0
112.5
100.0
87.5
75.0
62.5
50.0
37.5
25.0
T2 (Temperature °C)

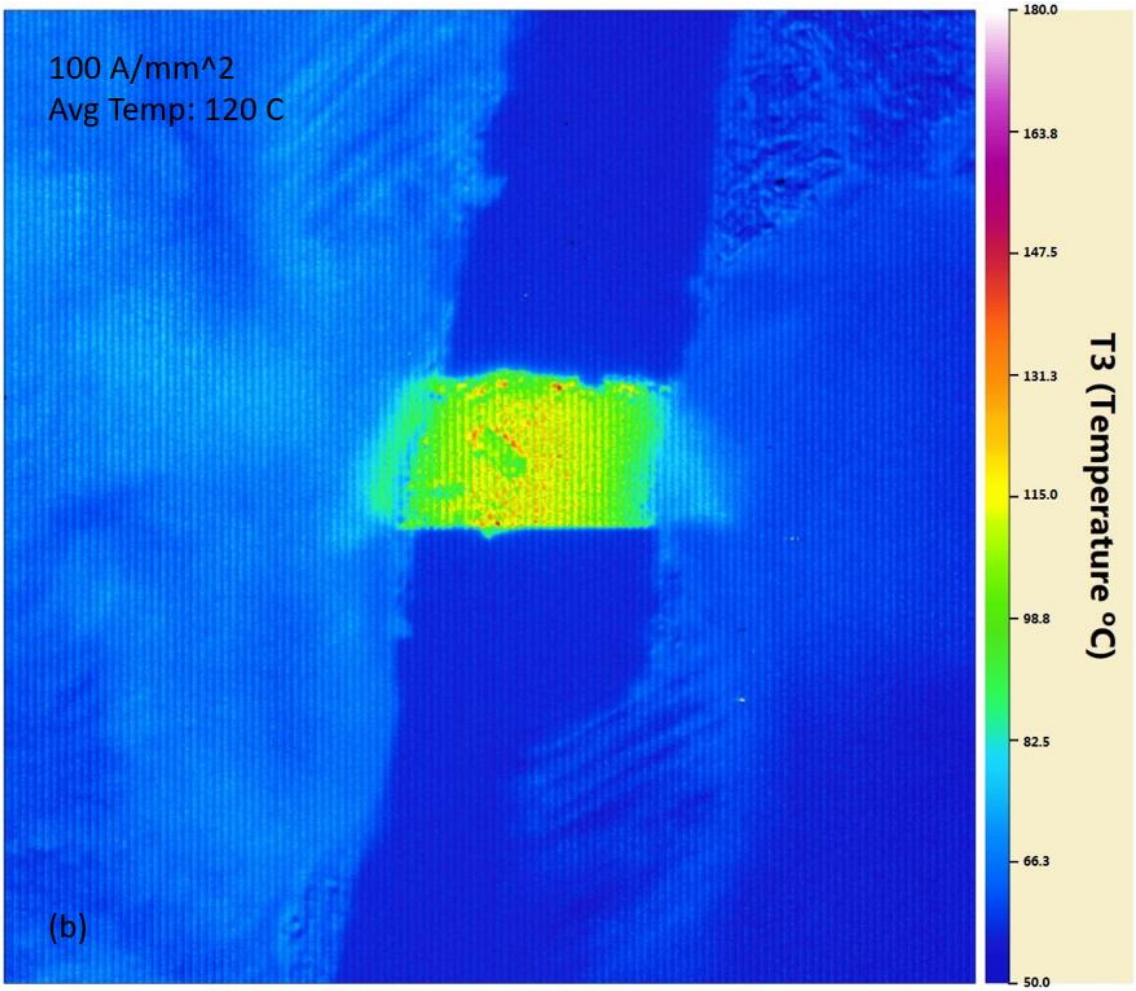
100 A/mm^2
Avg Temp: 120 C
(b)
180.0
163.8
147.5
131.3
115.0
98.8
82.5
66.3
50.0
T3 (Temperature °C)

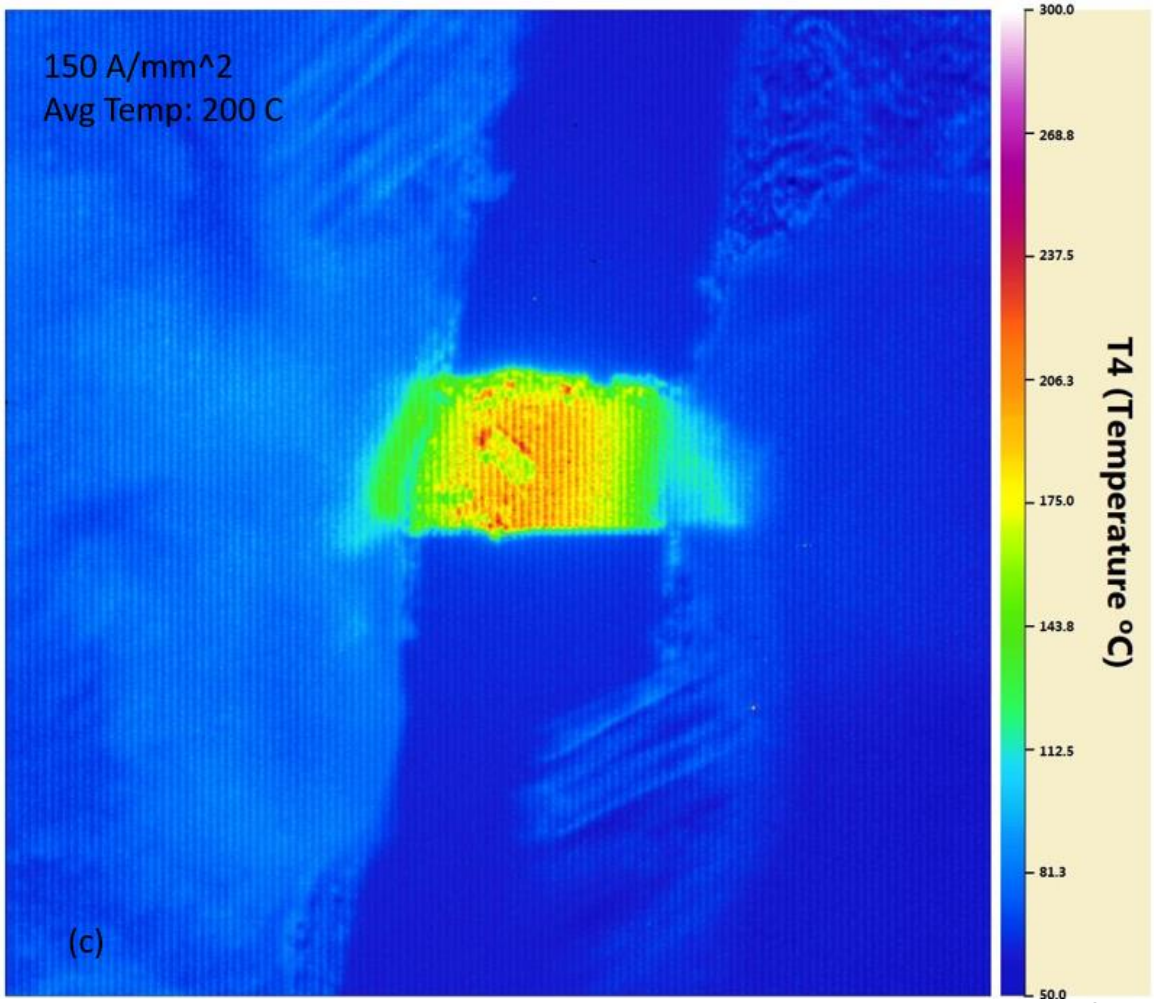

Figure 3-1: Thermal IR Temperature Measurements of a sample at (a) 50, (b) 100, and (c) 150 A/mm^2.

As-Received Sample

The as-received material was scanned under an EBSD capable SEM and the microstructure in the Figure 3-2 was identified. The texture of the grains appears to be elongated in one dimension. This should be expected from a metal that was made from an additive process due to the grains favoring growth in the build direction. After performing grain size analysis using ImageJ and the line intercept technique, the width of the columnar grains in the as received material was estimated to be around 40 µm. This grain size is typical of a 316L laser powder bed fusion process. From this EBSD scan, Figure 3-3 of the grain misorientation angle plot was made which shows a large fraction of the grains having a small misorientation angle. This means that there is a lot of residual stress in the material due to large contractions of the melt pool during solidification.

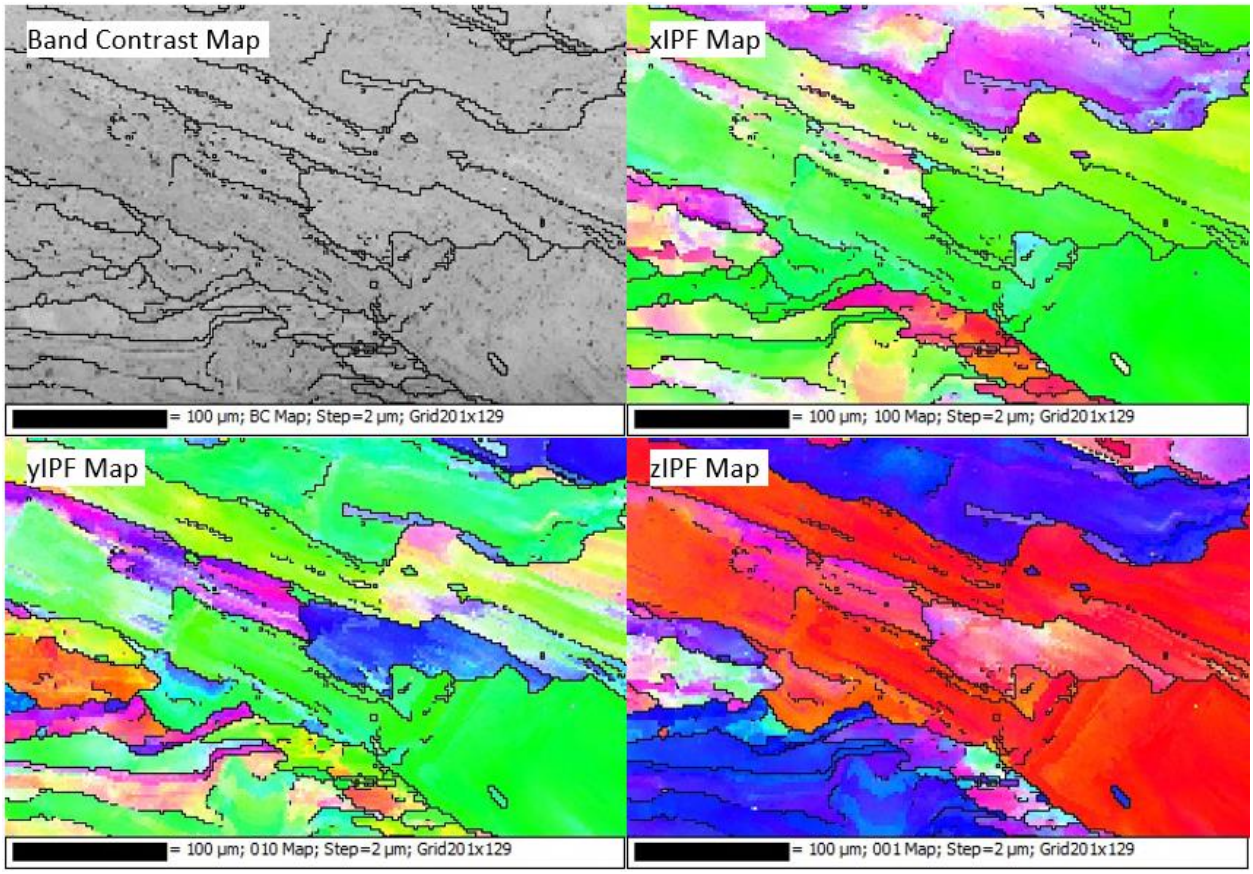

Figure **3-2**: EBSD shows the as-recevied columnar texture.

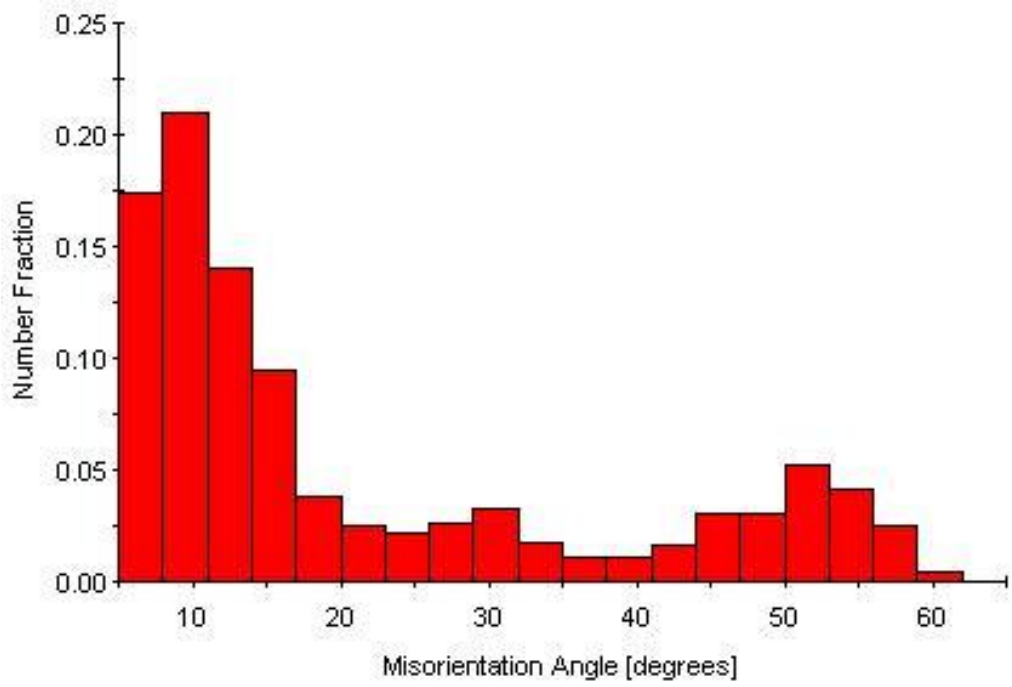

Figure 3-3: Misorientation angle plot for the as-received material.

Intermediate Annealed Sample

In order to identify the current density that will initiate grain growth in the additively manufactured 316 stainless steel sample, experiments were performed on samples that did not have any cooling effects. Performing these experiments on samples that were not cooled was a method of identifying the critical density earlier in the research than if we waited to design the experiments around a cooled stage. The first sample was only processed up to an intermediate current density of about 100 A/mm^2 due to heating effects in the electrical connections that caused the sample to lose the electrical connection. The sample appeared to have some changes on the surface as seen in Figure 3-4. The decision was made to perform an EBSD scan on this sample instead of re-soldering the sample and continue processing to a higher current density.

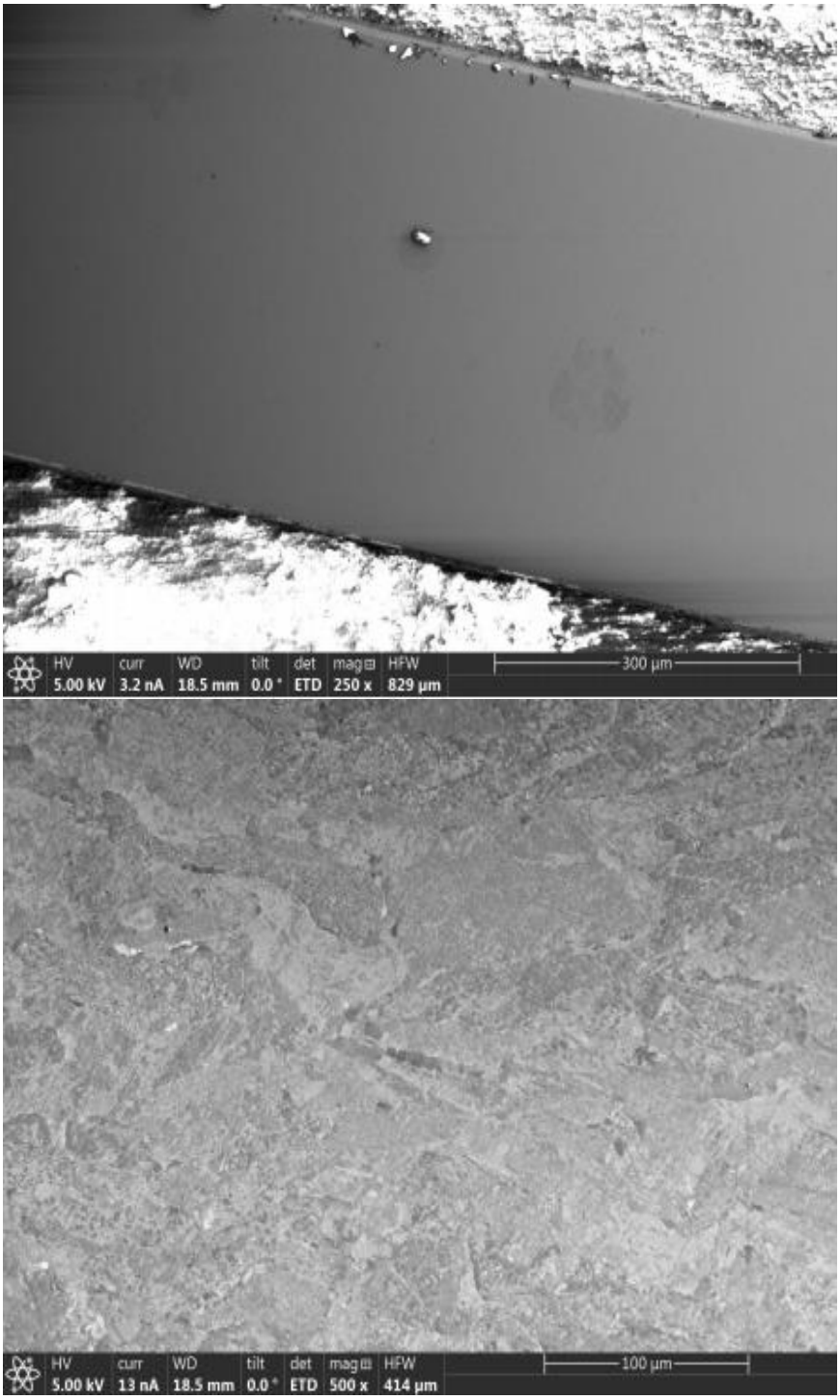

Figure 3-4: Before and after optical micrographs of the intermediate sample.

The EBSD scans, that can be seen in Figure 3-5, shows a mostly unchanged microstructure from the original elongated columnar grains. This is not surprising since, up to this point, the critical current

density was not known. In later experiments, the surface changes that signify grain growth would become obvious. Performing grain size analysis resulted in an estimation of grain width of about 33 μm.

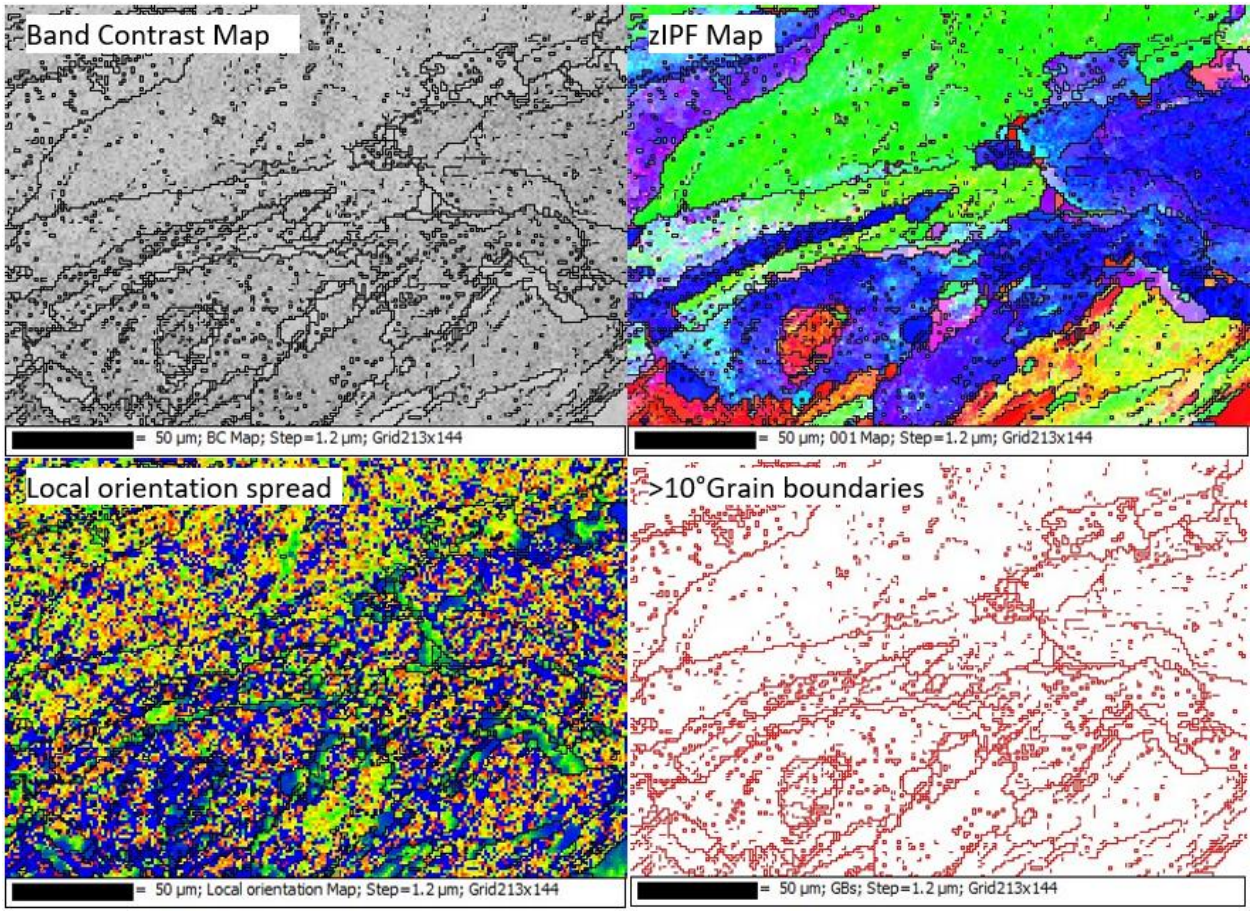

Figure 3-5: EBSD of the intermediate sample.

It can be seen in both the EBSD scans and the misorientation angle plots, shown in Figure 3-6, that there is a large fraction of small misorientation angles in the material. In fact, there seems to be a larger fraction of small angles in the intermediate sample than in the original as-received material. This could be explained by recovery in the material that allows for rearrangement of the dislocation substructures and dislocation tangles.

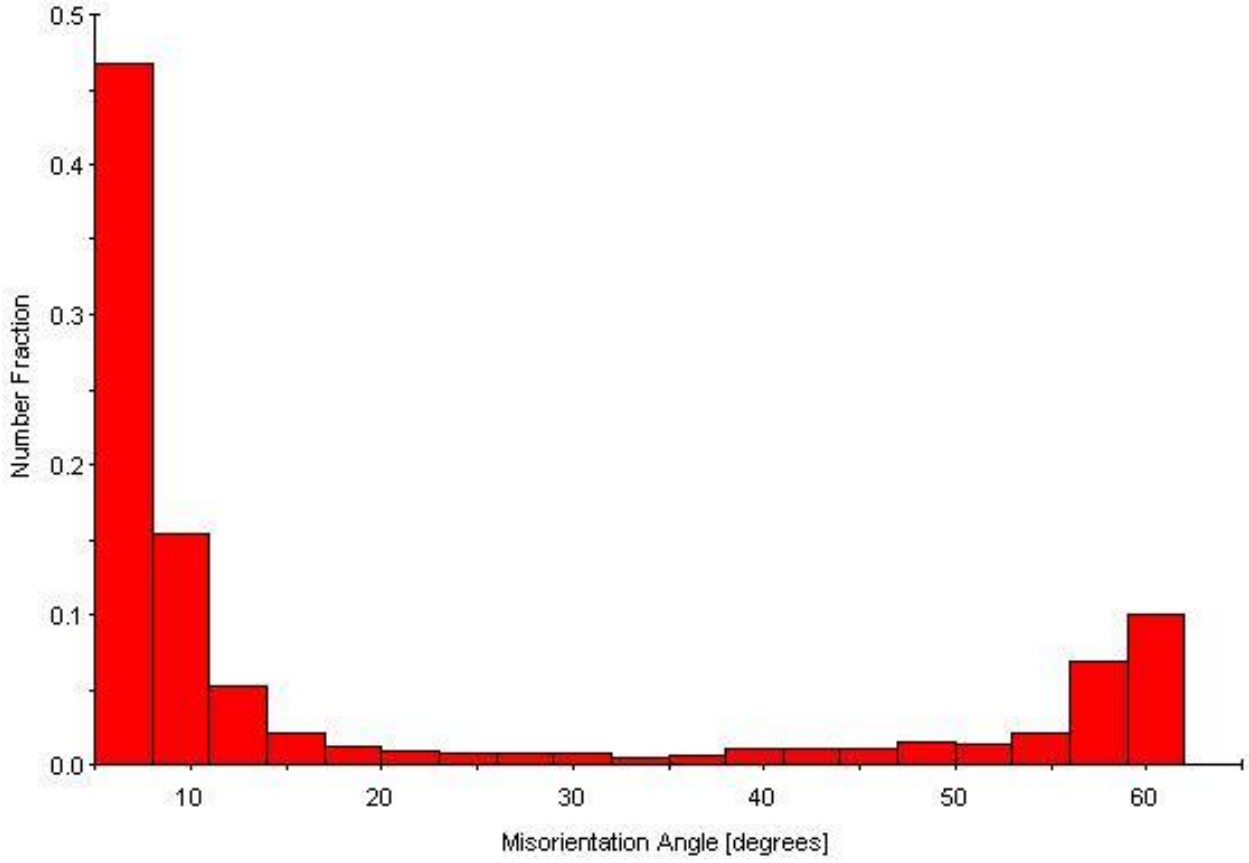

Figure 3-6**:** Misorientation angle plot for the intermediate sample.

Annealed Sample with No Cooling

The next sample was processed up to around 200 A/mm^2 and from the optical micrographs, as seen in Figure 3-7, there are some clear grains that are large and do not reflect the as-received columnar shape. The grains are identifiable due to the etching that occurs due to the grain boundary channeling that is an effect of the electron wind process.

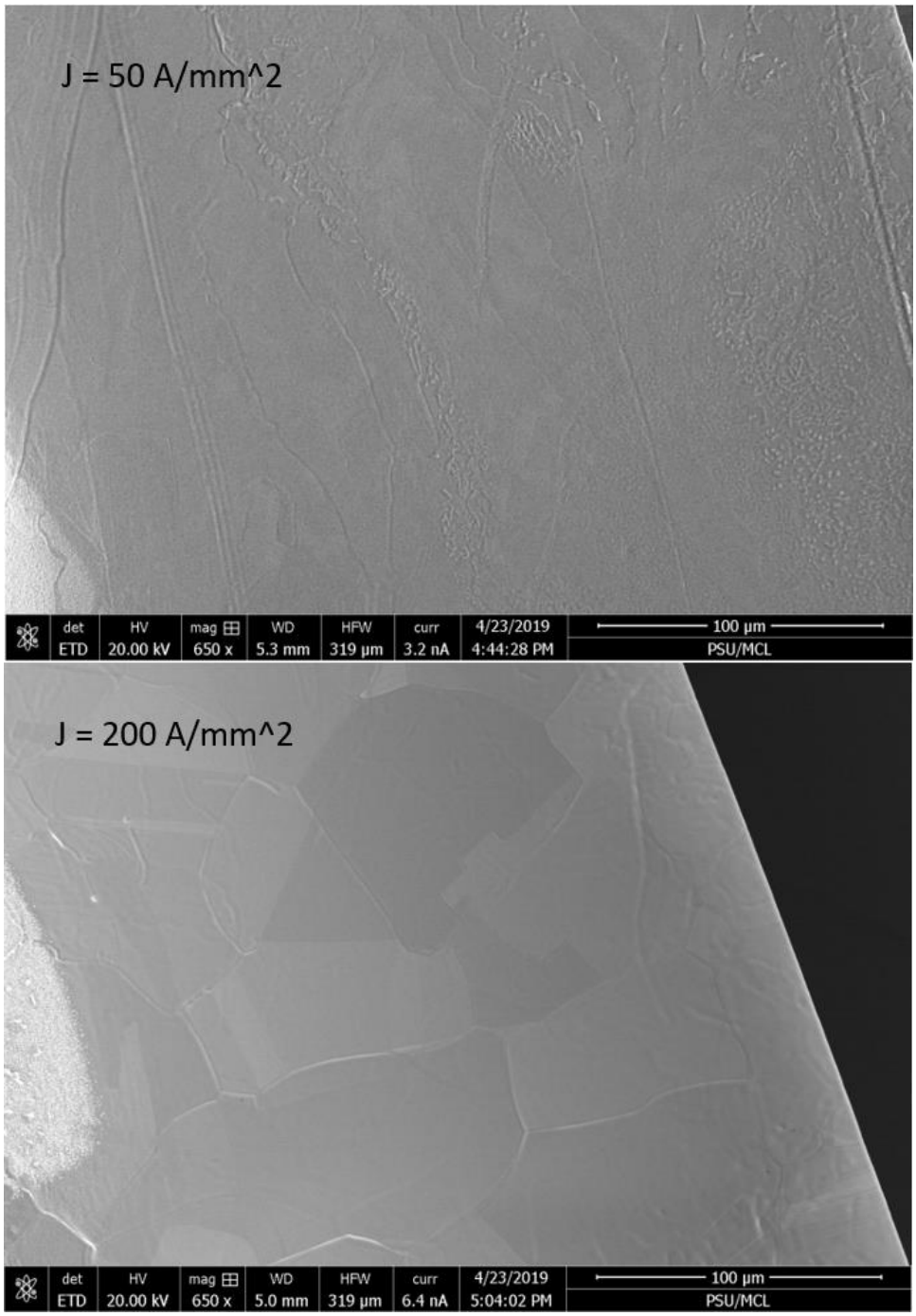

Figure 3-7: Optical micrographs of the annealed sample that was not coooled

It is worthy of noting that this sample was made before the sample preparation procedures were optimized to eliminate sample defects such as thickness variation across the sample. The sample variation came due to an unpredicted side effect of trying to make the sample thinner than the intermediate sample. This was done to eliminate the experimental failure of a lost electrical connection due to heating in the

solder. A thinner sample would allow for less current to achieve grain growth and therefore less heat produced from the Joule heating. This sample had a large thickness variation that can be seen in Figure 3-8, with the largest sample thickness measured being around 40 μm and the thinnest section being around 1 μm thick. It became obvious after processing that the thinnest areas underwent electromigration failure, as seen in Figure 3-9, where mass transport started to occur, and the largest areas did not undergo grain growth. The grain growth region occurred at a sample thickness somewhere in between the largest and thinnest sections. This complicated the estimation of the critical current density for this sample of 316 stainless steel. From this sample, the critical current density was estimated to be around 200 A/mm^2. This density would later be confirmed by samples that were processed with an even thickness across the sample.

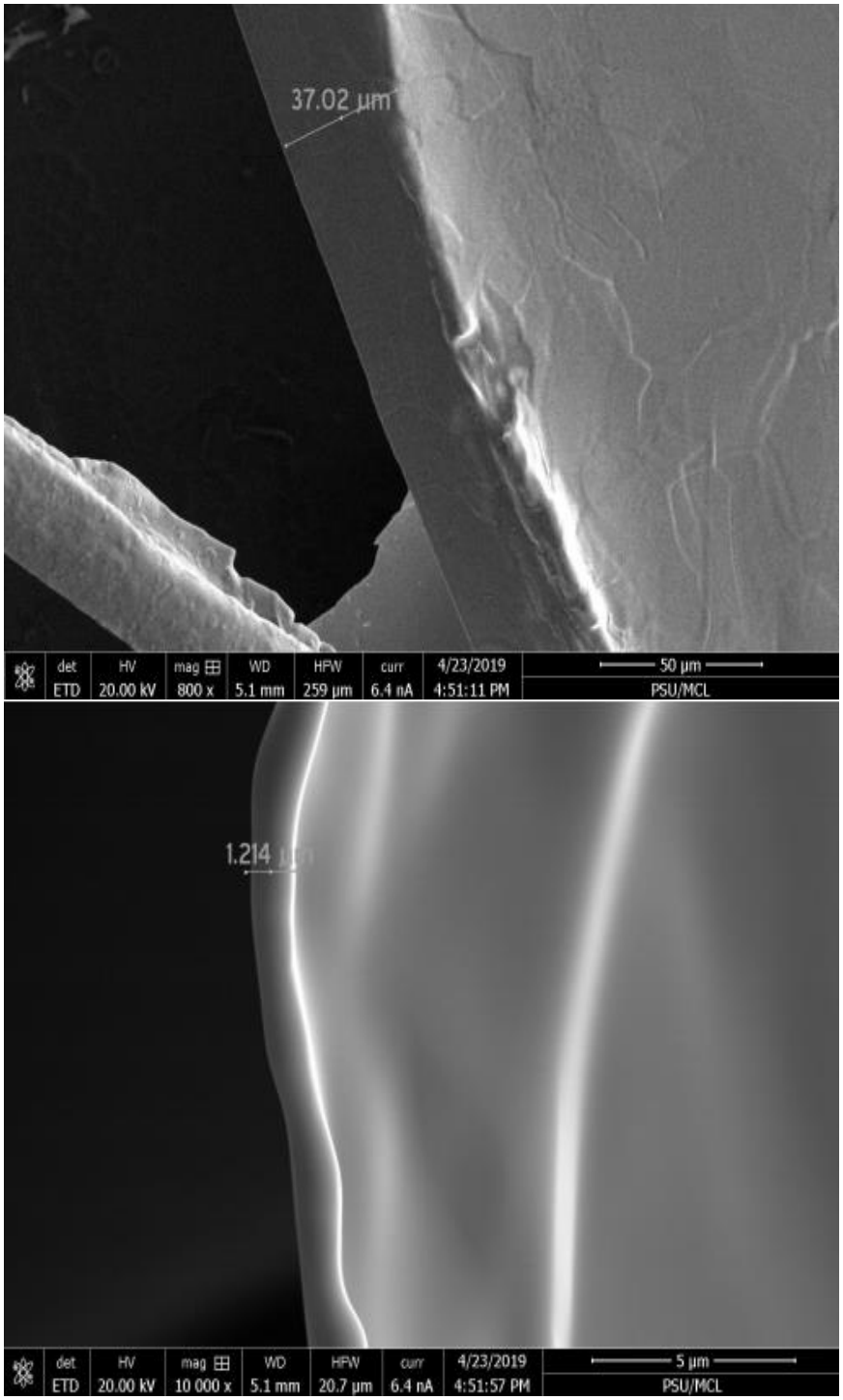

Figure 3-8: Optical micrographs that show the variation of thickness across the sample.

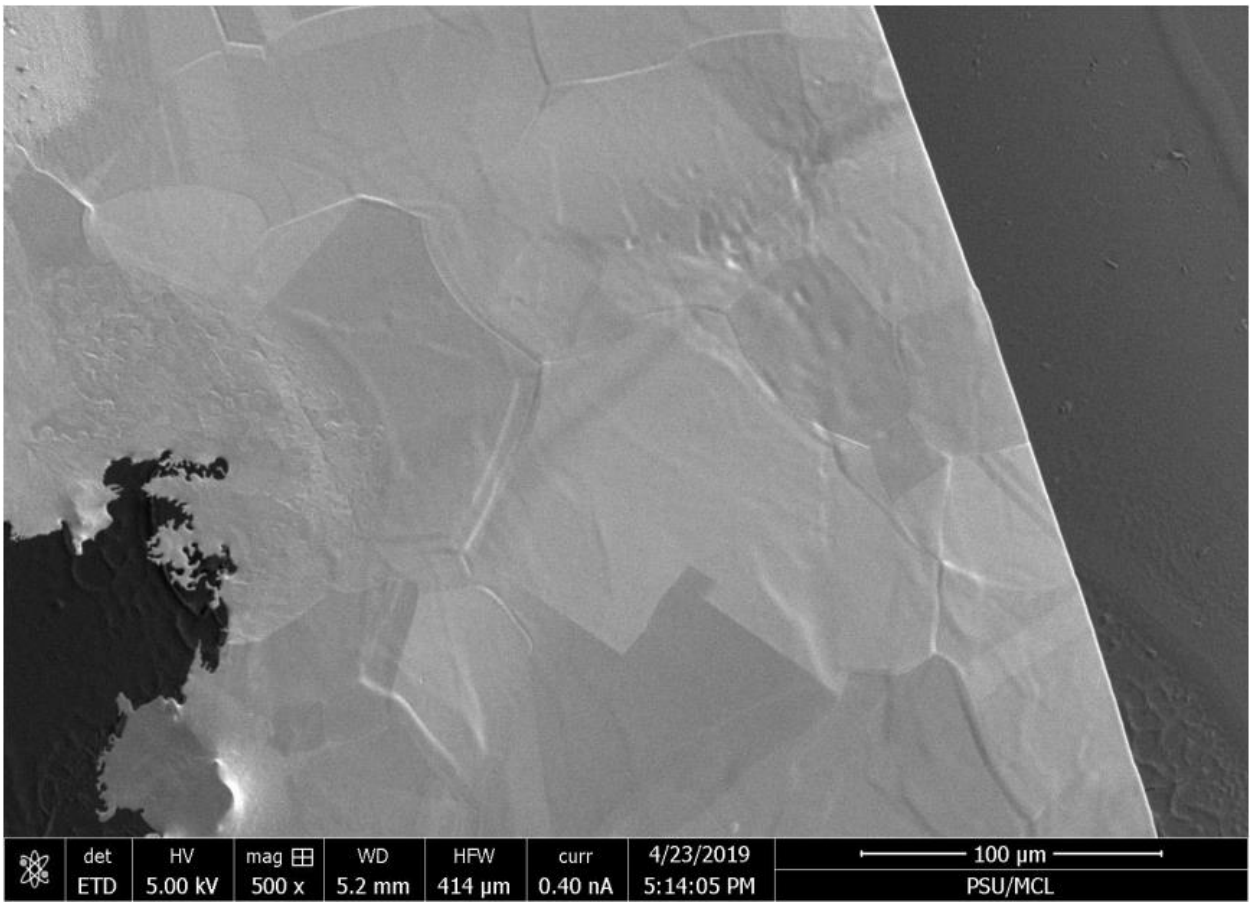

Figure 3-9: Areas that underwent electromigration and grain growth.

Multiple EBSD scans were taken on this sample across all ranges of thickness in the sample. Figure 3-10 shows locations (a) and (b) where grain growth occurred. The third location (c) shows a point where there was partial grain growth with the rest of the location maintaining the original microstructure. This is explained due to the thickness variation with the grain growth section having a thinner cross section then the rest of the scan location. The final location (d) shows that the cross section at this location was too large and did not experience any microstructural changes. It is also noteworthy of the large fraction of annealing twins that is present in the new microstructure of these locations. This shows that this electro-annealing process has a high strain rate applied to the grains during growth that creates the twinning phenomenon. Grain size analysis was performed on location (b) since it was the best image of an area of interest. The estimated average grain size from the intercept method using ImageJ came out to be around 75 µm.

(a)

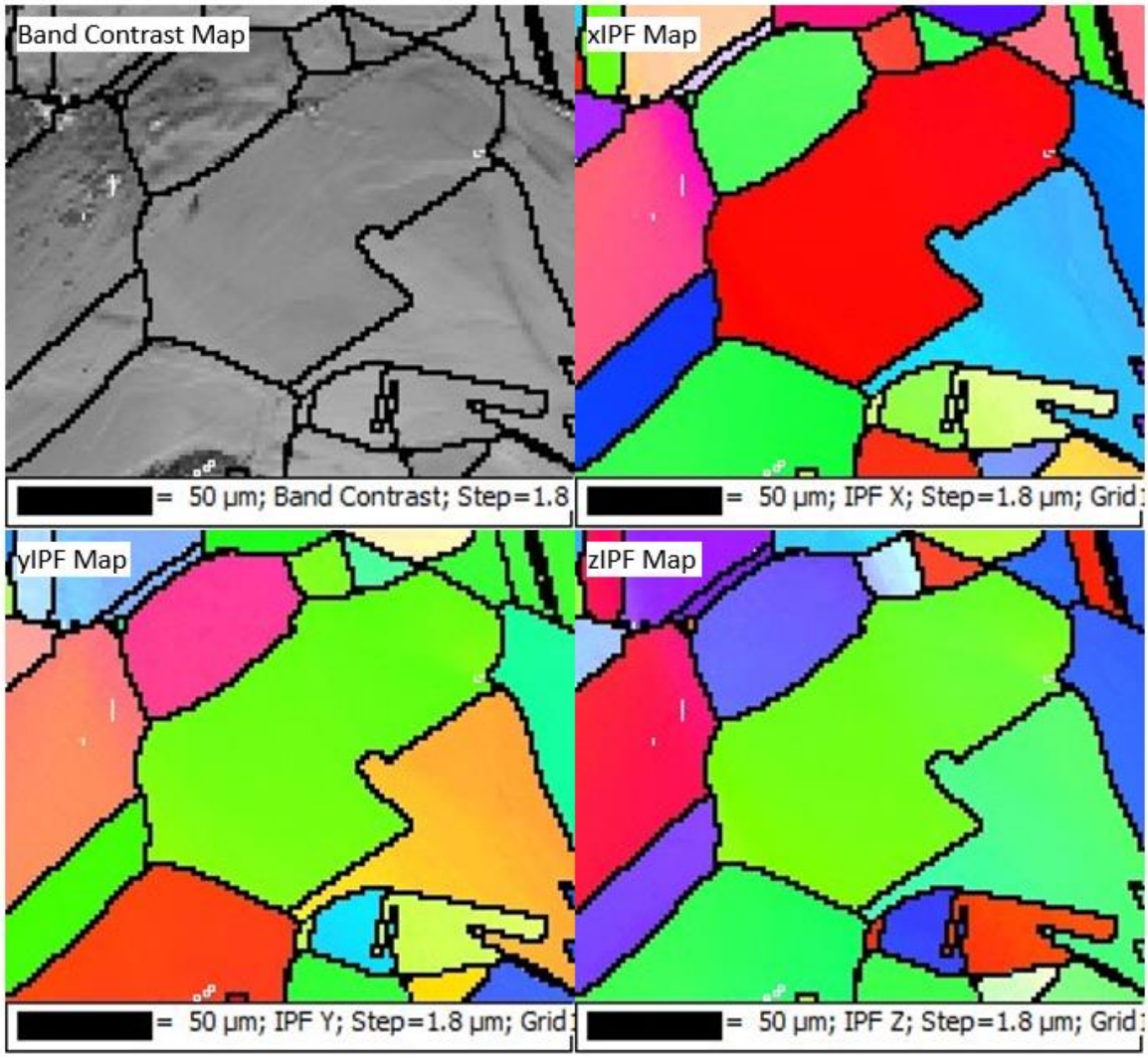
Band Contrast Map
xIPF Map
= 50 µm; Band Contrast; Step=1.8
= 50 µm; IPF X; Step=1.8 µm; Grid
yIPF Map
zIPF Map
= 50 µm; IPF Y; Step=1.8 µm; Grid
= 50 µm; IPF Z; Step=1.8 µm; Grid

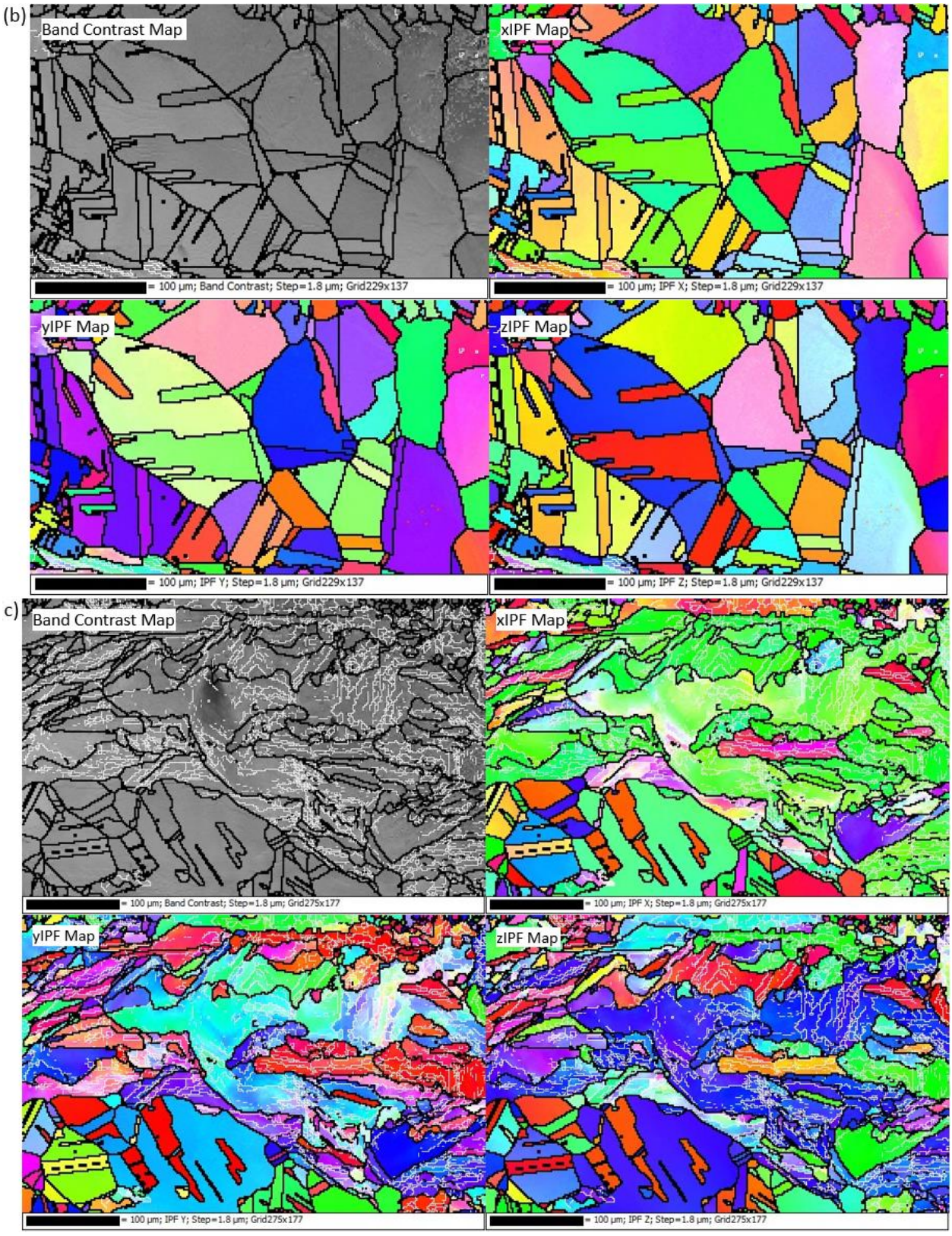
(b)
Band Contrast Map
xIPF Map
= 100 µm; Band Contrast; Step=1.8 µm; Grid229x137
= 100 µm; IPF X; Step=1.8 µm; Grid229x137
yIPF Map
zIPF Map
= 100 µm; IPF Y; Step=1.8 µm; Grid229x137
= 100 µm; IPF Z; Step=1.8 µm; Grid229x137
c)
Band Contrast Map
xIPF Map
= 100 µm; Band Contrast; Step=1.8 µm; Grid275x177
= 100 µm; IPF X; Step=1.8 µm; Grid275x177
yIPF Map
zIPF Map
= 100 µm; IPF Y; Step=1.8 µm; Grid275x177
= 100 µm; IPF Z; Step=1.8 µm; Grid275x177

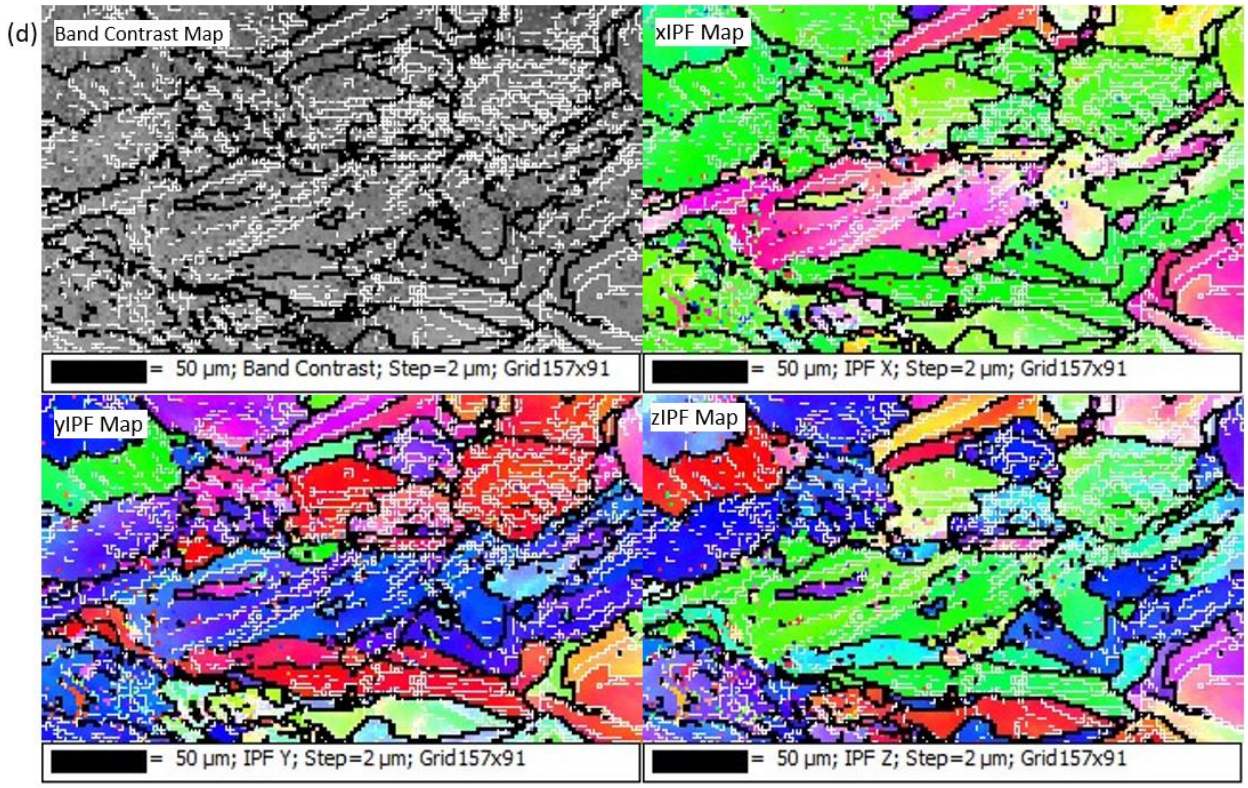

Figure 3-10: EBSD of the annealed sample showing the newly formed microstructure. (a) site 1, (b) Site 2, (c) site 3, (d) site 4

Plots of the misorientation angles were made for each of the EBSD scan locations and can be seen in Figure 3-11. Both of the two locations that showed large grain growth had almost entirely all high angle misorientations. This is the opposite of the as-received scan and demonstrates how the material is at a lower residual stress level. The third misorientation plot showed an approximately equivalent fraction of small angles to the fraction of large angles. This makes sense if you break down the plot into the components of the area that showed the original microstructure and the area that showed the new microstructure. The final plot shows a distribution very similar to the as-received material which agrees with the EBSD scan.

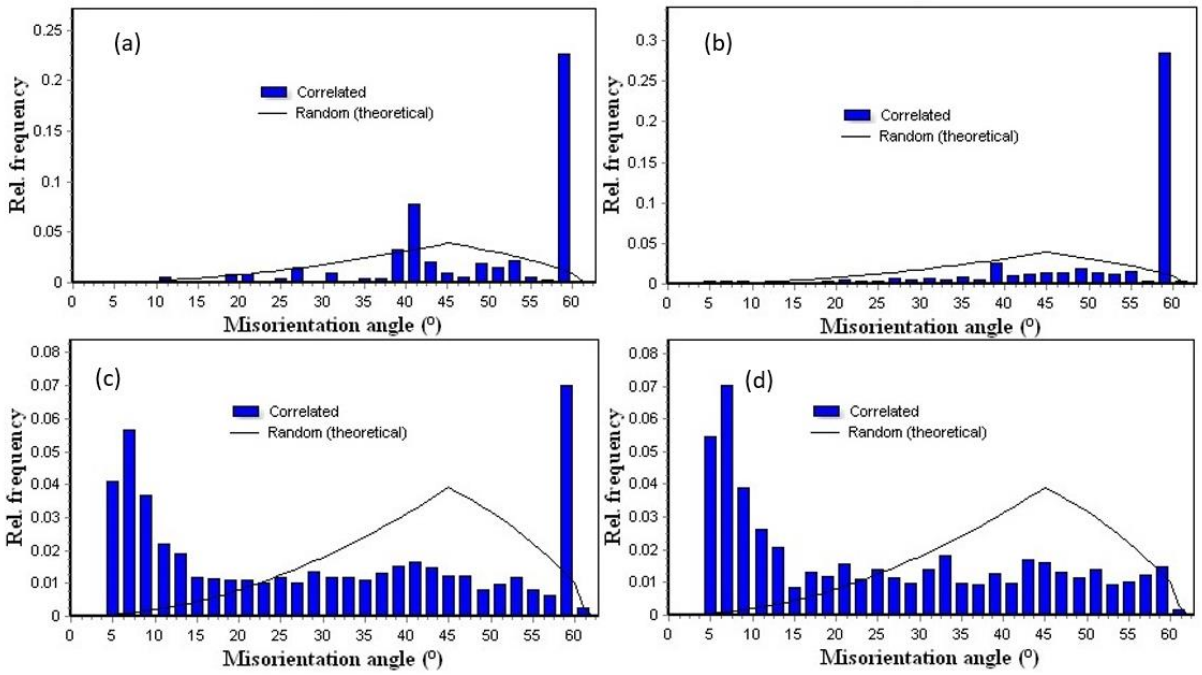

Figure 3-11: Misorientation angle distribution plots of the annealed sample at (a) site 1, (b) site 2, (c) site 3, and (d) site 4.

Sample with Localized Grain Growth

With a better idea of the critical current density required for grain growth, it was time to utilize a liquid nitrogen cooled stage to process the sample at room temperature. The results from the first sample of three that were processed at low temperatures can be seen in Figure 3-12. During the experiment, the temperature on the liquid nitrogen stage was held at 20°C. This sample shows a combination of small sized grains and large grains due to thickness variation in the sample. From visual inspection there appears to be some twinning in the larger grains but not in the smaller grains. The sample also appears to have been deformed during processing.

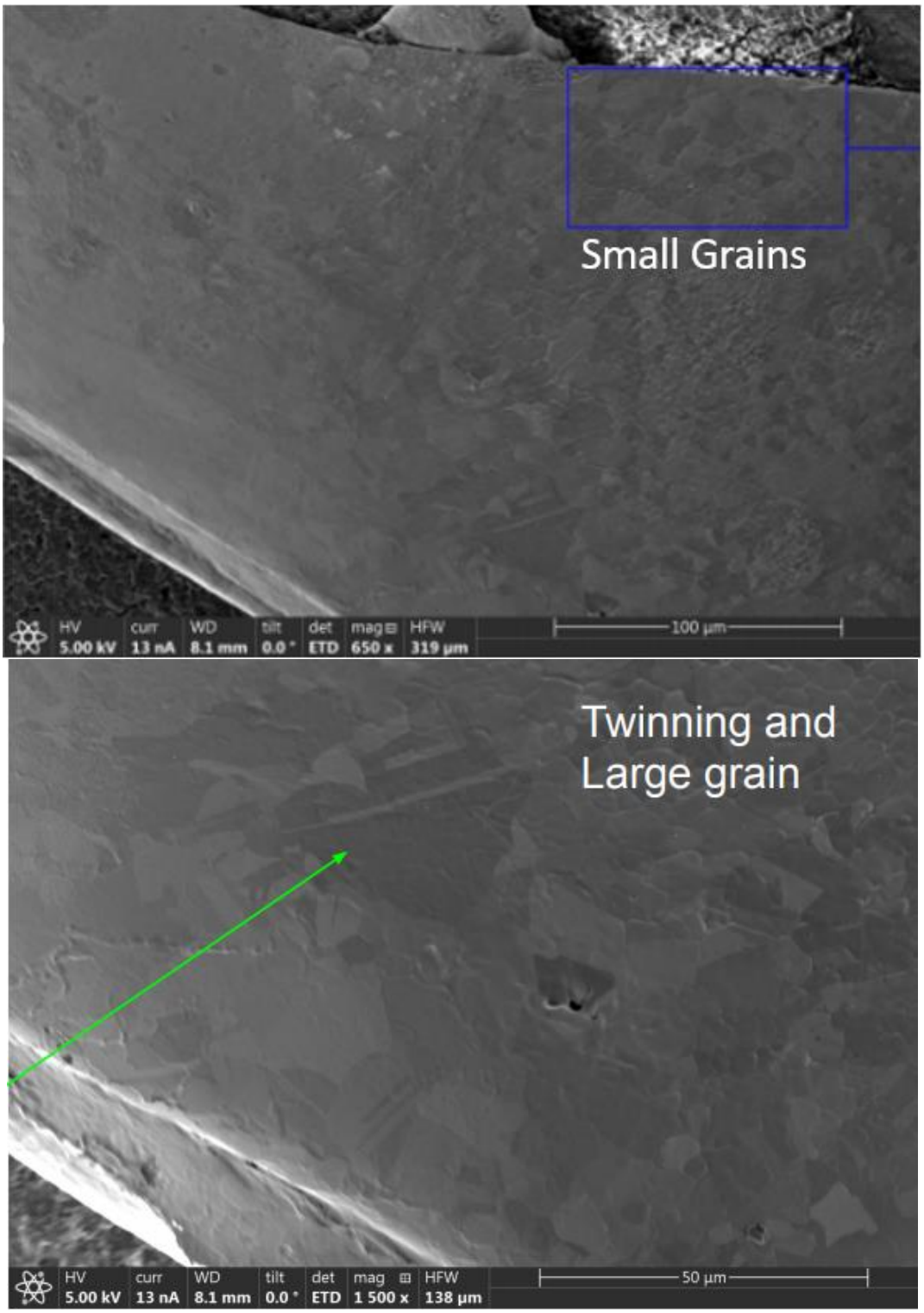

Figure 3-12: Optical micrographs showing small and large grains in the sample.

The EBSD scan taken in this sample shows a microstructure very different than the as-received microstructure. It is interesting to note that, in Figure 3-13, there are some areas where there appears to be some unchanged microstructure. Other samples with small grain sizes would similarly have larger portions of unchanged microstructure compared to samples with larger grain sizes. The scan also confirms that the smaller grains do not contain any annealing twins. Unfortunately, an EBSD scan of the area with larger grains was not possible due to the sample being deformed. Grain size analysis was performed on the scan location with a focus on the newly created grains in order to estimate the refined grain size. The estimation from ImageJ revealed the average size to be about 11 μm in diameter. Grain size analysis was not done for the areas of larger grain size due to the sample being deformed during processing.

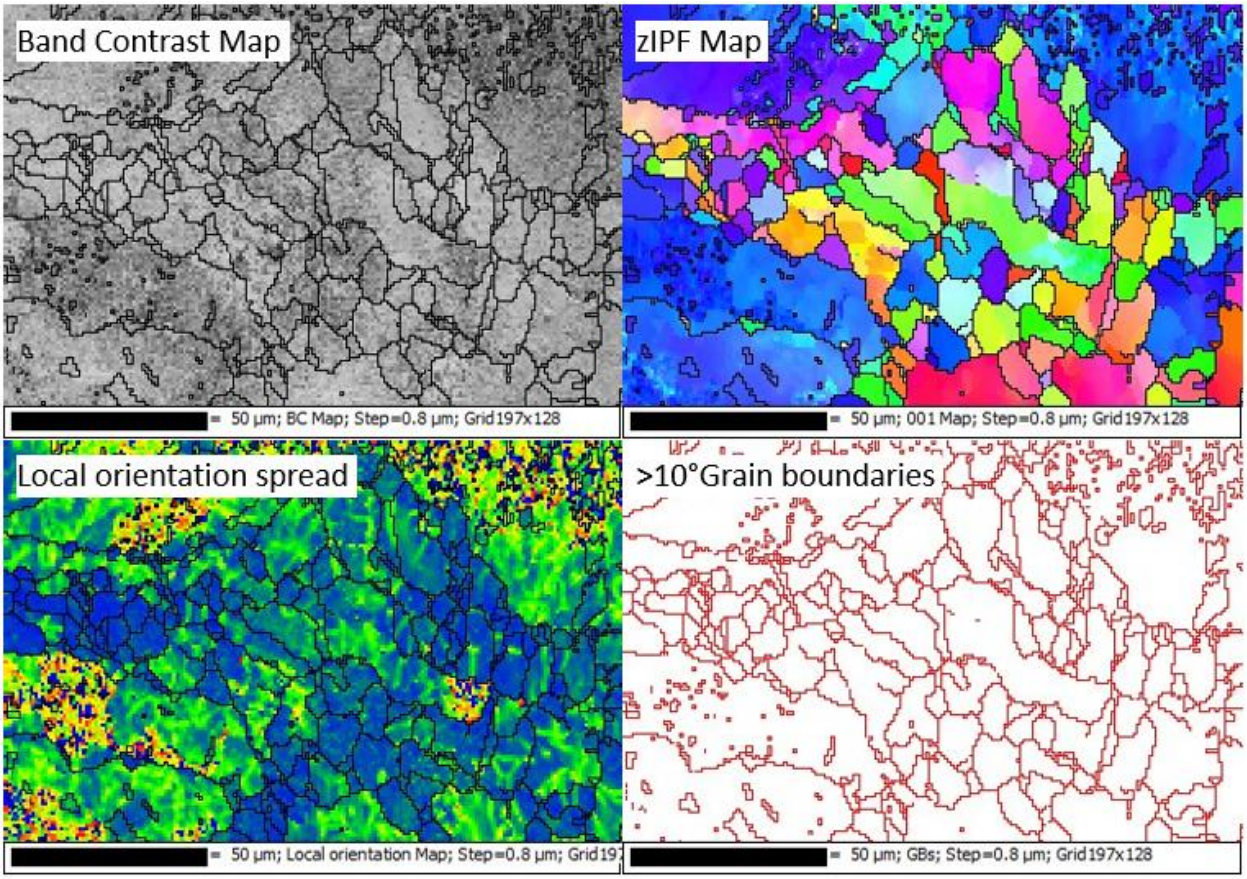

Figure 3-13: EBSD showing some small grains along with unchanged microstructure.

The Misorientation angle plot in Figure 3-14 shows a large fraction of high misorientation angles with a significant number of angles that are not high angles. This distribution agrees with the EBSD scan with the high angles coming from the large grains and the lower angles coming from the unchanged microstructure.

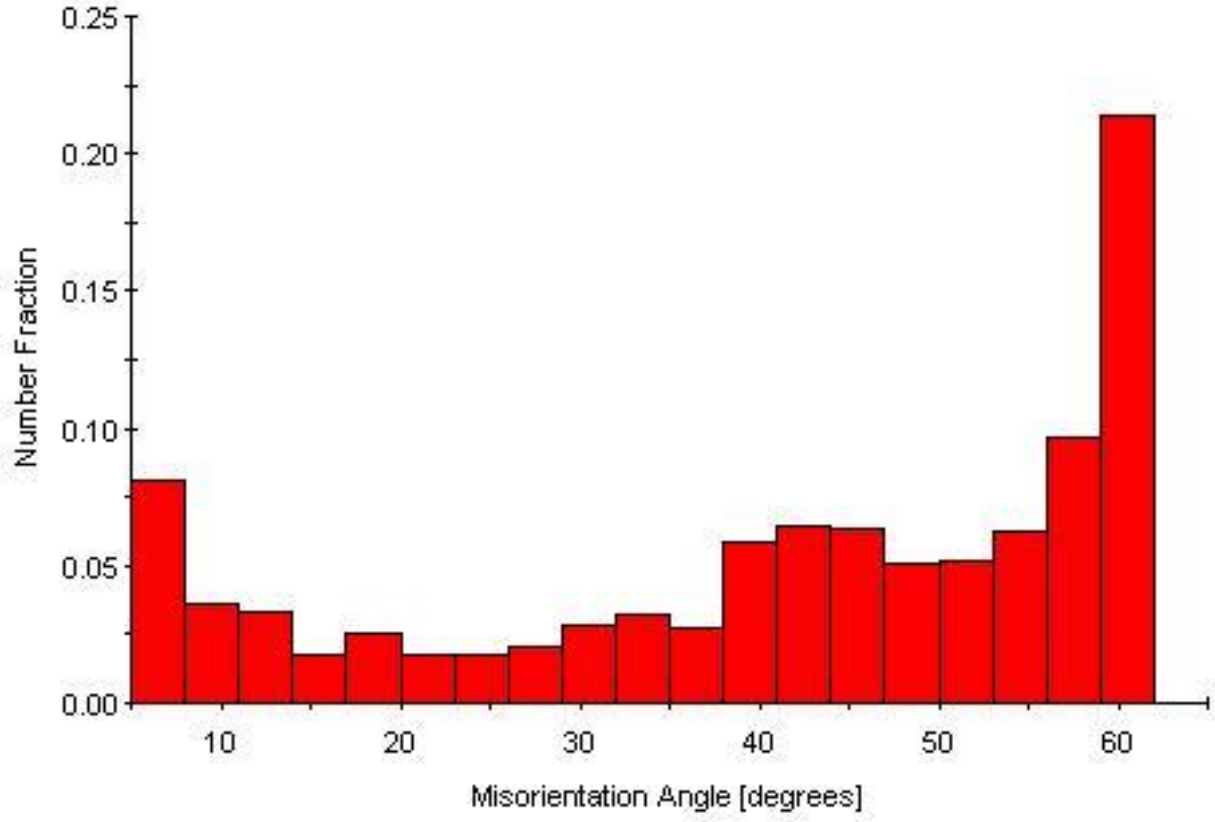

Figure 3-14: Misorientation angle distribution plot of the sample with localized grain growth.

Fully Annealed Sample at Room Temperature

The second sample that was processed at a low temperature achieved a large amount of grain growth. Optical micrographs of the sample can be seen in Figure 3-15. The top image shows the surface of the sample before processing. The middle image displays a magnified image of the surface after processing. The bottom image shows how grain growth occurred across the entire length of the sample.

The grain boundaries are clearly discernible due to large grain boundary grooving that occurred during the experiment. Twins are also visible inside the grains.

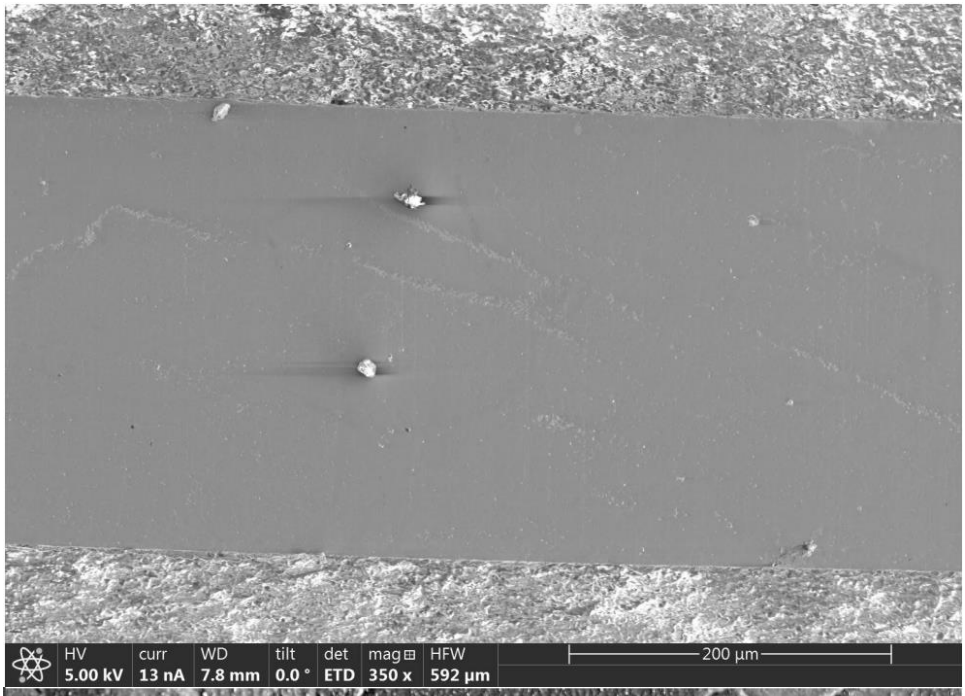

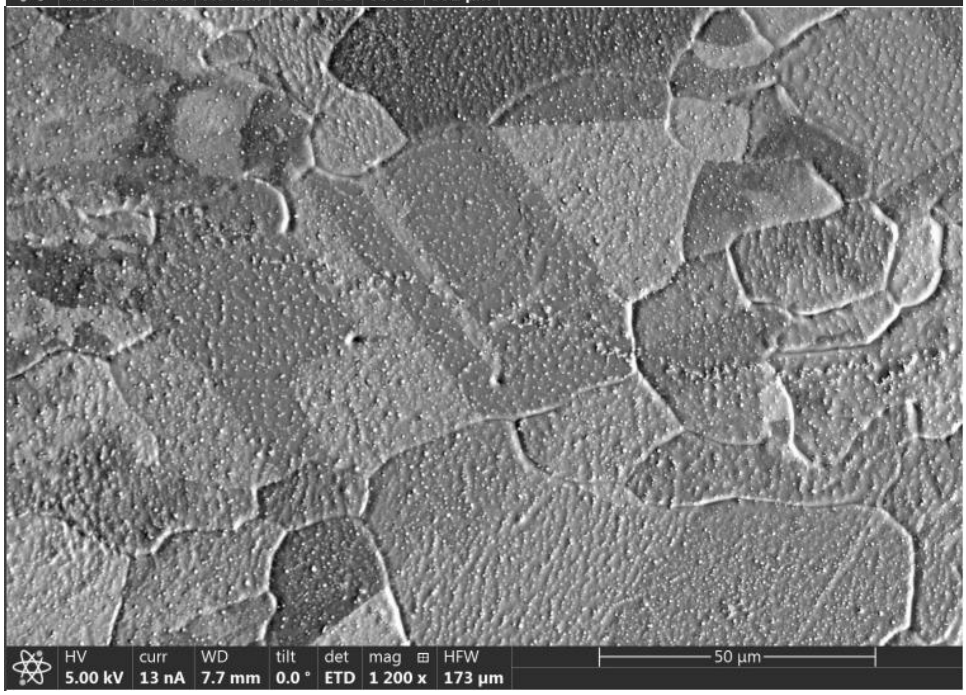

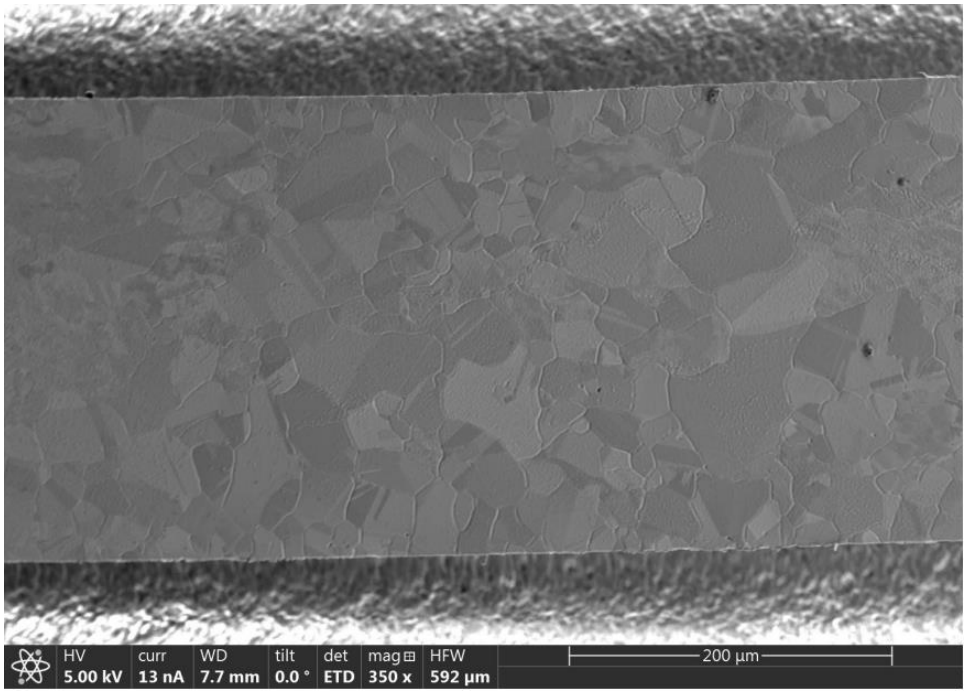

Figure 3-15: Optical micrographs of the sample surface before and after processing.

The EBSD scans of this sample confirms what was seen in the optical images with large sized grains and large amounts of annealing twins. Figure 3-16 shows the results of two different EBSD scan areas that were taken far apart from each other. The entire area for both scans shows enlarged equiaxed grains that underwent a high strain rate to produce annealing twins. The fact that both scans show the same microstructure even though they were taken at two locations on the sample that were far apart demonstrates how this sample was uniformly annealed across the entire sample. Grain size analysis was performed for the first scan location and the estimation showed the average grain size diameter to be 45 µm. This was also confirmed with grain size analysis on the optical images once again using ImageJ and a line intercept method.

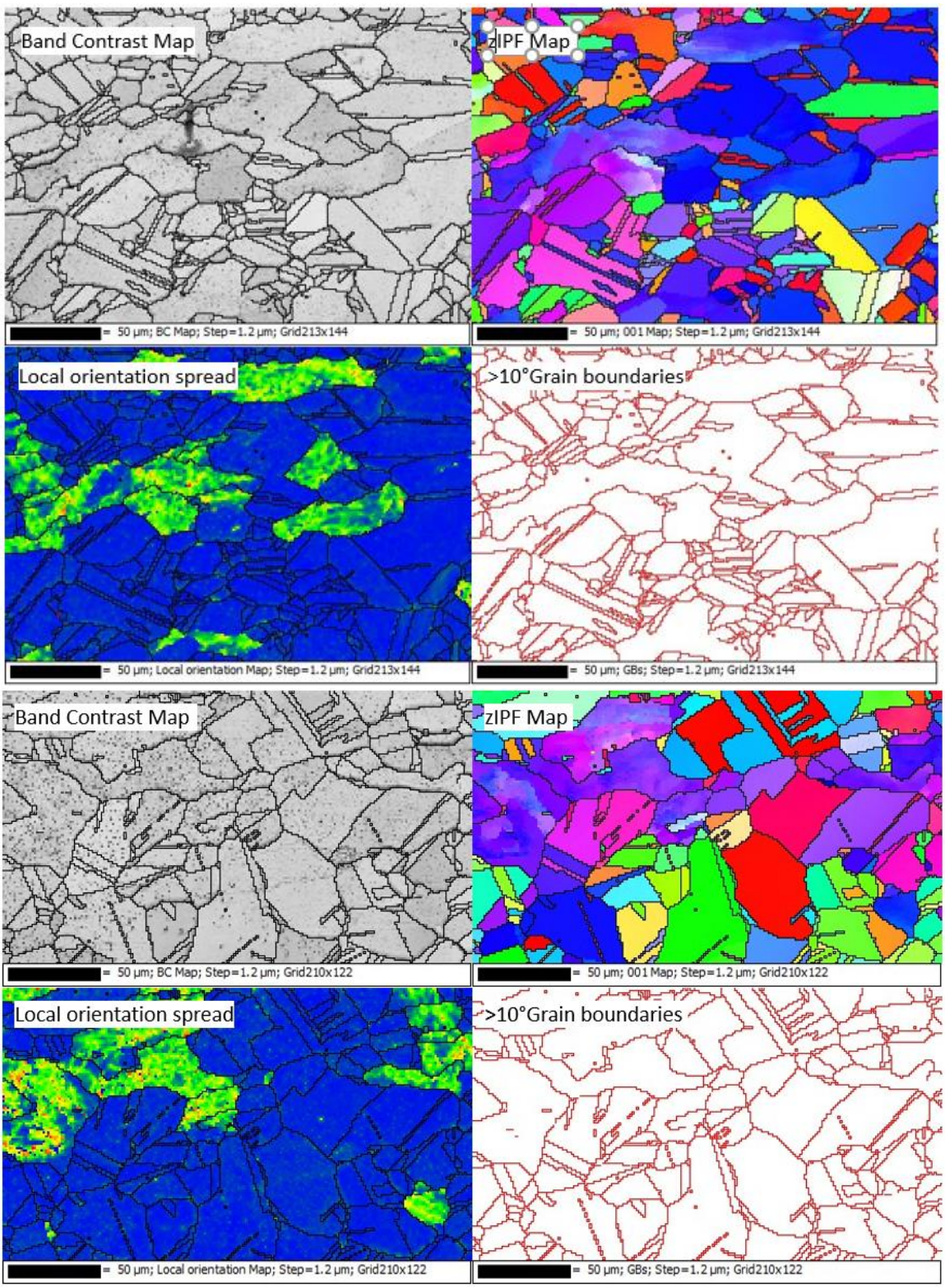

Figure 3-16: EBSD of two locations on the fully annealed sample. (Top) Location 1 (Bottom) Location 2

The misorientation angle plot shown in Figure 3-17 has almost entirely high misorientation angles which agrees with the EBSD scans and the Optical micrograph images. The distribution shows that the microstructure has achieved a lower residual stress state.

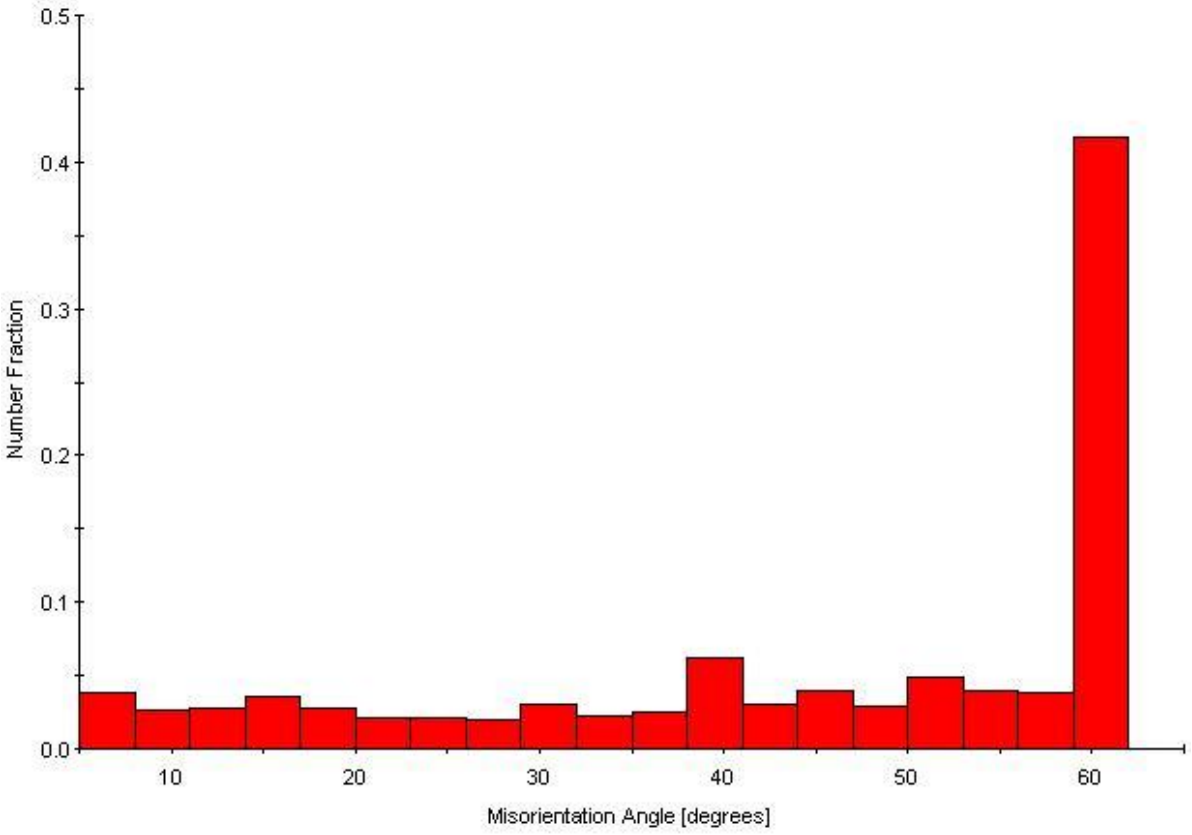

Figure 3-17: Misorientation angle plot of the fully annealed sample.

Sample Annealed Under a Short Period of Time

With a successfully annealed sample that was created while at room temperature, the next step forward was to use this process to refine the grain size in the sample. While grain refinement was not seen in the heated samples, there was evidence in the first cooled sample that there may be some processing conditions that would lead to grain refinement. From the first cooled sample, it was determined that smaller grains would form with larger current densities and the formation of smaller grains could also be impacted by the duration of the processing time. The sample in Figure 3-18 was processed up to 200

A/mm^2 with large steps of current levels to reduce the processing time. The first image was taken while the sample was being biased at half of the critical current density and shows some surface changes. The second picture was taken after processing and shows a significant amount of grain refinement occurred across the sample. The third picture shows a magnified image of an area of complete grain refinement. There also appears to be some differences in the amount of grain boundary grooving that occurs with some grooves being deeper and clearer than others. This may signify that some boundaries are more affected by the electron wind force than other boundaries. The final picture shows a region where the current density was not large enough to induce microstructural changes but is still of interest due to the cracks that appeared to have formed from the processing.

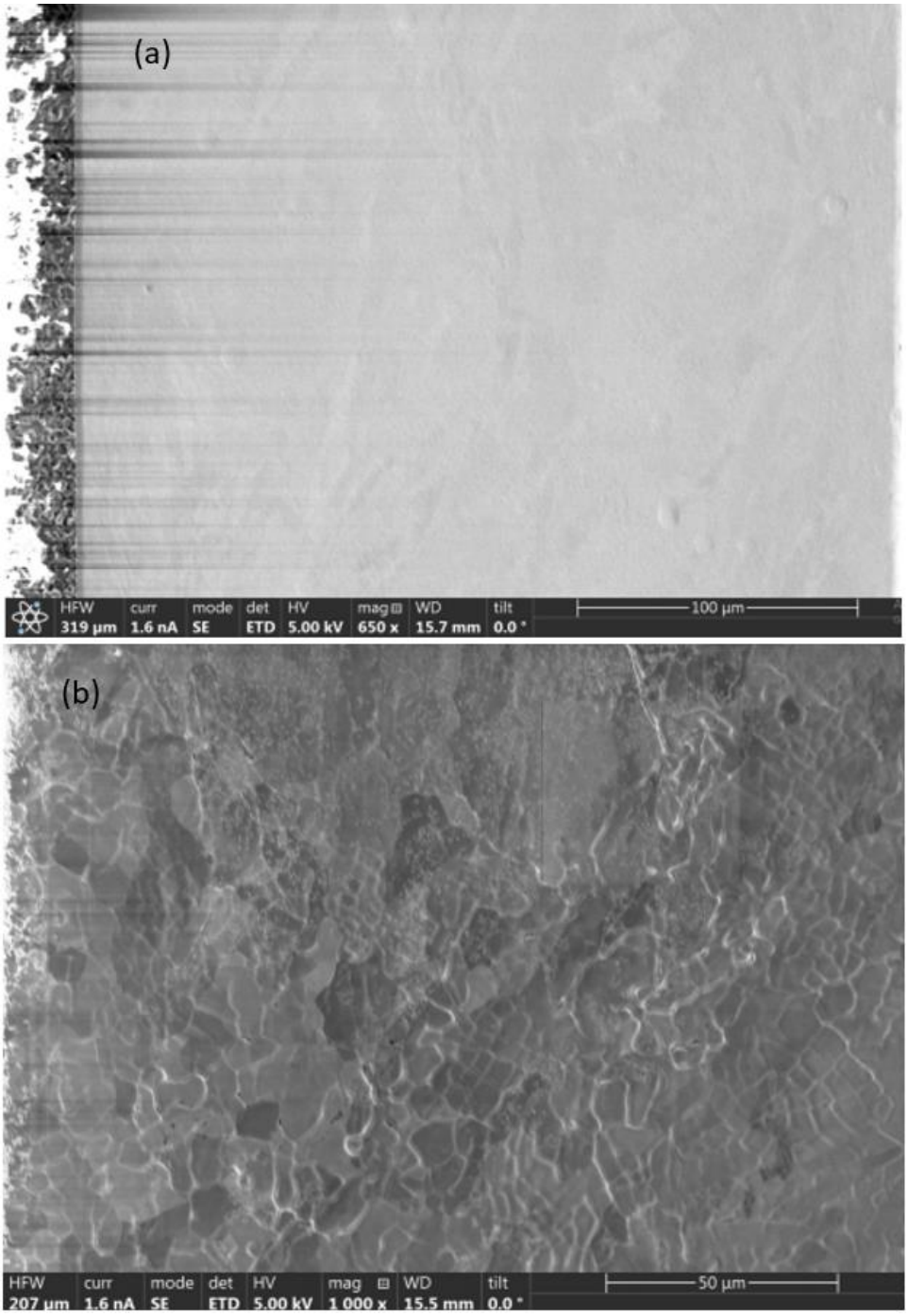
(a)
HFW 319 µm
curr 1.6 nA
mode SE
det ETD
HV 5.00 kV
mag 650 x
WD 15.7 mm
tilt 0.0 °
100 µm
(b)
HFW 207 µm
curr 1.6 nA
mode SE
det ETD
HV 5.00 kV
mag 1 000 x
WD 15.5 mm
tilt 0.0 °
50 µm

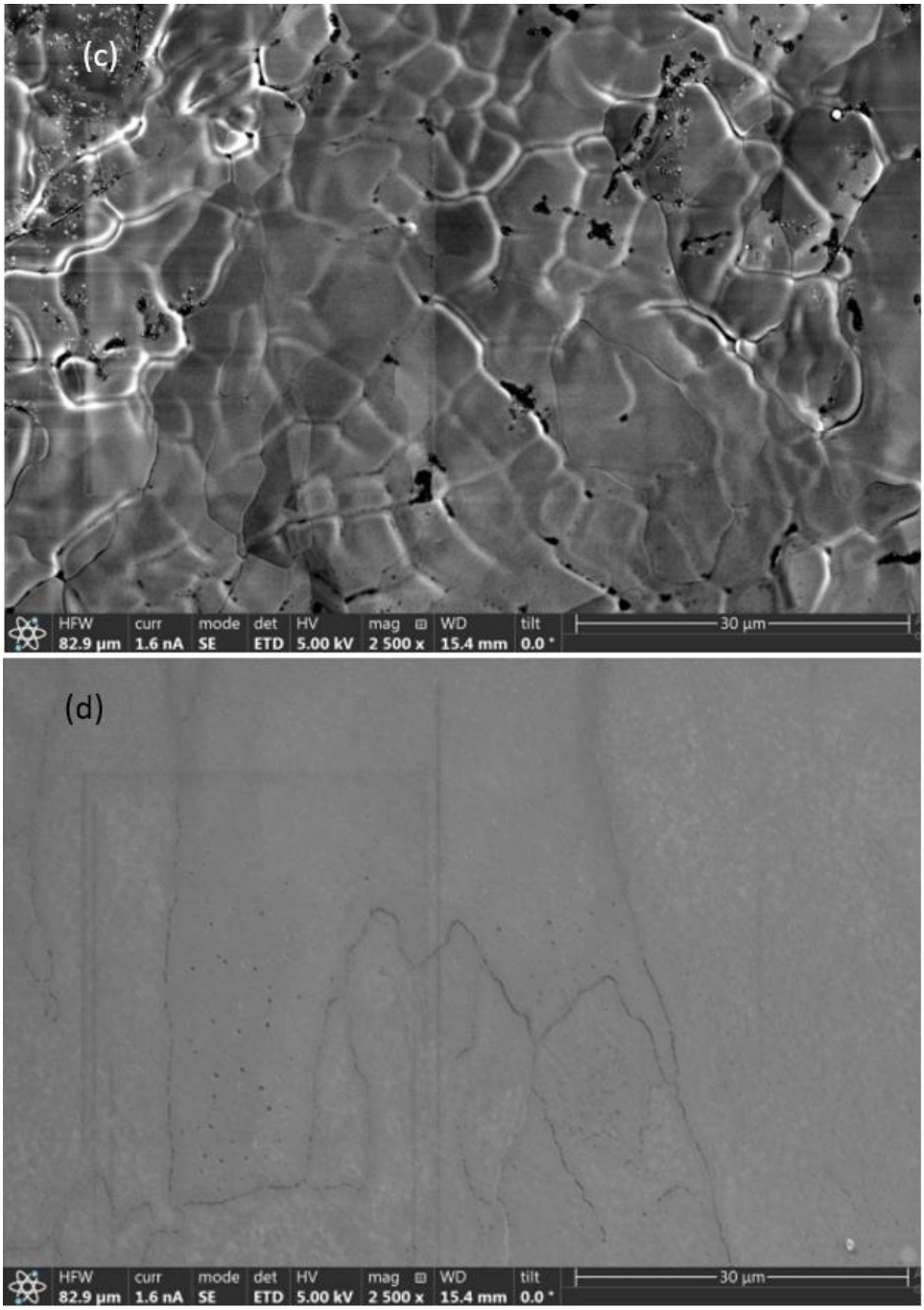

Figure 3-18: Optical micrographs of the sample processed for a short period of time: (a) very low current density, (b) post biasing surface, (c) magnified view of surface, (d) cracks that formed on the surface.

EBSD scans were taken at two different locations to see if the microstructure was consistent across the sample. The scans can be seen in Figure 3-19. The first location shows grains that were clearly created by grain boundary bulging from the original microstructure. The second location shows only

partial refinement with a large portion of the area retaining the original microstructure. The portion of retained original microstructure was seen in every sample that underwent grain refinement. Also, in every scan location focusing on smaller grain sizes, there were no instances of twinning in the grains. Grain size analysis on the first scan location revealed an estimated grain size to be approximately 15 μm. Analysis was not done on the second location since it almost entirely comprised of a single grain from the original microstructure.

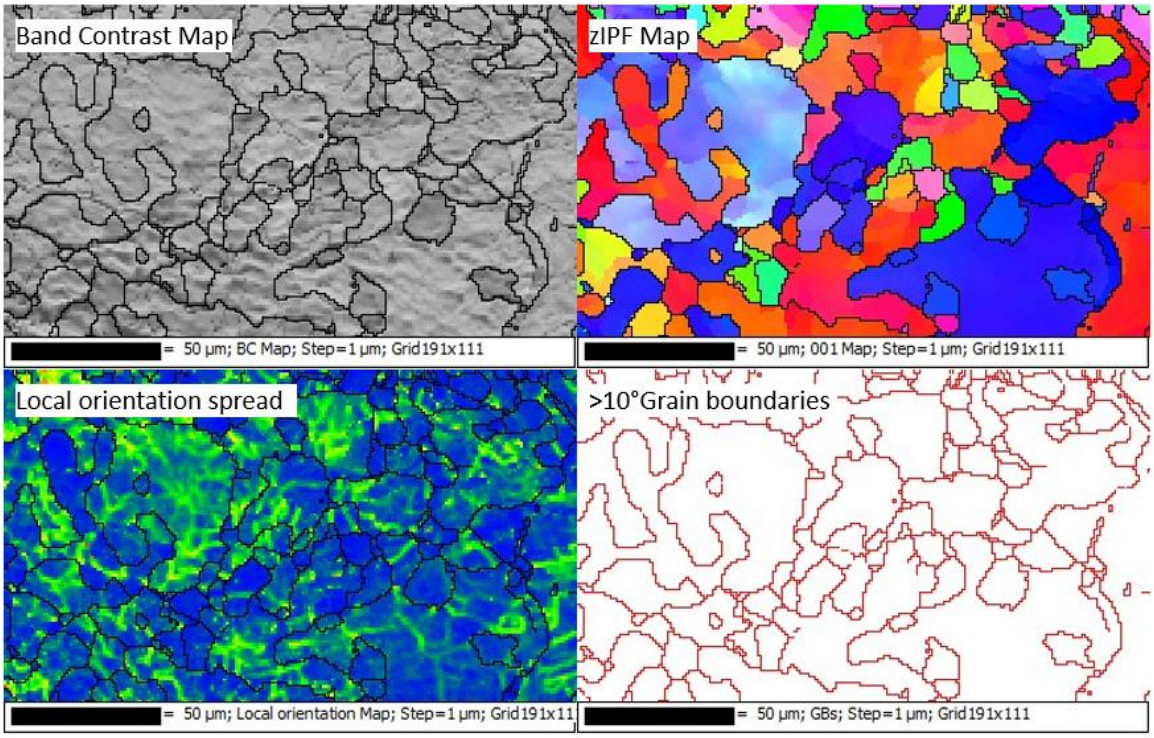

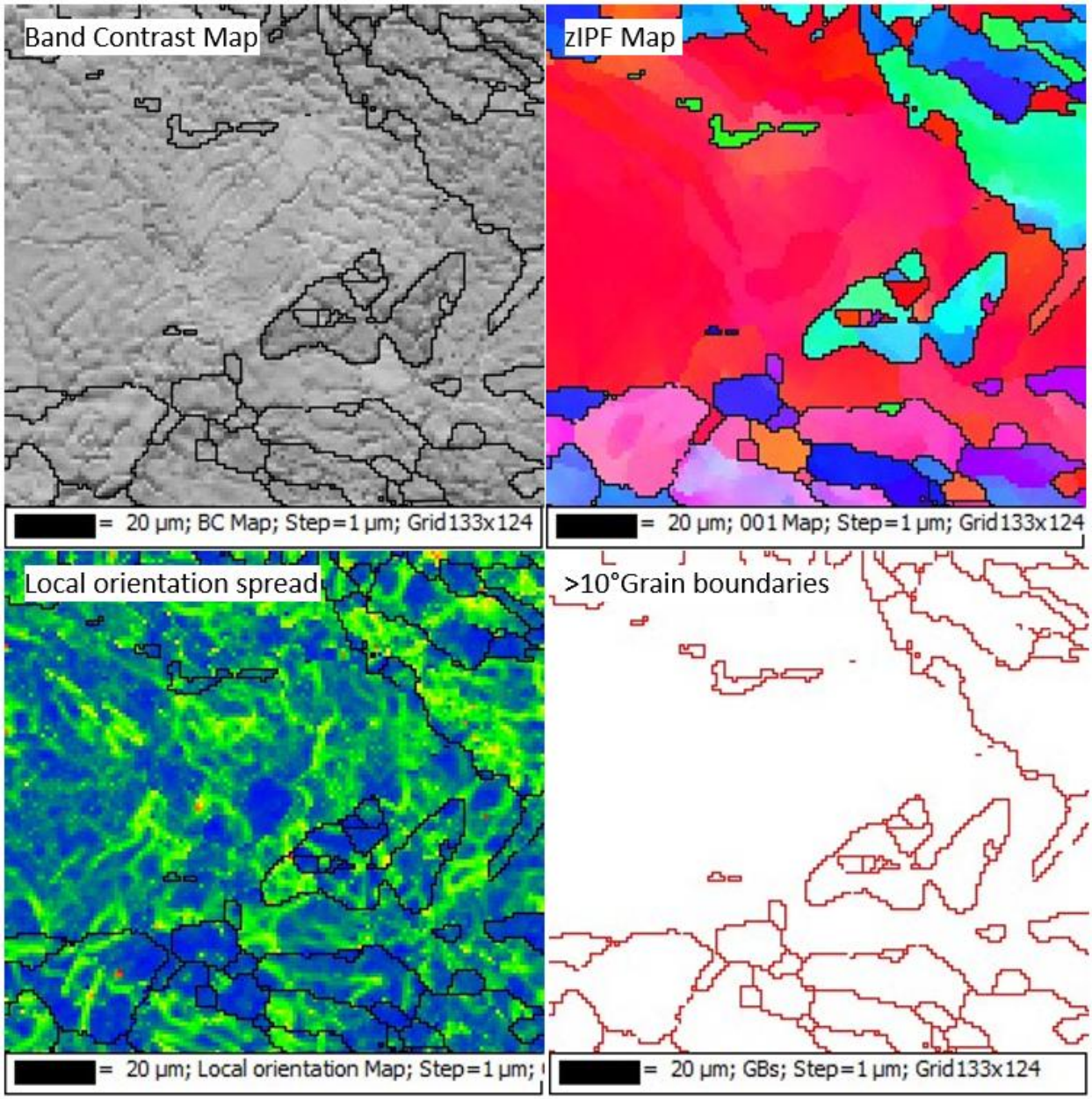

Figure 3-19: EBSD of the refined sample at two different locations. (top) Location 1 (bottom) Location 2

A plot of the distribution of misorientation angles was created for the second scan location and can be seen in Figure 3-18. The plot shows that the grains have either a high misorientation angle or a low misorientation angle. Once again, the high angles are coming from the areas of new microstructure and the low angles are coming from the original microstructure.

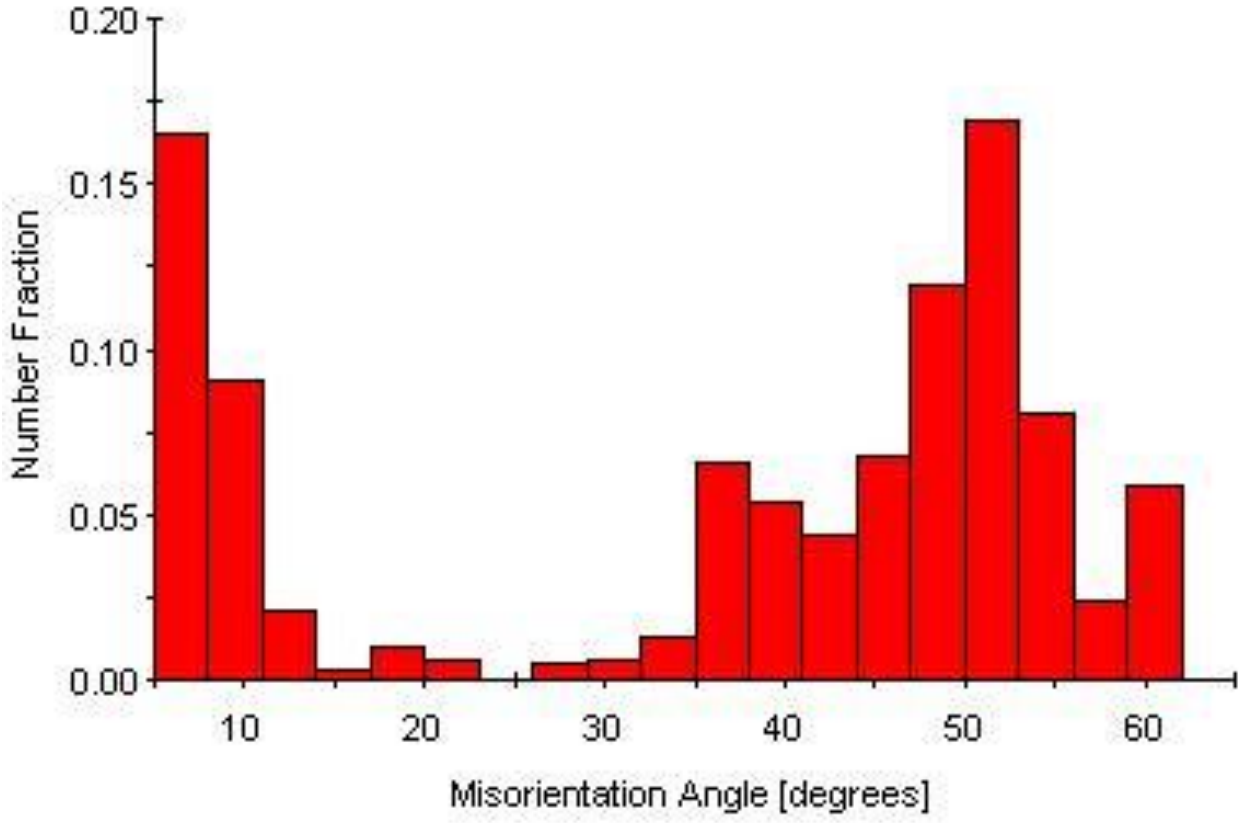

Figure 3-20: Misorientation angle plot of the sample processed for a short period of time.

Plot of Misorientation Angle Distribution for All Samples

A plot with all the misorientation angle distributions for each sample was made and can be seen in Figure 3-21. For most of the samples, there are very little fractions of grains that are in between the small misorientation angles and the large misorientation angles. The smaller angles represent high stored strain energy while the larger angles show that the grains have reformed under a more equilibrium condition. For the intermediate sample that was processed but retained the original microstructure, the fraction of small angles shifted to lower angles compared to the as-received distribution due to the material only going through a recovery step and not proceeding to grain bulging and growth. All other samples had a larger fraction of high angles after processing since they were able to reform the pre-existing grains.

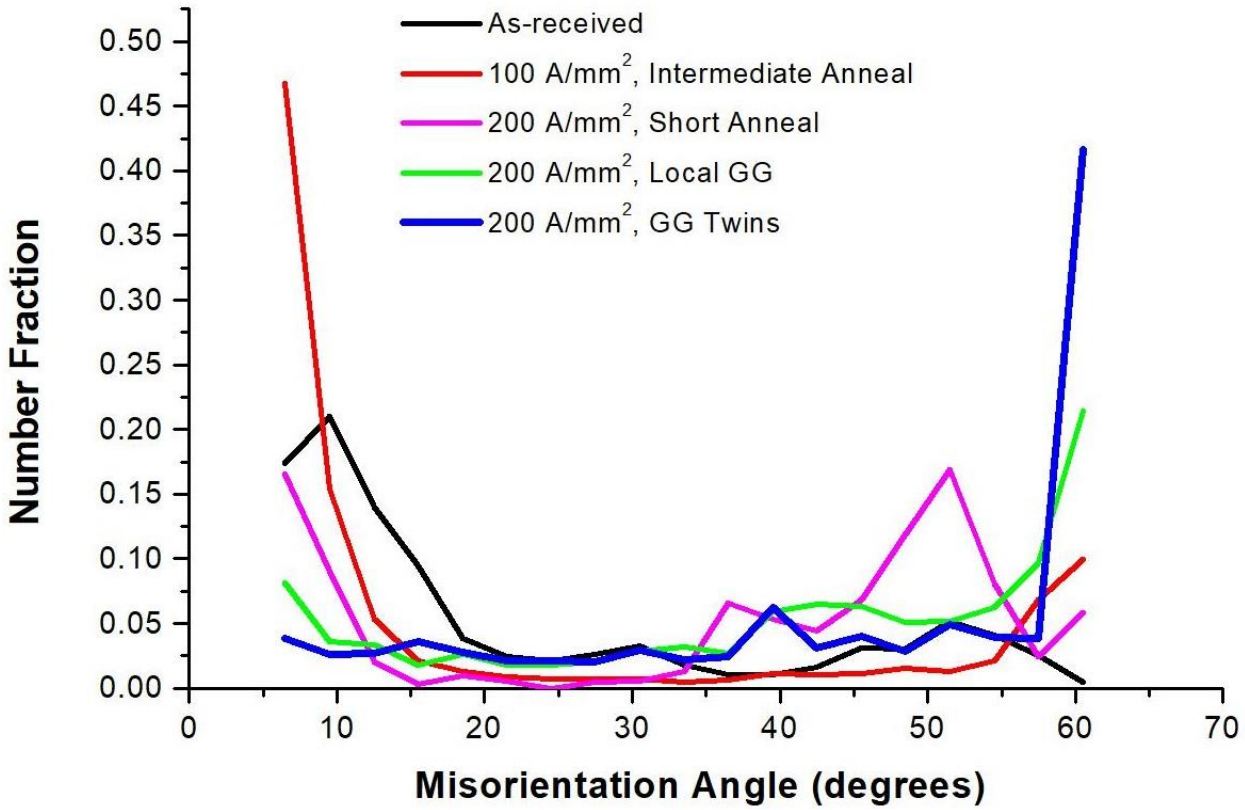

Figure 3-21: Plot of all misorientation distributions across all the samples.

X-ray Diffraction and Analysis

The X-ray diffraction analysis that was performed on the as-received material and the sample annealed at room temperature can be seen in Figure 3-22. There appears to be a clear difference between the size of the peaks seen in the two plots of intensity vs two-theta. The as received XRD plot shows that the largest peak is at 75° while the annealed sample does not even pick up a peak at the 75°. The annealed sample also did not reveal any peaks at 90° which was present in the as-received plot.

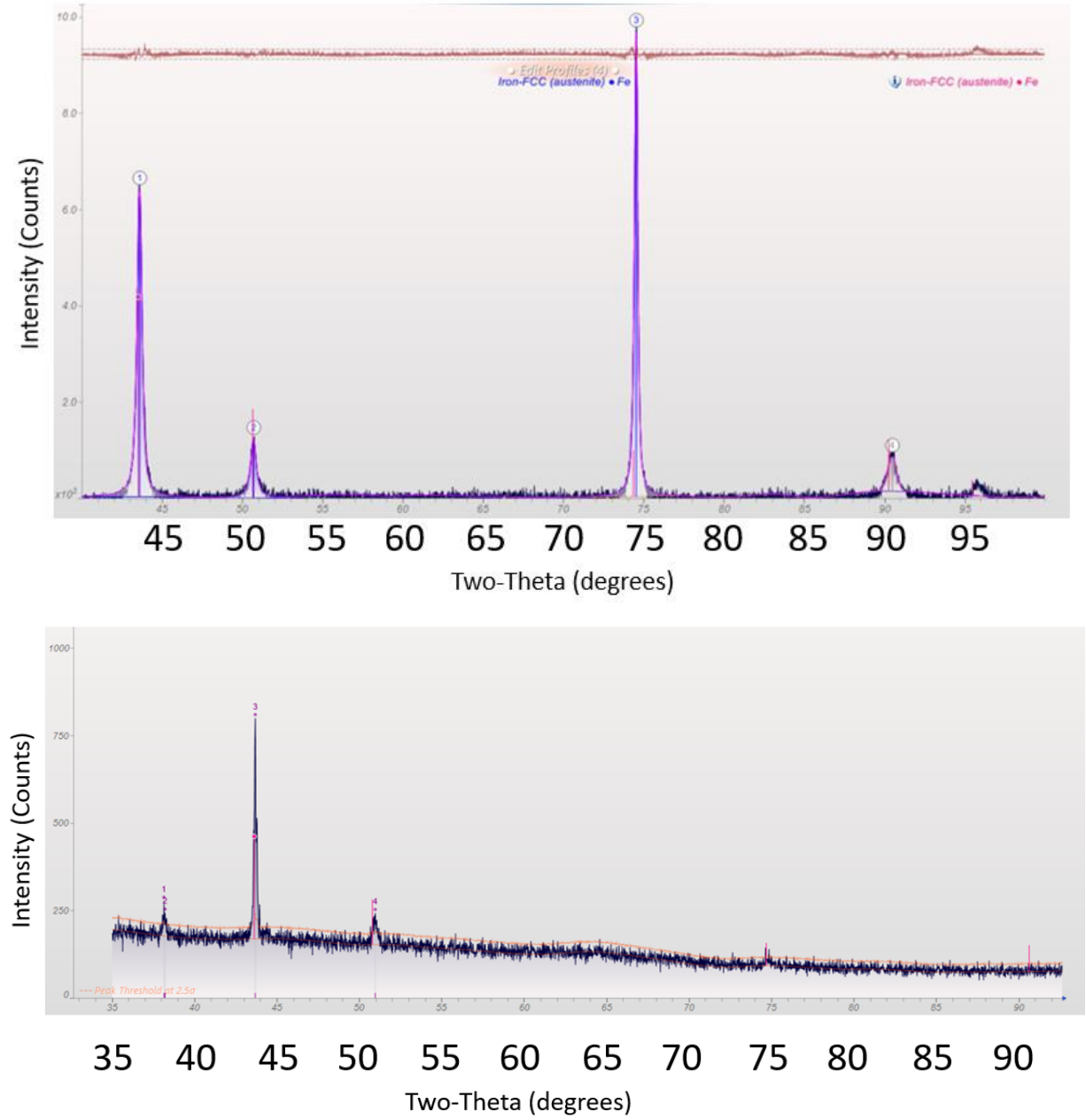

Figure 3-22: Intensity vs two-theta plot for the sample annealed at room termperature. (top: as-received, Bottom: annealed)

The Williamson-Hall analysis of crystallite size and strain can be seen in Figure 3-23. The size and strain were calculated for the as-received material but was not calculated for the annealed sample. This was due to a lack of discernible peaks in the intensity vs two-theta plot for the annealed sample. Some of the Williamson-Hall analysis can still be useful in comparing the before and after processing

states. The first image shows the estimated crystallite size and strain of the as-received material. The second image shows the estimated crystallite size in the annealed sample when strain is considered constant. This is not a terrible assumption since the misorientation angle distribution found in the sample annealed at room temperature had almost entirely large angles which could be inferred as very little strain left in the crystal. From this analysis, the annealed crystallite size is an order of magnitude larger than the as-received crystallite size. This would be expected from the electro-annealing process. The last image shows the analysis of crystallite strain in the annealed sample when size is considered infinitely large. This assumption is also not unreasonable since the average grain size seen in the EBSD scans were relatively large. Once again, the results of the annealed sample with much less crystallite strain compared to the as-received material would be expected from this electro-annealing process.

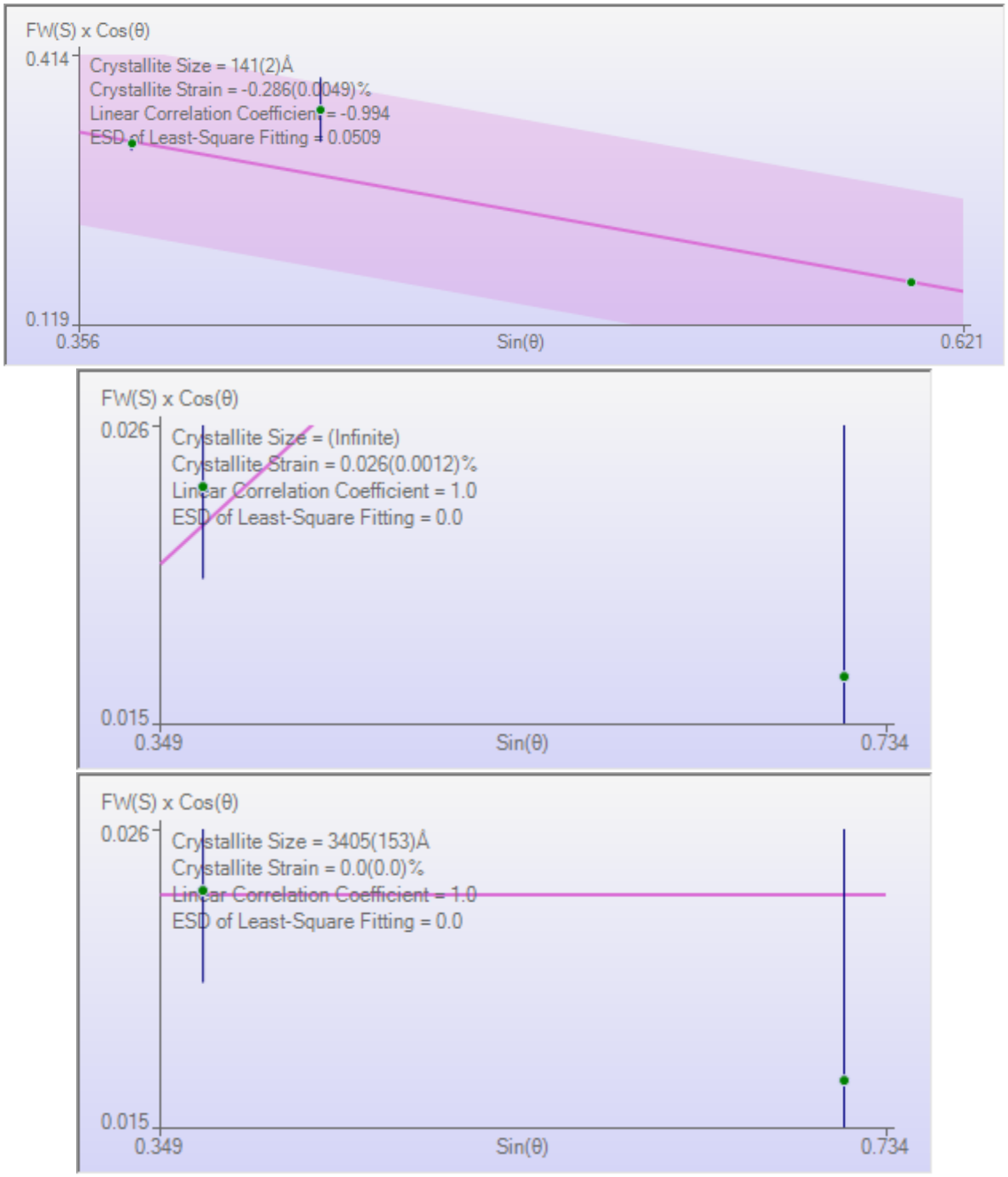

Figure 3-23: Williamson-Hall analysis of the x-ray diffraction data. (Top: as-received, Bottom two: Annealed)

Chapter 4

Discussion

Utilizing the electron wind force for strain induced grain boundary migration has proved to be very effective. After trial and error with some of the experiments, the processing conditions for achieving large amounts of grain growth in the 316 stainless steel created from a powder bed fusion process was obtained. These growths were experienced in short periods of time when a high current density was applied. Grain refinement proved to be more difficult than grain growth in this process. Grain refinement seems to be possible from the experiments performed, but complete refinement of the original microstructure would need more investigation. The short processing times in these experiments seems to be the most beneficial aspect of using this type of grain growth compared to the long times associated with traditional heat treatments. Even though this process requires large amounts of power, the short period of time at which this power is maintained results in a more energy efficient process compared to traditional heat treatments. If this process was to be practically applied in an industrial setting, solutions for managing the large currents and the possibility for surface contamination would need to be implemented.

Optical Images

Comparing the before and after images of each of the samples shows that there are clearly some surface changes that occur from processing. When the current density is half of the critical current density there is some discoloration and contrast differences on the surface which reflects what the EBSD scan revealed as dislocation tangles. With an adequate current density, images of the surface reveal clear microstructural differences as compared to the smooth initial surface. The detailed surface is due to the grain boundary grooving effect which is the equivalent of etching the sample. The detailed optical micrographs of the sample taken after processing allows for easy identification of when the sample has

been properly annealed. These images are detailed enough to make a qualitative guess as to the sample's average grain size without the need of an EBSD scan. Qualitative information on the fraction of annealing twins in the sample can also be gathered by analyzing optical images of these samples after electrically processing them.

EBSD

Each of the EBSD scans generally agreed with what was seen in the optical images. The EBSD scan of the first sample showed that the material underwent a recovery step that allowed for movement and rearrangement of the existing dislocations. The processing conditions for the second and fourth samples lead to equiaxed grains forming and growing into larger equiaxed grains. The third and fifth samples formed equiaxed grains out of the original microstructure but did not allow these grains to complete the grain growth. The new grains formed in these samples can be easily differentiated from the original microstructure since the original grains were columnar in shape. The original microstructure also contained more defects inside the grains compared to the newly formed grains. These results are typical of a strain induced grain boundary migration process where the grains bulge from the original shape and the newly created area have lower dislocation densities.

The EBSD scans of the second and fourth samples also revealed a large number of annealing twins. These twins formed due to the large strain rate that was applied to the grains during the grain growth stage. It is also not surprising that the twins formed in the samples with large grains since large grain sizes has been shown to promote the twinning phenomenon. This is also confirmed by the fact that no twins were found in the smaller grains formed in the third and fifth samples. These twins should be beneficial to the mechanical properties of the samples by increasing the strength and ductility of the samples. The large amounts of twin boundaries should restrict the movement and creation of dislocations. This means that the microstructure can be approximated as an equivalent microstructure of smaller

average grain size and therefore larger material strengths. As previously discussed, twins have also been shown to improve ductility of the material beyond what would be seen in a material of similar grain size but without twins.

One thing that cannot be realized through optical images of the sample is that the microstructures have much higher misorientation angles than in the as-received material in every sample that was processed at the critical current density of around 200 A/mm^2. This confirms that the annealing process has reduced the stored strain energy in the sample. The misorientation plots show that the samples that had higher fractions of large angles were processed to a point closer to equilibrium compared to the samples that contained a mixture of angles. This process of analyzing the misorientation angles acts as an easy way to establish optimum processing conditions that ensure complete reformation of the microstructure.

The EBSD scans of the samples that underwent grain refinement showed some unchanged microstructure after processing. It may be that these samples needed more processing time to allow for these grains to be consumed by the bulging grains. The other possibility is that if the samples were processed further, then the first grains to nucleate would start to grow while other grains are just starting to form. If grains are growing while others are just starting to reform, then the resulting microstructure would have substantial variation in grain size. This variation of grain size would explain the results of the third sample which had a combination of small and large grains. That being said, the result from the third sample is probably more related to the variation in thickness across the sample. If the samples need more processing time, then in order to achieve grain refinement the current density should be decreased to allow for more time for the process to take place. This is because, at $200A/mm^2$, the microstructural changes happen very quickly with the original microstructure changing into large grains in a matter of seconds. The samples that underwent grain refinement also saw a large rate of current increase up to the critical current density. This may have influenced the formation of more grain bulging sites and a larger number of small grains. If the speed at which the current level is increased to the critical level affects the

formation of smaller grains, then the process of refining the grain size would be difficult due to less time to detect surface changes. The most reliable way to create a grain refined sample would be to sacrifice on the grain size and allow for a little bit of grain growth to occur to ensure that all the original microstructure has been consumed.

X-ray Diffraction

The x-ray diffraction data gathered was crude but generally followed what was to be expected from a successful annealing process. The intensity vs two-theta plots showed some peak location and size changes. The location of maximum intensity peak shifted from 75° in the as-received material to 45° in the sample annealed at room temperature. This shift was due to the removal of the texture in the as-received material. The texture of columnar grains favoring the build direction in the additively manufactured material would create a texture that promotes a certain crystal orientation to receive more radiation than the other possible crystal orientations. With the annealed sample having a normalized equiaxed microstructure, this texture is removed and therefore the promotion of radiation on the specific orientation was also removed. This removal of the columnar texture is a sign of a successful grain growth process.

The comparison of estimated crystallite size and strain in the two scans also followed what would be expected in a successful annealing process. There was a significant reduction in crystallite strain in the annealed sample which agrees with the EBSD and misorientation distribution data. There was a significant increase in the estimated crystallite size for the annealed sample which also agrees with the EBSD data. It should be noted that the crystallite size measured in this process is not the average grain size but the average crystallite size. This measurement serves as a comparison of the average crystallite size before and after processing. With an increase in the average crystallite size, an increase in the average grain size could also be inferred. The assumptions made for the estimation of crystallite size and

strain of the annealed sample may reduce the accuracy of the estimations since the size and strain are not estimated simultaneously. That being said, there is a clear difference between the size and strain found in the as received and after processing scans.

The lack of enough peaks in the intensity plot for the sample annealed at room temperature to create an estimation of size and strain simultaneously was most likely due to the sample size. The sample was pushing the limits of what the XRD machine could handle since the machine could not focus the X-ray beam down to a small enough size. The beam size that was used was larger than the sample and thus included a lot of background radiation into the plot. This background radiation could have been large enough to wash out some of the peak data. The lack of peaks could also have been from a lack of radiation on the sample. With a very long exposure time across the two-theta range, the intensity from peaks would increase and should be larger than the background radiation intensity.

Current Density

From these experiments, the current density that appears to initiate microstructural changes in the additively manufactured 316 Stainless Steel is 200 A/mm^2. Each sample that underwent significant microstructural changes has had a current density that was approximately close to this value. Although the process will still occur at lower current densities, 200 A/mm^2 will create substantial changes on the order of seconds to a minute. The relationship between the current density and time to anneal a material is not a linear relationship. Current densities slightly below the critical value will result in substantially longer processing times. This nonlinear relationship also holds true for larger current densities which means that you can create large microstructural changes in a very short period of time. The differences in processing time at the different current densities may also create different resulting microstructure but this was not confirmed in this work. For instance, the key to grain refinement may be to have a larger current density

in order to process the sample very quickly which may result in more grains and smaller average grain size.

This critical current density measurement of 200 A/mm^2 is calculated by dividing the current used in the experiment by the cross-sectional area of the sample that was measured during sample preparation and thus serves as a rough estimate of the critical value. The thickness of the sample is measured using a micrometer at several points of the sample to get an average thickness in the center of the sample where the microstructural changes are going to occur. The width of the sample was confirmed inside of the SEM.

There is a wide variety of critical current density values measured in the literature, which is partly expected since each material should have a different critical value. For instance, the 600 A/mm^2 measured for processing a Zr-based alloy system is larger than the value measured in this experiment but makes sense when you consider the differences between a stainless steel and a ZR-based alloy system [38]. The 200 A/mm^2 measured in this experiment fits into the range of values found in other works utilizing the electron wind force.

Cooling Issues

While there is no doubt that the samples were processed at a low temperature compared to the temperatures seen in traditional annealing processes, the temperatures seen in the samples were probably higher than what was measured during the experiment. This is since the temperature was measured on the liquid nitrogen stage, which was a constant 20°C, and not on the surface of the sample. This is significant since the experimental setup had the sample in a free-standing configuration. This means that there was a slight air gap between the location of the microstructural changes and the cooling stage. Heat would be allowed to flow through the ends of the sample and then through the stage, but the air gap would cause heat to accumulate in the sample and raise the temperature of the material. The temperatures seen in

infrared temperature measurements in Figure 3-1 show relatively low temperatures especially when considering that these samples were not cooled at all. These temperatures were also confirmed with thermocouple measurements of experiments performed without any cooling stage.

There are ways to estimate how high the temperature actually was in the cooled samples. For instance, some of the samples were slightly deformed due to the material trying to expand but being restricted since it was effectively pinned by the electrical connections. This means that the temperatures in the sample were large enough for the sample to have a small size change. This is what first indicated that the sample temperatures were not the same as the cooling stage. A more promising temperature indication of the cooled samples was the fact that the solder had not re-melted during the experiment. This is significant when trying to claim low temperatures because the solder used in this experiment has a very low melting temperature even when compared to traditional solders. The experiments that were not cooled commonly had electrical connection issues due to the solder re-melting, so clearly the liquid nitrogen cooled stage was working to cool the sample.

A way to improve the temperatures in these experiments would be to directly mount the samples to the heat sink or stage in order to eliminate any air gaps. This was tried multiple times, but each attempt resulted in poor electrical connections. With more time, a sample setup that allowed for direct stage or heatsink contact with the sample could have been created.

Mechanical Characterization

Attempts to gather mechanical information on these samples were made but none of the data would be presentable due to errors in the process and problems that were encountered due to the samples. In terms of indentation, the sample sizes used in these experiments would restrict indentation to the nano-size scale. This becomes a problem due to the strict tolerances that nano-indentation requires. The error was determined to be partly caused from the method of mounting the sample to the substrate used in the

nano-indentation experiments. The sample was adhered by epoxy to a disposable metal disk that acts as the substrate. This disk is attached to the indentation machine through a magnet. The epoxy is required to minimize the compliance of the sample during the indentation. The procedure used for applying the epoxy calls for the epoxy to be applied to the substrate by hand and then place the sample on top of the epoxy. This method is flawed due to the unevenness of the epoxy layer that throws the parallelism out of tolerance. This was confirmed by the drift measurements taken before each indentation. This problem continued to occur for each sample that was indented on and even occurred in the bulk sample from which each of the experimental samples were cut from.

A solution to the epoxy problem would be to change the mounting mechanism used to attach the sample to the substrate of the nano-indenter. The only process that seemed reliable enough to get accurate indentation data from the samples post experiment was a hot mounting process. This would include placing the sample on a surface and placing a hard polymer powder on top of the sample and placing the magnetic disposable stage on top of the powder. The powder would then be sintered and pressed around the sample and stage in order to create a plastic puck that had flat surfaces with the sample surface exposed on one side and the stage exposed on the opposite side. This plastic puck could then be polished to meet the nano-indentation specifications. Unfortunately, the hot mounting machine available for use with these samples broke before accurate indentation data could be gathered from these samples.

Another way to gather mechanical data from these samples would be to create a tensile tester setup. This would require a custom setup due to these sample's unique size scale. The tester would also have to be used inside of an SEM or high-powered microscope in order to measure the displacement when the sample is loaded. With more time and resources this type of tensile tester would have been developed.

Gathering mechanical information on these samples would be interesting since it would allow for a process property relationship to be developed for this new type of annealing. It would also allow for the comparison between the mechanical strength and ductility of samples that were traditionally annealed and

annealed using the electron wind force. The mechanical data could also assess the effect of the large amounts of annealing twins on the strengths and ductility of the annealed material. These types of comparisons can only be speculated upon based on the differences of the resulting microstructure.

Chapter 5

Conclusion

The experiments performed in this study showed that the application of an electrical current is an effective way to anneal a material and has potential to refine microstructures. This study enhanced the knowledge of how the electron wind force, and not Joule heating, dominates the electro-annealing process by creating grain growth at temperatures close to room temperature. This study also provided new information related to how this unique method of strain induced grain boundary migration resulted in a large fraction of annealing twins. These twins formed due to the large strain rates induced by the electron wind force and the large average grain sizes that were obtained. Processing parameters related to achieving grain bulging and growth in 316 stainless steel were also developed with the key parameter being the critical current density of 200 A/mm^2. The success of this annealing process was demonstrated across the optical images taken, the EBSD data gathered, and the x-ray diffraction analysis. The large grain sizes and large fraction of annealing twins achieved through this electro-annealing process could be clearly identified in the optical images. The EBSD scans confirmed what was seen in the optical images and showed that the microstructure was at a near equilibrium state since the misorientation angle distributions heavily leaned towards high angles. Finally, the x-ray diffraction data confirmed that the stored strain energy was drastically reduced after processing the metal.

A current unique challenge that is encountered with this technology is the limitations on size that comes with the large current densities. The maximum size obtained in this study was only in the micron scale due to the available power supplies and cooling solutions. Examples of large amounts of current can be seen in field assisted sintering technology and in electric arc furnaces that have current in excess of 10,000 Amps. With these types of power supplies, parts with cross sectional areas in the centimeters squared size range could be processed. Sadly, the size scale available for this study limited what could be done in terms of analysis such as mechanical testing. While this study was not able to establish a

relationship between the processing parameters and the resultant mechanical properties, there is no doubt that the mechanical properties should be drastically different from the as-received state due to the drastically different microstructures.

The area of post processing is still dominated by heat treatment. Effect of other stimuli (such as electrical current, as described in this thesis) is under-researched and has questions left unanswered. Practical applications of this technology could revolutionize the manufacturing industry and become a standard post processing step due to the energy savings and unique results that have been established by this and other studies. Scaling this technology to meet industrial applications needs to be done. The next logical step in researching this technology would be to increase the sample size. The application of this technology to a standard dog bone shaped sample would require unique power supply and cooling solutions but would undoubtedly result in an excellent process-property relationship and bring this technology one step closer to the industry.

References

[1] Tammas-Williams, S., et al. “Porosity Regrowth during Heat Treatment of Hot Isostatically Pressed Additively Manufactured Titanium Components.” *Scripta Materialia*, vol. 122, 2016, pp. 72–76., doi:10.1016/j.scriptamat.2016.05.002.

[2] Humphreys, F. John., et al. *Recrystallization and Related Annealing Phenomena*. Elsevier, 2017.

[3] Paggi, A., et al. “Strain Induced Grain Boundary Migration Effects on Grain Growth of an Austenitic Stainless Steel during Static and Metadynamic Recrystallization.” *Materials Characterization*, vol. 107, Sept. 2015, pp. 174–181., doi:10.1016/j.matchar.2015.07.003.

[4] Beck, Paul A., and Philip R. Sperry. “Strain Induced Grain Boundary Migration in High Purity Aluminum.” *Journal of Applied Physics*, vol. 21, no. 2, 1950, pp. 150–152., doi:10.1063/1.1699614.

[5] Hosseini, E., and V. A. Popovich. “A Review of Mechanical Properties of Additively Manufactured Inconel 718.” *Additive Manufacturing*, vol. 30, 2019, p. 100877., doi:10.1016/j.addma.2019.100877.

[6] Debroy, T., et al. “Additive Manufacturing of Metallic Components – Process, Structure and Properties.” *Progress in Materials Science*, vol. 92, 2018, pp. 112–224., doi:10.1016/j.pmatsci.2017.10.001.

[7] Pinkerton, A.J.: Advances in the modeling of laser direct metal deposition. Journal of Laser Applications 27(S1), S15001 (2015). doi:doi:http://dx.doi.org/10.2351/1.4815992

[8] Meredith, S. D., et al. “Impact of Composition on the Heat Treatment Response of Additively Manufactured 17–4 PH Grade Stainless Steel.” *Materials Science and Engineering: A*, vol. 738, 19 Dec. 2018, pp. 44–56., doi:10.1016/j.msea.2018.09.066.

[9] Leung, Chu Lun Alex, et al. “The Effect of Powder Oxidation on Defect Formation in Laser Additive Manufacturing.” *Acta Materialia*, vol. 166, Mar. 2019, pp. 294–305., doi:10.1016/j.actamat.2018.12.027.

[10] Muñiz-Lerma, Jose, et al. “A Comprehensive Approach to Powder Feedstock Characterization for Powder Bed Fusion Additive Manufacturing: A Case Study on AlSi7Mg.” *Materials*, vol. 11, no. 12, 27 Nov. 2018, p. 2386., doi:10.3390/ma11122386.

[11] Bai, Yun, et al. “Effect of Particle Size Distribution on Powder Packing and Sintering in Binder Jetting Additive Manufacturing of Metals.” *Journal of Manufacturing Science and Engineering*, vol. 139, no. 8, 1 June 2017, doi:10.1115/1.4036640.

[12] Khairallah, Saad A., et al. “Laser Powder-Bed Fusion Additive Manufacturing Physics of Complex Melt Flow and Formation Mechanisms of Pores, Spatter, and Denudation Zones.” *Additive Manufacturing Handbook*, 2017, pp. 613–625., doi:10.1201/9781315119106-33.

[13] Aboulkhair, Nesma T., et al. “Reducing Porosity in AlSi10Mg Parts Processed by Selective Laser Melting.” *Additive Manufacturing*, vol. 1-4, Oct. 2014, pp. 77–86., doi:10.1016/j.addma.2014.08.001.

[14] Esmaeilizadeh, Reza, et al. “On the Effect of Spatter Particles Distribution on the Quality of Hastelloy X Parts Made by Laser Powder-Bed Fusion Additive Manufacturing.” *Journal of Manufacturing Processes*, vol. 37, Jan. 2019, pp. 11–20., doi:10.1016/j.jmapro.2018.11.012.

[15] Matthews, Manyalibo J., et al. “Denudation of Metal Powder Layers in Laser Powder Bed Fusion Processes.” *Acta Materialia*, vol. 114, May 2016, pp. 33–42., doi:10.1016/j.actamat.2016.05.017.

[16] “Principles of Welding” by Robert W. Messler, Jr. Copyright © 1999 John Wiley & Sons, Inc (ISBN: 0-471-25376-6).

[17] Wang, Zhuqing, et al. “Effect of Processing Parameters on Microstructure and Tensile Properties of Austenitic Stainless Steel 304L Made by Directed Energy Deposition Additive Manufacturing.” *Acta Materialia*, vol. 110, 15 May 2016, pp. 226–235., doi:10.1016/j.actamat.2016.03.019.

[18] Carroll, Beth E., et al. “Anisotropic Tensile Behavior of Ti–6Al–4V Components Fabricated with Directed Energy Deposition Additive Manufacturing.” *Acta Materialia*, vol. 87, 2015, pp. 309–320., doi:10.1016/j.actamat.2014.12.054.

[19] Kuzminova, Yulia, et al. “Structure Control of 316L Stainless Steel through an Additive Manufacturing.” *Letters on Materials*, vol. 9, no. 4s, 2019, pp. 551–555., doi:10.22226/2410-3535-2019-4-551-555.

[20] Dehoff, R. R., et al. “Site Specific Control of Crystallographic Grain Orientation through Electron Beam Additive Manufacturing.” *Materials Science and Technology*, vol. 31, no. 8, 10 Dec. 2014, pp. 931–938., doi:10.1179/1743284714y.0000000734.

[21] Zhang, X., et al. “Nanoscale-Twinning-Induced Strengthening in Austenitic Stainless Steel Thin Films.” *Applied Physics Letters*, vol. 84, no. 7, 10 Feb. 2004, pp. 1096–1098., doi:10.1063/1.1647690.

[22] Chuang, Tung Han, et al. “Effects of Annealing Twins on the Grain Growth and Mechanical Properties of Ag-8Au-3Pd Bonding Wires.” *Journal of Electronic Materials*, vol. 41, no. 11, 2012, pp. 3215–3222., doi:10.1007/s11664-012-2225-0.

[23] Lu, Lei, et al. “Ultrahigh Strength and High Electrical Conductivity in Copper.” *Science*, vol. 304, no. 5669, 16 Apr. 2004, pp. 422–426., doi:10.1126/science.1092905.

[24] Fullman, R. L. “Formation of Annealing Twins during Grain Growth.” *Journal of Applied Physics*, vol. 21, no. 10, 1950, pp. 1069–1070., doi:10.1063/1.1699536.

[25] Pham, M. S., et al. “Twinning Induced Plasticity in Austenitic Stainless Steel 316L Made by Additive Manufacturing.” *Materials Science and Engineering: A*, vol. 704, 17 Sept. 2017, pp. 102–111., doi:10.1016/j.msea.2017.07.082.

[26] Christian, J. W., and S. Mahajan. “Deformation Twinning.” *Progress in Materials Science*, vol. 39, 1995, pp. 1–157., doi:10.1016/0079-6425(94)00007-7.

[27] Varin, R. A., and J. Kruszynska. “Control of Annealing Twins in Type 316 Austenitic Stainless Steel.” *Acta Metallurgica*, vol. 35, no. 7, 1987, pp. 1767–1774., doi:10.1016/0001-6160(87)90122-2.

[28] Yin, Y. J., et al. “Mechanism of High Yield Strength and Yield Ratio of 316 L Stainless Steel by Additive Manufacturing.” *Materials Science and Engineering: A*, vol. 744, 28 Jan. 2019, pp. 773–777., doi:10.1016/j.msea.2018.12.092.

[29] Pande, C. S., et al. “Effect of Annealing Twins on Hall–Petch Relation in Polycrystalline Materials.” *Materials Science and Engineering: A*, vol. 367, no. 1-2, 25 Feb. 2004, pp. 171–175., doi:10.1016/j.msea.2003.09.100.

[30] Steinmetz, David R., et al. “Revealing the Strain-Hardening Behavior of Twinning-Induced Plasticity Steels: Theory, Simulations, Experiments.” *Acta Materialia*, vol. 61, no. 2, 2013, pp. 494–510., doi:10.1016/j.actamat.2012.09.064.

[31] Conrad, H., et al. “Effect of an Electric Field on the Superplasticity of 7475 Al.” *Scripta Metallurgica*, vol. 23, no. 5, 1989, pp. 697–702., doi:10.1016/0036-9748(89)90514-0.

[32] Waryoba, Daudi, et al. “Low Temperature Annealing of Metals with Electrical Wind Force Effects.” *Journal of Materials Science & Technology*, vol. 35, no. 4, 2019, pp. 465–472., doi:10.1016/j.jmst.2018.09.069.

[33] Ho, Paul S, and Thomas Kwok. “Electromigration in Metals.” *Reports on Progress in Physics*, vol. 52, no. 3, 1989, pp. 301–348., doi:10.1088/0034-4885/52/3/002.

[34] Basaran, Cemal, and Minghui Lin. “Damage Mechanics of Electromigration Induced Failure.” *Mechanics of Materials*, vol. 40, no. 1-2, 2008, pp. 66–79., doi:10.1016/j.mechmat.2007.06.006.

[35] Saito, Daiki, et al. “Damage of Flexible Electronic Line Printed With Ag Nanoparticle Ink Due to High-Current Density.” *ASME 2019 International Technical Conference and Exhibition on Packaging and Integration of Electronic and Photonic Microsystems*, 2019, doi:10.1115/ipack2019-6408.

[36] Wang, Jingze, et al. “Electromigration Mechanism of Indium-44Tin-6Zinc Alloy.” *Journal of Electronic Materials*, vol. 48, no. 10, 2019, pp. 6849–6856., doi:10.1007/s11664-019-07471-5.

[37] Li, Chao, et al. “Pulse Current-Assisted Hot-Forming of Light Metal Alloy.” *The International Journal of Advanced Manufacturing Technology*, vol. 63, no. 9-12, 2012, pp. 931–938., doi:10.1007/s00170-012-3934-5.

[38] Islam, Zahabul, et al. “Current Density Effects on the Microstructure of Zirconium Thin Films.” *Scripta Materialia*, vol. 144, 2018, pp. 18–21., doi:10.1016/j.scriptamat.2017.09.032.

[39] Bertolino, N., et al. “Electromigration Effects in Al-Au Multilayers.” *Scripta Materialia*, vol. 44, no. 5, 2001, pp. 737–742., doi:10.1016/s1359-6462(00)00669-2.

[40] Waryoba, Daudi, et al. “Recrystallization Mechanisms of Zircaloy-4 Alloy Annealed by Electric Current.” *Journal of Alloys and Compounds*, vol. 820, 2020, p. 153409., doi:10.1016/j.jallcom.2019.153409.

[41] Zhou, Yizhou, et al. “Crack Healing in a Steel by Using Electropulsing Technique.” *Materials Letters*, vol. 58, no. 11, 2004, pp. 1732–1736., doi:10.1016/j.matlet.2003.10.049.

[42] Zhou, Yizhou, et al. “Recrystallized Microstructure in Cold Worked Brass Produced by Electropulsing Treatment.” *Materials Letters*, vol. 58, no. 12-13, 2004, pp. 1948–1951., doi:10.1016/j.matlet.2003.11.035.

[43] Zhang, W., et al. “Evolution of Microstructures in Materials Induced by Electropulsing.” *Micron*, vol. 34, no. 3-5, 2003, pp. 189–198., doi:10.1016/s0968-4328(03)00025-8.

[44] Samuel, Edwin I., et al. “Accelerated Spheroidization Induced by High Intensity Electric Pulse in a Severely Deformed Eutectoid Steel.” *Journal of Materials Research*, vol. 25, no. 6, 2010, pp. 1020–1024., doi:10.1557/jmr.2010.0140.

[45] Hulbert, Dustin M., et al. “A Discussion on the Absence of Plasma in Spark Plasma Sintering.” *Scripta Materialia*, vol. 60, no. 10, 2009, pp. 835–838., doi:10.1016/j.scriptamat.2008.12.059.

[46] Deng, Shenghua, et al. “Direct Current-Enhanced Densification Kinetics during Spark Plasma Sintering of Tungsten Powder.” *Scripta Materialia*, vol. 143, 15 Jan. 2018, pp. 25–29., doi:10.1016/j.scriptamat.2017.09.009.

[47] Kondo, Takayuki, et al. “Influence of Pulsed DC Current and Electric Field on Growth of Carbide Ceramics during Spark Plasma Sintering.” *Journal of the Ceramic Society of Japan*, vol. 116, no. 1359, 2008, pp. 1187–1192., doi:10.2109/jcersj2.116.1187.

[48] Kim, Moon-Jo, et al. “Electric Current-Induced Annealing during Uniaxial Tension of Aluminum Alloy.” *Scripta Materialia*, vol. 75, 2014, pp. 58–61., doi:10.1016/j.scriptamat.2013.11.019.

[49] Fan, Rong, et al. “Influence of Grain Size and Grain Boundaries on the Thermal and Mechanical Behavior of 70/30 Brass under Electrically-Assisted Deformation.” *Materials Science and Engineering: A*, vol. 574, 2013, pp. 218–225., doi:10.1016/j.msea.2013.02.066.

[50] Jones, Joshua J., and Laine Mears. “Thermal Response Modeling of Sheet Metals in Uniaxial Tension During Electrically-Assisted Forming.” *Journal of Manufacturing Science and Engineering*, vol. 135, no. 2, 2013, doi:10.1115/1.4023366.

[51] Han, Ke, et al. “EBSD Study of the Effect of Electropulsing Treatment on the Microstructure Evolution in a Typical Cold-Deformed Ni-Based Superalloy.” *Materials Characterization*, vol. 158, 2019, p. 109936., doi:10.1016/j.matchar.2019.109936.

[52] Yang, Zhi Nan, et al. “Effect of Electropulsing Treatment on Microstructure and Mechanical Properties of a Deformed ZrTiAlV Alloy.” *Materials*, vol. 12, no. 21, 2019, p. 3560., doi:10.3390/ma12213560.

[53] Xu, W., et al. “Additive Manufacturing of Strong and Ductile Ti–6Al–4V by Selective Laser Melting via in Situ Martensite Decomposition.” *Acta Materialia*, vol. 85, 15 Feb. 2015, pp. 74–84., doi:10.1016/j.actamat.2014.11.028.

[54] Karthik, G. M., et al. “Additive Manufacturing of an Aluminum Matrix Composite Reinforced with Nanocrystalline High-Entropy Alloy Particles.” *Materials Science and Engineering: A*, vol. 679, 2 Jan. 2017, pp. 193–203., doi:10.1016/j.msea.2016.10.038.

[55] Jinoop, A. N., et al. “Laser Additive Manufacturing Using Directed Energy Deposition of Inconel-718 Wall Structures with Tailored Characteristics.” *Vacuum*, vol. 166, Aug. 2019, pp. 270–278., doi:10.1016/j.vacuum.2019.05.027.